University of Alberta

Novel Spectroscopic Probes for Detecting DNA Damage

by

Amira F. El-Yazbi

A thesis submitted to the Faculty of Graduate Studies and Research
in partial fulfillment of the requirements for the degree of

Doctor of Philosophy

Department of Chemistry

Spring 2013
Edmonton, Alberta

To my parents

To my husband Amr and daughters Hana and Karma

Abstract

Absorption of UV light by nucleic acids can result in the formation of molecular lesions leading to mutagenesis, carcinogenesis, and cell death. Thus, understanding DNA damage is important for elucidating the molecular mechanisms of disease. Much effort has been focused on developing methods for detecting DNA damage. However, almost all of the proposed methods consist of multi-step procedures, are limited to a specific type of damage, require expensive instruments, and/or suffer from a high level of interference. In this thesis, I present some novel simple, mix-and-read fluorescent assays for the detection of DNA damage. The goal is to design probes that are superior to conventional fluorescent molecular beacons (MBs) in detecting DNA damage. The first approach was to design MBs with modified DNA backbones. For this purpose, locked nucleic acid (LNA) and chimeric RNA-DNA (chMB) MBs were designed. The results show that chMBs are more sensitive and selective for DNA damage than LNA MBs that have comparable selectivity to conventional MBs. However, these probes show a signal that is inversely proportional to the amount of damage. Therefore, the second approach was to design probes that give signals directly proportional to the amount of damage. For this purpose, probes with 2-aminopurine (2AP) were designed. Such probes show no fluorescence for undamaged DNA and fluorescence for damaged DNA. 2AP probes offer high sensitivity and selectivity comparable to MBs, but are expensive, especially with an increasing number of 2APs in the probe to increase sensitivity. Thus, the hypochromism probe was designed. For this probe, the absorbance signal increases with increasing amount

of damage. Results show that the hypochromism probe is more selective and more than ten times cheaper than conventional MBs, but less sensitive. The need for a sensitive, selective and inexpensive probe was the motivation to design the Tb^{3+}/hairpin probe. Single-stranded DNA greatly enhances the Tb^{3+} emission, but duplex DNA does not. Undamaged DNA targets will hybridize with the hairpin with no emission. The Tb^{3+}/DNA hairpin probe proves to be the cheapest, most sensitive and selective probe for the quantification of DNA damage of all the probes presented here.

Table of Contents

List of Tables

List of Figures

List of Abbreviations

2AP	2-aminopurine
A	adenine
C	cytosine
CE-LIF	capillary electrophoresis with laser-induced fluorescence
chMB	chimeric RNA-DNA molecular beacon
CPD	cyclobutyl pyrimidine dimers
DNA	deoxyribonucleic acid
Dabcyl	4-(4'-dimethylaminophenylaz)-benzoic acid
EDTA	ethylenediaminetetraacetic acid
ELISA	enzyme-linked immunosorbent assay
F	fluorescence
FAM	6-carboxyfluorescein
FISH	fluorescence in-situ hybridization
FRET	Förster or fluorescence resonance energy transfer
G	guanine
GC	gas chromatography
HPLC	high performance liquid chromatography
IC	internal conversion
IR	infrared
IS	internal standard
ISC	intersystem crossing
LNA-MB	locked nucleic acid molecular beacon

LOD	limit of detection
LOQ	limit of quantitation
MB	molecular beacon
MS	mass spectrometry
P	phosphorescence
PCR	polymerase chain reaction
Ph	photochemical reaction
Q	quenching
RIA	radioimmunoassay
RNA	ribonucleic acid
ROS	reactive oxygen species
SNP	single nucleotide polymorphism
SP	smart probe
T	thymine
TLC	thin layer chromatography
T_m	melting temperature
U	uracil
UV	ultraviolet
UVA	ultraviolet A (320-400 nm)
UVB	ultraviolet B (280-320 nm)
UVC	ultraviolet C (320-400 nm)
UV-Vis	UV-Visible

Chapter 1

General Introduction

1.1. DNA structure and components

Chemical degradation studies in the early years of the twentieth century on material extracted from cell nuclei established that the high molecular-weight "nucleic acid" was actually composed of individual acid units, termed nucleotides. Four distinct types were isolated – guanylic, adenylic, cytidylic and thymidylic acids.[1] These could be further cleaved to phosphate groups and four distinct nucleosides. The latter were subsequently identified as consisting of a deoxypentose sugar and one of four nitrogen-containing heterocyclic bases. Thus, each repeating monomer unit in a nucleic acid polymer comprises these three units linked together – a phosphate group, a sugar, and one of the four bases. In a nucleic acid, individual nucleoside units are joined together in a linear manner, through phosphate groups attached to the 3' and 5' positions of the sugars (Figure 1.1).

The bases are planar aromatic heterocyclic molecules and are divided into two groups – the pyrimidine bases, thymine and cytosine and the purine bases, adenine and guanine. Their structures are shown in Figure 1.2. Thymine is replaced by uracil in ribonucleic acids, which also has an extra hydroxyl group at the 2' position of the ribose sugar groups. Nucleic acid and oligonucleotide sequences use single-letter codes for the five unit nucleotides; A, T, G, C and U. The prefix "d", as in d(CGAT), emphasizes that the oligonucleotide is a deoxyribose one rather than being an oligoribonucleotide. The prefix "r" denotes ribonucleotides.

The realization that the planar bases can associate in particular ways by means of hydrogen bonding was a crucial step in the elucidation of the structure of DNA. The important early experimental data of Chargaff showed that the molar ratios of adenine:thymine and cytosine:guanine in DNA were both unity.[1,2] This led

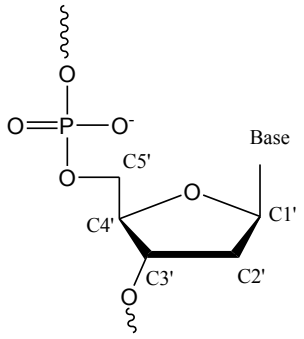

Figure 1.1. The organization of repeating units in a polynucleotide chain.

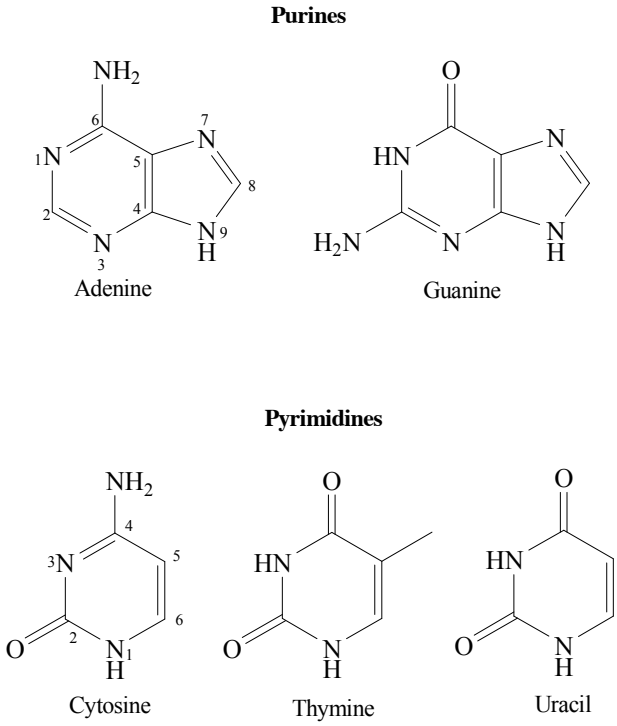

Figure 1.2. Structures of the five nucleobases. The atomic numbering scheme for the ring atoms is shown on the first member of each group.

Watson and Crick to the proposal that in each of these pairs the purine and pyrimidine bases are held together by specific hydrogen bonds, to form planar base pairs. In native, double-helical DNA, the two bases in a base pair necessarily arise from two separate strands of DNA and hold the DNA double helix together with intermolecular hydrogen bonds.[3] The AT base pair has two hydrogen bonds compared to three in a GC one (Figure 1.3).

1.2. Damaging effect of UV light on DNA

The sun emits energies at wavelengths that range through 17 orders of magnitude, from 10^{-4}nm to 10^{12} nm.[4] The vast majority of this energy is biologically irrelevant; short wave radiation such as high energy particles, x-rays, and gamma rays are expended by atomic collisions in the upper atmosphere, and long wavelength far infrared, microwaves, and radio waves do not have sufficient energy to influence biochemical reactions. Although UV radiation comprises a minute portion of the total solar output of energy, its biological impact is immense.

Nucleic and amino acids are considered the primary chromophores of UV radiation. RNA and proteins are encoded by DNA and are readily replaced by the cellular machinery. DNA, on the other hand, requires an intact copy of itself for replication, and any errors made during the replication process can result in mutation, loss of fitness, and cell death. Such errors would result in acute and chronic health effects. Tanning and sunburn are well-known examples of the acute effects of excessive UV exposure. On the other hand, skin aging and cancer represent the chronic outcomes of excessive exposure.

Skin cancer is the most common form of human cancer. The three most prominent forms are basal cell carcinoma, squamous cell carcinoma, and malignant melanoma. The first two variants contribute about 90 to 95% of all skin cancer incidents, while 5 to 10% are due to malignant melanoma, which is the most dangerous form of skin cancer due to its rapid metastasis.[5,6] Worldwide, the number of new skin cancer incidents was estimated by the World Health

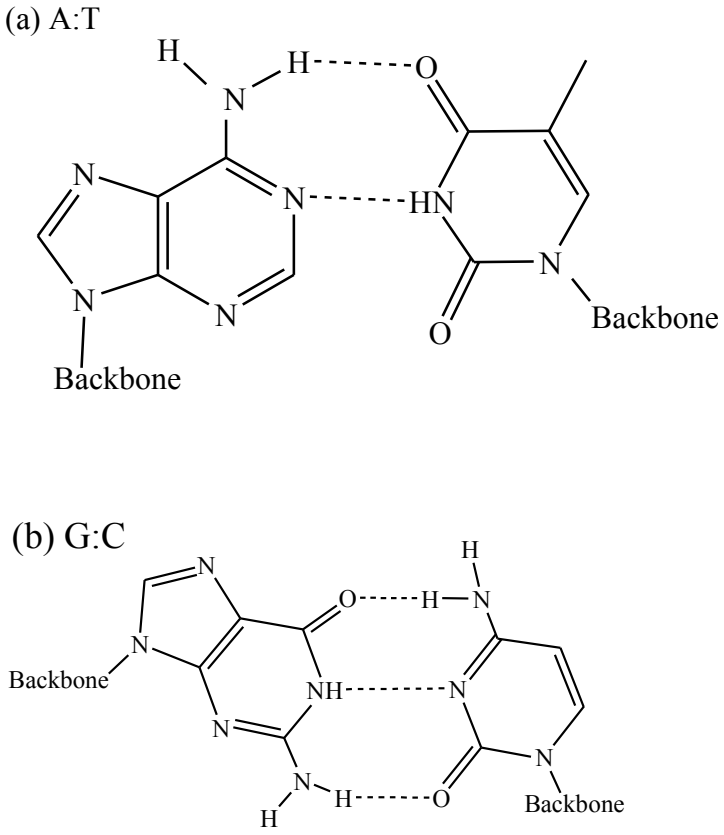

Figure 1.3. (a) AT and (b) GC base pairs, showing Watson-Crick hydrogen bonding.

Organization (WHO) to be around 130,000 cases, with about 35,000 deaths directly linked to skin cancer.[7] Tumour incidence and mortality correlate directly to UV exposure.[8] Basal and squamous cell carcinomas are most prevalent on the faces and trunks of men and on the faces and legs of women. Tumour incidence is increased in individuals working in occupations with high exposure, such as ranchers or fisherman, and the protective action of skin pigmentation results in lower cancer rates in dark-skinned populations compared to lighter-skinned populations.[8] The importance of UV damage and its repair in humans is exemplified by genetic diseases that greatly increase the risk of sunlight-induced skin cancer. In one such disease, xeroderma pigmentosum,[9] a failure in the DNA repair process is associated with a major increase in the rate of squamous and basal cell carcinoma and melanoma.[9,10]

UV radiation is composed of three regions.[11] UVC (200 to 280 nm) is not present in ambient sunlight, as wavelengths below ~295 nm are absorbed by ozone molecules in the stratosphere.[11] UVC light has been of major importance in experimental studies. It is readily produced by low-pressure mercury sterilizing lamps. The peak wavelength of mercury sterilizing excitation (254 nm) coincides with the peak of DNA absorption (260 nm), and thus causes maximum photochemical damage to DNA. On the other hand, almost 10% of UVB (280 to 320 nm) radiation reaches the earth's surface. It overlaps the upper end of DNA and protein absorption spectra and is the UV range mainly responsible for the environmental and pathological effects through direct photochemical damage to DNA. Therefore, it is a potent and ubiquitous carcinogen responsible for much of the skin cancer in the human population today.[12,13] UVA (320 to 400 nm) is photocarcinogenic and is involved in photoaging but is weakly absorbed by DNA and proteins. In contrast to the direct induction of DNA damage by UVC and UVB light, UVA produces damage indirectly through highly reactive chemical intermediates.[14] Similar to ionizing radiation, UVA induces the formation of oxygen and hydroxyl radicals, which in turn, react with DNA to form monomeric photoproducts, such as cytosine and thymine photohydrates, photooxidation

products (such as 8-oxodeoxyguanine), as well as strand breaks and DNA-protein cross-links.[11,15]

The relationship between the frequencies of the photoproducts and their biological effects depends on the cytotoxic and mutagenic potentials of the individual lesion. Hence, even though a photoproduct may occur at a low frequency, its structure and location may elicit a potent biological effect. It may not alter the genetic code and, hence, not affect normal metabolism, or it may produce a truncated or partial RNA transcript encoding a dysfunctional protein. Also, it may result in activation of an oncogene or inactivation of a tumour suppressor gene, thereby initiating the carcinogenic process.[8]

1.3. UV-induced DNA Photoproducts

1.3.1. Cyclobutane Pyrimidine Dimers

Cyclobutane dipyrimidines (CPDs) constitute the major DNA photoproducts upon exposure to UVB light. They arise from a [2π+2π] cycloaddition of the C_5=C_6 of adjacent pyrimidine bases (Figure 1.4). Four diastereomers may be generated from thymidine according to the position of the pyrimidine moieties with respect to the cyclobutane ring (*cis*/*trans* stereochemistry) and on the relative orientation of the two C_5–C_6 bonds (*syn*/*anti* regiochemistry).[16] Due to steric constraints, only *syn* isomers can be generated within DNA and oligonucleotides. Moreover, the *cis*-*syn* form is produced in large excess with respect to the *trans*-*syn* diastereomer.[16] The latter photoproduct is only present within single-stranded and denatured DNA.

CPDs have been reported to be formed preferentially at the major p53 mutational hotspot in UVB induced mouse skin tumors.[17] The biological effects of CPDs have been extensively studied in microbes and mammals. CPDs have been reported to inhibit the progress of DNA polymerases.[18] Mammalian RNA polymerase II has been reported to stall at both CPDs and 6–4PPs.[18,19] There is evidence that the stalled RNA polymerase II remains bound to the site of the obstruction.[20] Therefore persisting lesions may not only reduce the overall

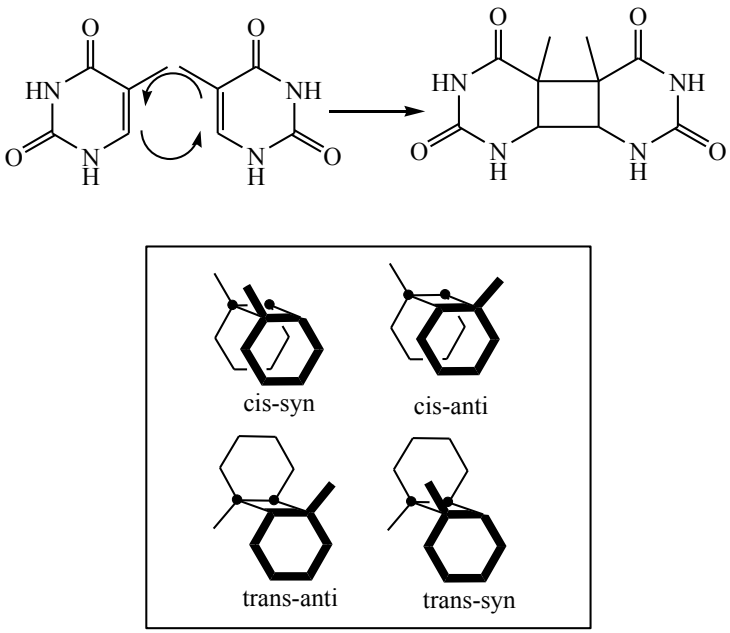

Figure 1.4. Formation of thymine cyclobutane dimer. The inset shows the different diastereoisomers.

concentration of free RNA polymerase but also, eliminate transcription of the gene in which they are located. Every CPD acts as a block to transcription and replication, and only a small fraction of dimers results in a mutation.[21,22] Therefore, these DNA lesions, if unrepaired, may interfere with DNA transcription and replication and can lead to misreading of the genetic code causing mutations and death.

The formation of CPDs can be reversed upon UVC irradiation through the photo-induced splitting of the cyclobutane ring. The residual absorption that CPDs exhibit at 254 nm allows their photoreversion into the starting pyrimidine bases or into uracil when cytosine-containing CPDs undergo deamination as a result of hydrolytic substitution of the C_4 amino function by an OH group.[23,24] Deamination may be involved in mutagenesis since the presence of uracil-containing photoproducts induces the predominant incorporation of adenine at the site of uracil resulting in C→T transition mutations.[25] In addition, photoreversion by the photolyase repair enzyme in some organisms[26] is expected to lead to the release of a uracil residue in place of the original cytosine.

1.3.2. Pyrimidine [6-4] pyrimidinone photoproducts and related Dewar valence isomer

The formation of pyrimidine [6-4] pyrimidinone adducts involves a singlet excited state. It represents the second class of pyrimidine photoproducts in terms of quantitative importance. They also arise from a [2π+2π] cycloaddition involving the C_5=C_6 double bond of the 5′-end pyrimidine and the C_4=O carbonyl group of the 3′-end thymine. This leads to the formation of an unstable oxetane intermediate.[27] An azetidine intermediate is generated when the 3′-end base is a cytosine, through cycloaddition of its C_4=NH imino group. Spontaneous rearrangement of the oxetane or azetidine intermediate gives rise to the pyrimidine [6-4] pyrimidinone adducts (Figure 1.5). The pyrimidinone ring allows the [6-4] lesions to exhibit fluorescence properties, with excitation and emission maxima around 320 and 380 nm, respectively. Detailed NMR investigations show that the [6–4] lesions strongly change the B conformation of the DNA duplex.[28] They

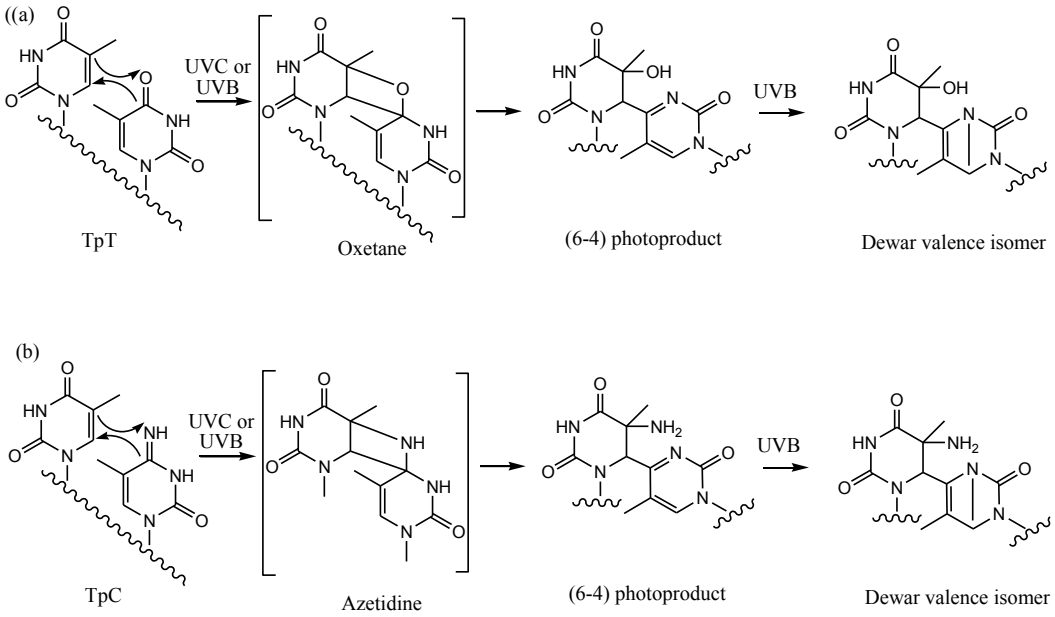

Figure 1.5. Formation of the pyrimidine [6-4] pyrimidinone photoproduct and the Dewar valence photoisomes from a dipyrimidine site through an oxetane (a) or an azetidine (b) intermediates.

induce a bend or a kink of 44° at the lesion site in the DNA duplex. [29,30] The 5′-T of a T-T [6-4] lesion is still paired in the Watson–Crick modus. The 3′-T, however, pairs preferentially with a guanine resulting in T→C transition mutations.[29,31,32] The [6-4] adducts exhibiting a cytosine only at their 5′-end may undergo deamination as the amino group of a 3′-end cytosine is transferred to the C_5 position of the 5′-end base upon formation of the photoproduct and therefore it cannot be hydrolyzed. Deamination of a 5′-C of a C-T [6-4] lesion would also result in C→T transition mutations. It should be added that both the [6-4] adduct and the Dewar valence isomer of the dinucleoside monophosphate dCpdT undergo deamination about 100 times more slowly than the corresponding *cis-syn* CPD.[23]

A second interesting property of the [6-4] photoproduct is photoisomerization into the related Dewar valence isomers upon exposure to UVB radiation (Figure 1.5).[33] Taylor[33,34] clarified that the pyrimidinone substructure of the [6-4] lesion is the rearranging unit. The structural effect of the Dewar valence isomer on the DNA duplex is substantially different compared to the [6-4] adduct.[28,35] DNA repair enzymes appear to recognize this lesion as an abasic site.[36] Whereas the CPDs, and to a lesser extent, the [6-4] adducts, can still instruct polymerases (mis-instruction), the Dewar valence isomer seems to be fully noninstructional. Polymerases, however, which are forced to read through a noninstructional site preferentially incorporate an adenine. This feature of polymerases is known as the A rule.[36] This A rule seems to govern the mutagenicity of the Dewar valence isomer.

The pyrimidine nucleobases have the highest quantum yields for photoreactivity, with thymine ~ uracil > cytosine. The three main UVB-induced dimeric photoproducts appear to be generated within cellular DNA in the following decreasing order of importance *cis-syn* T<>T > [6-4] TC adduct > T<>C. In contrast, CT and CC sites exhibit a low photoreactivity as inferred from the low yield of formation of both CPDs and [6-4] adducts at these

sequences.[37] Cadet, *et. al*.[38,39] proposed that CPDs are produced preferentially at TT and TC sites whereas CC and CT bipyrimidine sites are poorly photoreactive. However, CC photoproducts, although generated in low yields, exhibit a high mutagenic potential, leading to the characteristic UV-induced transition mutation CC → TT, which may imply deamination.[40,41] Insight into the type of DNA photodamage responsible for inducing skin cancer comes from the analysis of the mutations found in the p53 tumour suppressor gene of skin cancers.[42,43] Unlike proto-oncogenes, which require specific mutations to become activated, tumour suppressor genes can be inactivated by a much broader range of mutations and thus retain the signature of the carcinogen. When the p53 genes of basal and squamous cell carcinomas were sequenced, a large number of C→T mutations at dipyrimidine sites were discovered as well as the tandem CC → TT mutation.[42,43]

1.3.3. Photodimers of purine bases

The purine nucleobases are relatively photostable compared to pyrimidine bases. Thus, they have much lower quantum yields for photochemistry. This class of photoproducts arises from the dimerization of adjacent adenine residues (Figure 1.6).[44] The primary event in the photodimerization involves cycloaddition of the N_7=C_8 double bond of the 5'-A with the C_6-C_5 single bond of the 3'-A.[45] Two distinct homodimers of A have been reported upon the formation of the unstable A photodimer, the A=A and AA* photoproducts (Figure 1.6).[44-46] Also, heterodimers of A-T arise from the addition of adenine to a neighboring thymine upon exposure to UVB radiation.[47,48] The quantum yields of formation of this heterodimer are very low.[49,50] However, the adenine-containing lesions may contribute to the biological effects of UV light since the A-T adduct has been shown to be mutagenic.[51]

1.3.4. Monomeric photoproducts

Recently it has been shown that UVB is able to induce the formation of 8-oxo-7,8-dihydroguanine (8-oxoG) in DNA (Figure 1.7).[52-55] The mechanism of

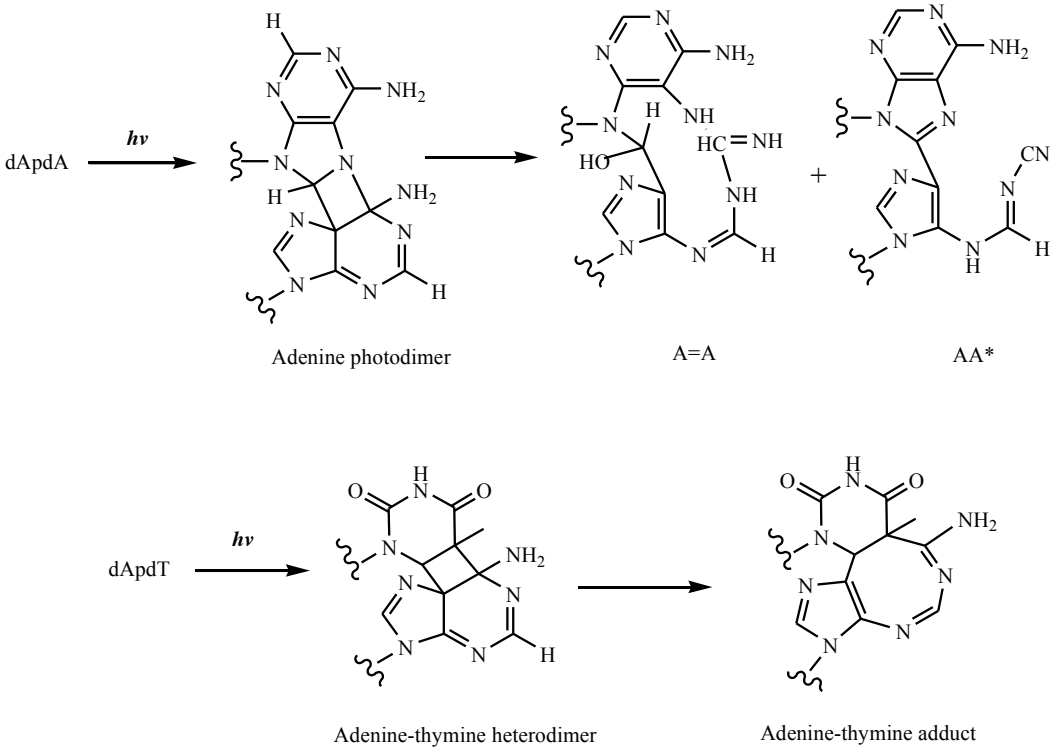

Figure 1.6. The formation of adenine-containing dimeric photoproducts upon UV exposure. The fate of the unstable photodimer (A=A) is also shown.

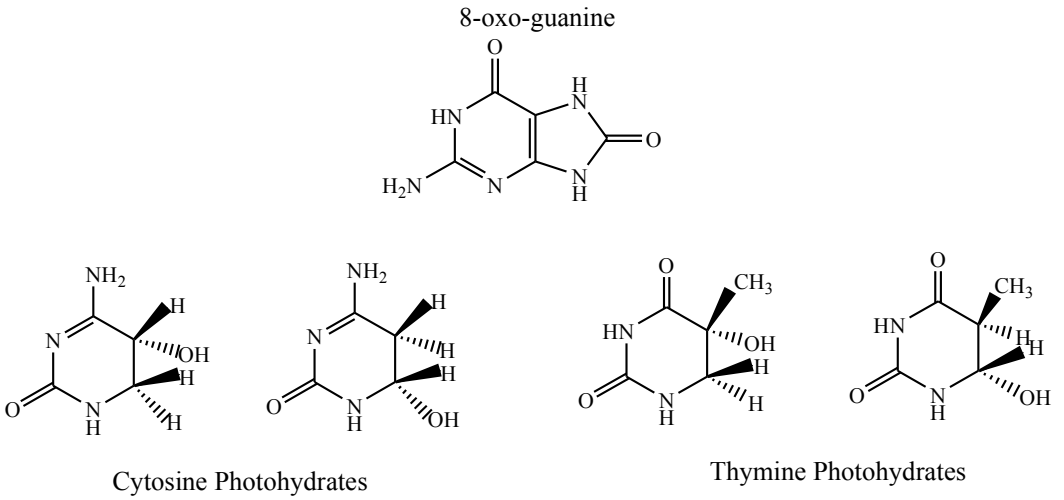

Figure 1.7. Structure of monomeric UV-induced photoproducts.

the UVB-induced formation of 8-oxoG was recently proposed through the oxidation of the 2'-deoxyguaninosine moiety as a result of its reaction with either singlet oxygen [56,57] or a hydroxyl radical.[54]

Other UV-induced DNA photoproducts that have received a lot of attention in early model studies are the pyrimidine photohydrates. Pyrimidine photohydrates (Figure 1.7) are produced through the photocatalytic addition of water across the C_5=C_6 bond in pyrimidines with the subsequent formation of either a 6- hydroxy-5-hydroderivative or a 5- hydroxy-6-hydroderivative. The photohydration reaction occurs efficiently within DNA or RNA monomers. It is suggested to involve the nucleophilic addition of a water molecule to a reactive excited intermediate.[14] Experimental data showed that UVC-induced formation of photohydrates in isolated DNA is a minor photochemical event with a yield of formation which is about two orders of magnitude lower than that of CPDs.[8] The relative efficiency in the formation of pyrimidine photohydrates with respect to CPDs was found to be even lower, by a factor of 10, in cellular DNA due to the lower accessibility of water molecules for hydration of the pyrimidine moieties in compacted cellular DNA. This suggests a minor contribution of pyrimidine hydrates to the overall biological effect of UV radiation.

1.4. Detection of UV-induced DNA damage

Numerous methods have been developed for the specific and general detection and quantification of DNA photoproducts. Methods for detecting individual lesions (Figure 1.8) require either quantitative acidic hydrolysis (base release) or enzymatic digestion (release of nucleosides, nucleotides, or short oligonucleotides), followed by separation of the individual lesions of interest from the overwhelming majority of normal DNA constituents. Finally, the complex mixture of DNA lesions is analyzed. For the general methods, the DNA is kept intact and lesions are measured either by hybridization probes, immunological methods or by the nicking activity of DNA repair enzymes in association with

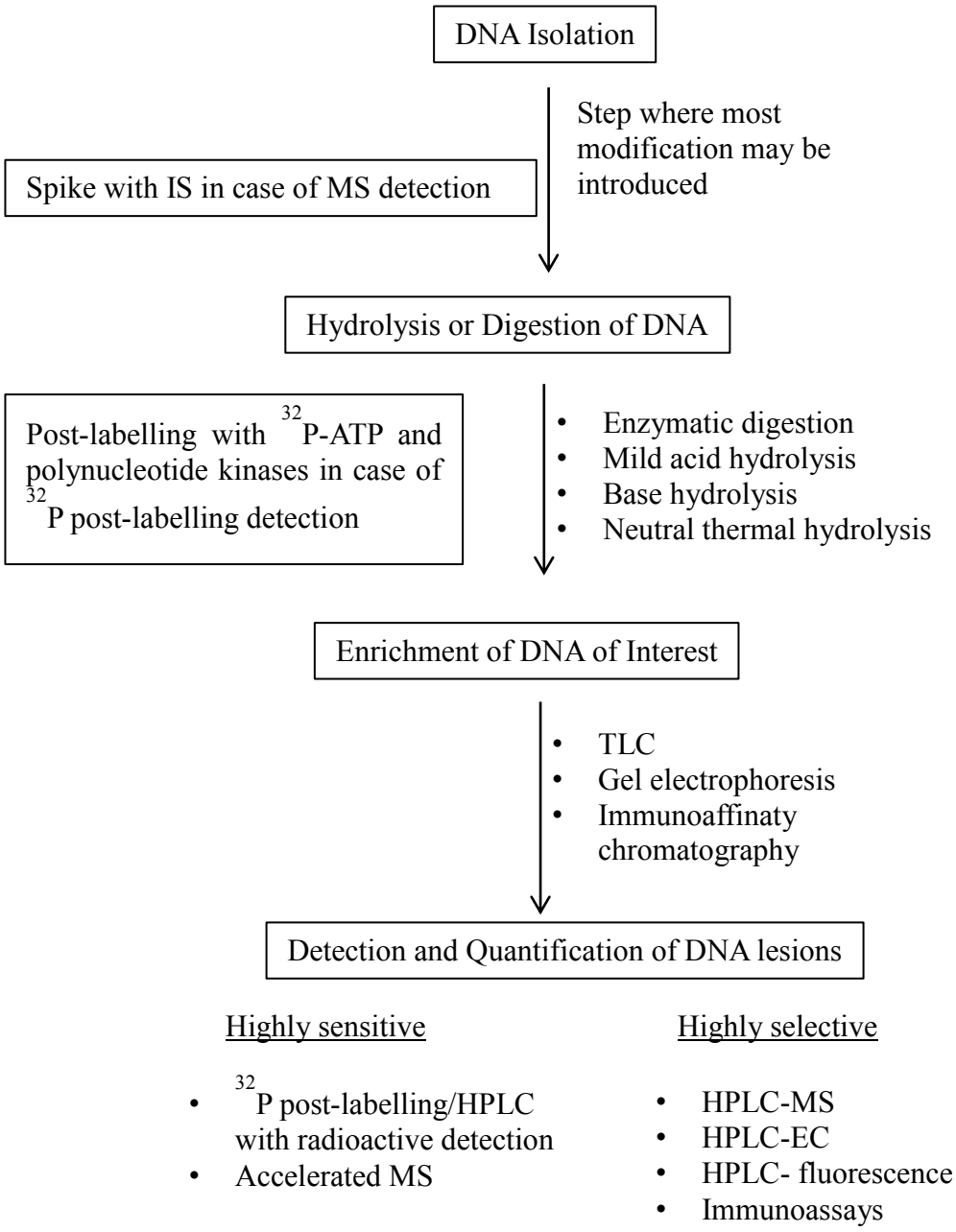

Figure 1.8. Scheme for quantification of individual DNA lesions. IS, MS, TLC, and EC are abbreviations for internal standard, mass spectrometry, thin layer chromatography and electochemical detection, respectively.

sedimentation and gel-sequencing techniques that quantify the number of strand breaks.

1.4.1. Chromatographic assays

The first attempts to assess the formation of CPDs within cellular DNA involved paper chromatographic analysis following the acidic hydrolysis of radioactive-labeled DNA, allowing the isolation and characterization of *cis-syn* CPDs (T<>T). Then, thin-layer chromatography (TLC), and high-performance liquid chromatography (HPLC) were adapted to the analysis of this and other DNA lesions. The only available sensitive detection at that time was the radioactive measurement of the content of HPLC fractions, therefore, all of these procedures required pre-labelling of the DNA sample with a radioactive tracer as ^{3}H-thymidine[58,59] and the subsequent hydrolysis to free bases or nucleotides by enzymatic digestion or treatment in strong acid at high temperature. It should be noted that these procedures were time consuming and required a large amount of sample. The availability of hydrophobic stationary phases including octadecylsilyl silica gel (ODS) packing material has offered the advantage of strongly retaining thymine due to the occurrence of hydrophobic interactions more than the targeted *cis-syn* T<>T allowing its efficient separation from the DNA hydrolysis products.[58,59] However, measurements of other UV-induced DNA lesions suffered from the presence of a co-eluting radioactive contaminant that arose from a self-radiolysis process.[60] A few years later, a non-radioactive HPLC-fluorescence assay was suggested for the measurement of the fluorescent pyrimidine [6-4] pyrimidinone photoproducts, which represent a major class of UV-induced DNA photolesions.[61,62] Mild hydrolysis of irradiated DNA by hydrogen fluoride stabilized with pyridine quantitatively induces the release of three base photoadducts, including T-C, T-T, and C-T [6-4] adducts followed by efficient separation by HPLC and quantification by on-line fluorescence detection. Unfortunately, other photolesions are not fluorescent and thus cannot be detected using this method.

Development of ^{32}P-postlabeling procedures obviated the need for pre-labeling and expanded the sample repertoire available to chromatographic techniques. Randerath and co-workers[63] developed these methods to measure carcinogen - DNA adducts. Damaged DNA is first digested enzymatically to nucleoside 3'-monophosphates or very short oligonucleotides (depending on the enzymes used for digestion and the damage to DNA) that are then enzymatically radiolabeled by incubation with ^{32}P-labeled ATP and phage T4 polynucleotide kinase. A variety of techniques, including two-dimensional TLC and HPLC, have been used to analyze the different UV-induced photolesions.[64-69] ^{32}P-postlabeling assays have the advantage of being highly sensitive, require only small amounts of the DNA sample, and allow the detection of different types of UV-induced DNA photoproducts in one sample. However, this type of assay includes multiple sample handling steps which makes the procedure more elaborate, time consuming and liable to human errors.

Recently, an HPLC–MS/MS method with electrospray ionization (ESI) detection mode has been used for the selective detection of UV-induced DNA lesions.[65,70] The first step involves enzymatic digestion of DNA extracted from UV-irradiated cells by several enzymes into nucleotides or nucleosides. The digested matrix produced depends on the type of enzymes or hydrolysis reagents used. It is always recommended to use enzymes or reagents that would result in a cleaner matrix so that it would facilitate the separation of the DNA lesions from normal nucleotides or nucleosides. For example, in order to separate T<>T photolesions from the cytosine-containing photolesions, a deamination step was carried out in order to produce the uracil derivatives of the latter, which were then separated by HPLC and selectively detected by tandem MS. This technique allowed the quantitative detection of the twelve possible bipyrimidine adducts at TT, TC, CT and CC sequences.[38,39] In addition using different modes of the tandem mass spectrometric measurement as the sensitive multiple reaction monitoring (MRM) mode or the selected ion monitoring (SIM) mode allows the selective quantification of CPD from [6-4] photoproduct for a given bipyrimidine

sequence.[71] It should be noted that using tandem mass spectrometry coupled with ESI offers high selectivity and high resolution for measuring UV-induced DNA lesions. However, the major limitation to this technique would be the elaborate sample pre-treatment as the more steps included in the sample pre-treatment, the more the sample loss during sample transfer and solvent exchange, and the more the introduction of sample contaminants.

Gas chromatography-MS has also been used for the detection of CPD lesions. It requires an additional trimethylsilylation step as well as the use of an isotopically labelled internal standard.[72,73] Generally gas chromatography is not commonly used for the detection of UV-induced photolesions as the derivatization of the photodimers to be volatile enough for GC analysis is difficult.

On-line electrochemical detection coupled with HPLC separation represents a sensitive and accurate method for the measurement of readily oxidizable compounds. It has been successfully applied to the specific determination of the oxidized pyrimidine components,[74] including 5-hydroxyuracil, 5-hydroxycytosine and 8-oxoG in cellular and biological fluids.[75]

1.4.2. Electrochemical assays

Electrochemical methods offer a sensitive, selective, low cost and miniaturized device for the detection of DNA damage.[76-81] Owing to its intrinsic electroactivity and surface activity, it is possible to analyze DNA electrochemically without any labeling.[76-86] The label-free approaches proved to be particularly useful in structure-sensitive DNA analysis and/or for the detection of DNA damage. In such cases, changes in the electrochemical response of a DNA molecule accompanying change in the nucleobase accessibility is monitored, such as, the formation of strand breaks and the opening of the DNA double helix, or in the nucleobase electroactivity, such as, a loss of the guanine oxidation signal upon chemical damage of the guanine moiety. Unfortunately this technique is limited to the detection of DNA lesions that can undergo redox reactions. Adenine, cytosine, and guanine undergo redox processes at the mercury electrode while guanine and

adenine are oxidizable at carbon and some other solid electrodes. Also the signal can be affected by changes in DNA structure.[82-84] 8-oxoguanine has been detected via its oxidation signal at carbon electrodes.[85,86] The UV-induced DNA lesions such as thymine dimers could not be detected directly. However they were detected indirectly through measuring the distortions of DNA double helix and relating it to the presence of these lesions.[82,83]

1.4.3. Gel Electrophoresis

Many types of photodamage can be converted into single-strand breaks in DNA by enzymatic or biochemical treatment. Strand breaks induced directly in DNA by UV and breaks produced at sites of photoproducts by targeted enzymatic or biochemical procedures can be quantified by agarose gel electrophoresis. The sensitivity of these procedures requires maintenance of high-molecular-weight DNA throughout the extraction and analytical procedures. Specific cleavage at the lesion site can be achieved by using purified glycosylase-endonucleases from various prokaryotic hosts, primarily *E. coli*. These enzymes combine a glycosylase that cuts the base from the sugar, leaving an apyrimidinic (AP) site, and an AP endonuclease that cleaves the phosphodiester backbone on either side of this site. These enzymes range from the CPD-specific T4 phage endonuclease V[87,88] and 8-oxodeoxyguanine-specific oxoguanine glycosylase to more broad-spectrum reagents like endonuclease III and formamido glycosylase that cut a variety of photohydrates and photooxidative products.[89] Nonenzymatic cleavage of alkali-labile sites, such as AP sites or Dewar pyrimidinones, also produces quantifiable strand breaks using alkaline agarose gel electrophoresis.

1.4.4. Polymerase Chain Reaction (PCR)

PCR is one of the most reliably used techniques for detecting DNA damage as the amplification stops at the site of the damage.[90] Ligation-Mediated Polymerase Chain Reaction (LMPCR) allows the mapping within DNA at the nucleotide resolution of dimeric pyrimidine photoproducts and particularly of CPDs.[91-93] Interestingly these sites of CPD formation correspond to the major p53 mutational

hot spots in mouse skin tumors.[94] Recently, for the mapping of pyrimidine [6-4] pyrimidinone photoproducts, Terminal transferase-Dependent PCR (TDPCR)[95,96] has been used. TDPCR depends on cohesive-end ligation to the 3′ ends of DNA molecules resulting from primer extension, followed by controlled ribonucleotide tailing by terminal deoxynucleotidyl transferase.[95] TDPCR has the advantage of using low doses of UVC for mapping [6-4] photoproduct over LMPCR. An immuno-coupled PCR (ICPCR) assay has been used by Karakoula et al.[97] to estimate T<>T (thymine dimer) formation at the gene level and to compare gene and global levels of T<>T within human genomic DNA. A PCR-based SINE (short interspersed DNA element)-mediated detection method was developed by Wang et al.[98] for UVB induced DNA damage and repair detection in mammalian genomes which utilize the abundance, dispersion and conservation of SINEs. This assay is also based on the template activity of the DNA region between SINEs, which is amplified by using primers bound to the SINE.[98]

1.4.5. Immunological detection

Immunological detection has long been recognized as a potentially powerful tool in the analysis of genotoxin-modified DNA. As early as 1966, Levine and co-workers prepared antibodies against UV-induced photoproducts of DNA.[99] Since then, antibodies have been derived against several DNA lesions, including cyclobutane-pyrimidine dimers, and [6-4] photoproducts.[14,61] The main advantages of immunochemical detection are specificity (especially if monoclonal antibodies are used), sensitivity (subfemtomole level), and simplicity once antibodies have been generated. Like other haptens, modified bases must be linked to macromolecules to elicit an immune response. The principal methods employed in the preparation of immunogens are the synthesis of modified nucleosides or nucleotides that are then covalently coupled to proteins such as bovine serum albumin or keyhole limpet haemocyanin, and the modification of single- or double- stranded DNA, which is then electrostatically bound to methylated bovine serum albumin.

Problems of cross-reactivity have occurred when damaged polymeric DNA has been used as an immunogen. This became evident when a polyclonal antiserum raised against UV-irradiated DNA recognized all the thymine- and cytosine-containing CPDs together with [6-4] photoproducts, but with a different affinity for each major class of damage.[100] Thus, if damaged DNA is to be used as the immunogen, it is important to choose conditions that greatly favor the production of a single type of damage over any other. For example, the ratio of CPDs to other photoproducts can be enhanced by acetophenone photosensitization of DNA when the DNA is exposed to 313 nm radiation.[14]

Numerous monoclonal and polyclonal antibodies were raised against CPDs, [6-4] photoproducts and related valence Dewar isomers for ELISA, radioimmunoassay (RIA) and immuno-dot-blot measurements in nuclear DNA together with immunostaining detection of photoproducts in tissues.[101-105] The most commonly used technique is ELISA, in which the primary antibodies, when bound to the antigen, are detected by secondary antibodies linked covalently to an enzyme such as alkaline phosphatase or peroxidase. Substrates for the enzymes are added and yield products with intense absorption at visible wavelengths. Other substrates have used either primary antibodies coupled to radioactive isotope in radioimmunoassays (RIA) or secondary antibodies conjugated to fluorescent compounds, such as fluorescein isothiocyanate (FITC).

Immunodetection has been particularly effective for studying the induction and repair of UV-induced photoproducts. Nikaido and coworkers[103,106] established monoclonal antibodies recognizing CPDs and [6-4] photoproducts. Using autoradiography to detect tritiated antibodies, they were able to observe [6-4] photoproducts in human cells exposed to very low radiation doses. In contrast to normal proficient human cells, which removed more than 80% of their initial damage within 4 h of post-irradiation, cells derived from a patient with xeroderma pigmentosum showed almost no repair within 8 h.[103] In the detection of very low quantity of CPDs in bacterioplankton and marine viruses caused by UVB

radiation, RIA was found to be very effective.[107-109] Specific RIAs were used to monitor antibody binding sites associated with CPDs and [6-4] photoproducts. Using this technique, the biological role of [6-4] photoproducts can be measured.[110] CPDs were detected in active *Mycobacterium parafortuitum* and *Serratia marcescens* cells, using fluorescent Alexa Fluor 488 and radiolabeled ^{125}I secondary antibodies as reporters.[11]

With an ELISA protocol,[103] T<>T are shown to be excised from DNA in irradiated human cells more slowly than [6-4] photoproducts; removal of the latter was virtually completed within 12 h of post-irradiation, whereas at 24 h, half of the T<>T still remained. DNA damage can be detected and quantified very efficiently by immune-slot-blot system utilizing chemiluminescent detection,[112] secondary antibodies conjugated to alkaline phosphatase enzymes[113] and secondary antibodies conjugated to radioactive iodine.[114] Antibodies to modified nucleosides are also possible.[115] Immuno-slot-blot assay is used to detect very low levels of adduct in very small amounts of DNA. It is a very sensitive and specific assay. Recently it was used to detect CPDs, [6-4l esions and their Dewar valence isomers in UV-irradiated mammalian cells.[116]

1.4.6. Comet Assay

The comet assay (Figure 1.9) is a single-cell gel electrophoresis technique based on the principal that DNA with nicks release fragments that migrate farther in an electric field than undamaged DNA.[117] Cells are embedded in agarose, layered on glass slides, and treated with a cell lysis solution to liberate DNA. Slides are then exposed to alkali to denature DNA and electrophoresed under alkaline conditions. Following electrophoresis, gels are neutralized and stained with cyber green, ethidium bromide, propidium iodide, or other suitable fluorescent dye to visualize tails of DNA extending from cells.[118] Images are captured using a fluorescence microscope equipped with an imaging system. These tails have the appearance of comets that increase in length and size as DNA damage increases. Tailing may be quantified by measuring tail length, tail area, or tail moment, which is the product

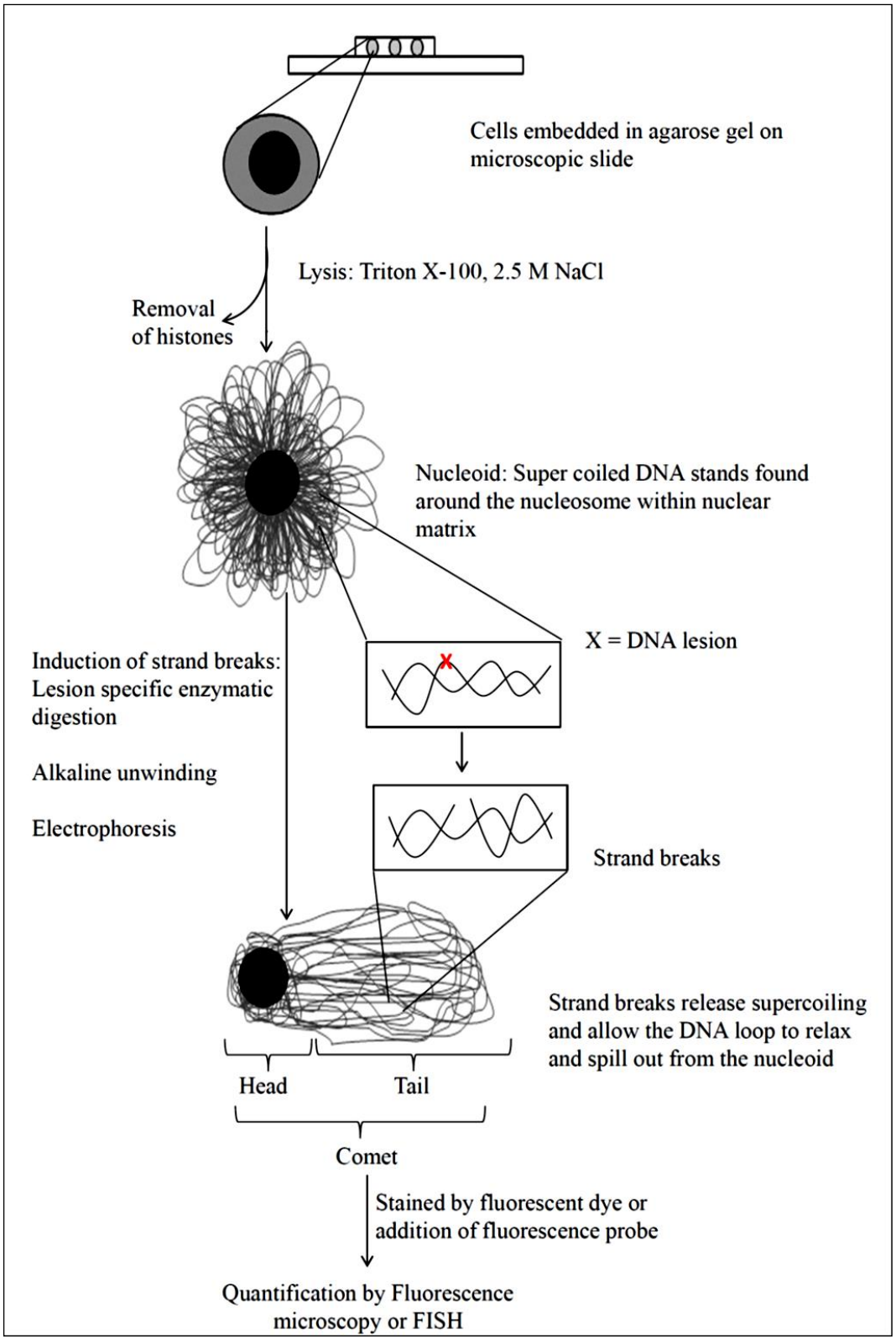

Figure 1.9. General principle of the comet assay

of the comet length and the fraction of fluorescence in the tail.[119,120]

Lesion-specific endonucleases extend the usefulness of the method to investigate different kinds of damage. For example, T4 endonuclease V for UV-induced CPDs was used and the comet tail length and area were significantly increased, and were easily discernable from background after subjecting a keratinocyte cell line to UVB.[121] Also in a modified comet assay, CPDs were detected with an indirect immunofluorescence detection using a specific monoclonal antibody.[122] DNA repair can be studied by treating cells with damaging agent and monitoring the damage remaining at intervals during incubation.[121] An important feature of the assay is that damage is detected at the level of individual cells. Also, combining the comet assay with fluorescent in situ hybridization (FISH), using labeled probes to particular DNA sequences, increased the resolution of the assay and allowed detection of DNA damage and repair at the level of single genes or DNA sequences.[123,124]

1.4.7. Absorbance techniques

DNA has a main absorbance band around ~260 nm, which represents the $\pi\pi^*$ transitions of nucleobases. The 260 nm absorbance band is seen to decrease with UV irradiation time. Monitoring the absorbance changes of the 260 nm absorbance band of a DNA sample UV irradiation and correlating these spectral changes to the UV exposure time, hence, the radiation dose, gave an idea about the kinetics of UV-induced DNA damage.[125,126] These results are expected and indicate UV-induced damage to the oligonucleotides due to the formation of CPDs and [6-4] photoproduct resulting in a loss of the C_5=C_6 double bond.[125,126] In addition an absorbance band at ~330 nm indicates the formation of the pyrimidine pyrimidinone [6-4] photoproduct and is seen to increase with increasing irradiation time.[125,126] Comparing spectral changes of unirradiated controls with UV irradiated and mismatched samples shows significant differences. This allows the detection of UV-induced DNA damage[125,126] and DNA mismatches.[126] In general, the attractive advantages of absorbance techniques, mainly, being inexpensive and simple, promoted their use in most of

the analytical assays but its low sensitivity made it necessary to move to other more sensitive techniques such as fluorescence measurments. Fluorescence techniques preserve the advantage of simplicity, however, the cost of the technique will be dependent on the cost of the fluorescent probe used.

1.4.8. Fluorescent Probes

The high sensitivity of fluorescence detection, due to the zero background nature of the technique, allowed the development of numerous bioanalytical fluorescent assays for measuring UV-induced DNA damage. In this thesis, the design and performance of several fluorescent probes will be discussed. Therefore, it is beneficial to briefly discuss fluorescence spectroscopy here.

Fluorescence Spectroscopy

When a molecule is excited by absorption of light, it returns to its ground state by a combination of several radiative and non-radiative relaxation processes (Figure 1.10).[129,130] Fluorescence and phosphorescence are forms of radiative relaxation while vibrational relaxation, internal conversion (IC) and intersystem crossing (ISC) are forms of non-radiative relaxation.[129] The simple Jablonski diagram of Figure 1.10 can be used to explain these processes. In the presence of other species, there could also be bimolecular interaction, electron transfer and non-radiative energy transfer processes taking place. This process is called quenching. In addition, unimolecular or bimolecular photochemical reactions can occur. The fluorescence process corresponds to the relaxation of the molecule from the singlet excited-state to the singlet ground-state with the emission of light.[130] Its relatively short lifetime of $\sim 10^{-9}$ s means that it can favourably compete with intersystem crossing and phosphorescence. Phosphorescence is the relaxation of the molecule from the triplet excited-state to the singlet ground state with the

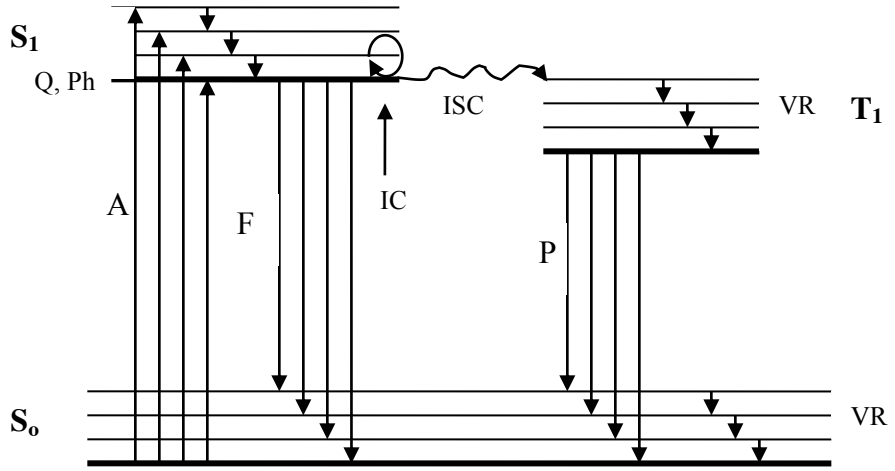

Figure 1.10. Jablonski diagram showing the absorption of light (A) by a molecule and its excitation from the ground state (S_o) to the excited-state (S_1). In the excited-state, the different relaxation processes that take place are indicated (F = fluorescence, P = phosphorescence, IC = internal conversion, ISC = intersystem crossing, VR = vibrational relaxation, Q = quenching and Ph = photochemical reaction). Note that P is from a different state (T_1) compared to F which originates from S_1.

emission of light. Because this is a classically forbidden transition, it has a long lifetime and a slow rate (10^{-2} – 100 s).[129]

Factors affecting fluorescence

The chemical structure and the surrounding environment are basically the main factors which influence fluorescence.[129] The structure of a good fluorophore should be rigid, flat, have a high extinction coefficient and a high fluorescence quantum yield. A rigid structure minimizes internal conversion, which competes with fluorescence. Compounds with aromatic rings of low energy $\pi\pi^*$ transitions possess the highest fluorescence intensity. The fluorescence intensity of conjugated aromatic hydrocarbons increases with increasing number of rings and degree of condensation.[129] Fused ring structures also make good fluorophores. In addition, a good fluorophore will have a low tendency to undergo intersystem crossing. Usually, molecules with no heavy atoms and no lone pairs of electrons are better fluorophores than those with these characteristics. The presence of species which can quench the fluorescence signal can also affect the fluorescence. For instance, the presence of molecular oxygen is known to reduce fluorescence intensity. Because it is a ground-state triplet, oxygen promotes intersystem crossing and conversion of molecules to the triplet state.[129] Thus, the careful choice of a fluorophore is essential for the design of sensitive analytical probes.

A number of fluorescence assays for probing DNA damage have been proposed. Typically, fluorescence methods offer enhanced sensitivity and the potential for use *in situ* or *in vivo*.[90] Some of the recently developed fluorescent assays for the detection of UV-induced DNA damage will be discussed below.

1.4.8.1 Affinity Capillary electrophoresis with laser-induced fluorescence detection (CE-LIF)

Immunochemical recognition with capillary electrophoresis (CE) and laser-induced fluorescence detection (LIF) is a well-established technique for the detection of DNA damage. Since 1998 in which thymine glycols were detected in irradiated A 549 cells (a human lung carcinoma cell line) with a detection limit as

low as 10^{-21} mol.[131] The fast (seconds) and efficient separation and a small sample volume (nl range) requirement of CE with the sensitive detection of LIF combined with the specificity provided by monoclonal antibodies to a single lesion limits sample manipulation to DNA extraction, incubation with antibodies, and capillary electrophoresis. Therefore, this reduces potential artifacts caused by chemical or enzymatic DNA digestion and makes affinity CE-LIF a powerful technique for bioanalysis, leading to a single molecule detection limit.[132] Affinity CE-LIF was successfully used for the detection of CPD lesions in human normal fibroblast CRL-2522 cells after UVB irradiation at low doses relevant to environmental exposure.[133] In addition, CRL-2522 cells were also exposed to two different DNA-damaging agents, UV light and benzo(a)pyrene. Comparison of the result between non-combined and combined exposures did not show significant differences between formation of benzo(a)pyrene adducts and UV lesions in cells. Unfortunately, the determination of the [6-4] photoproduct lesions was not possible because of the high background from the cellular DNA.[133]

1.4.8.2 Molecular Beacons (MBs)

MBs are oligonucleotide probes with a stem-loop structure (Figure 1.11), containing a fluorescent dye on one end and a quencher on the other.[134-137] In the absence of target DNA, the fluorophore and the quencher are in close proximity, so there is minimal fluorescence due to Förster resonance energy transfer (FRET) from the fluorophore (donor) to the quencher (acceptor). However, in the presence of the complementary target sequence, the MB hybridizes with the target, resulting in a significant increase in fluorescence. If the target is subjected to UV-light, UV-induced DNA lesions will be formed, and the hybrid formed between the MB and the damaged target is less stable since the DNA target is no longer perfectly complementary to the loop of the MB. Thus, the fluorescence is lower for this hybrid compared to that formed between the undamaged DNA and the MB. In 2005, Yarasi, et. al.[125] demonstrated the use of DNA MBs in the detection of UV-induced damage in poly dT and poly rU strands. The fluorescence intensity of the damaged DNA decreased with the increase of UV-exposure time, hence

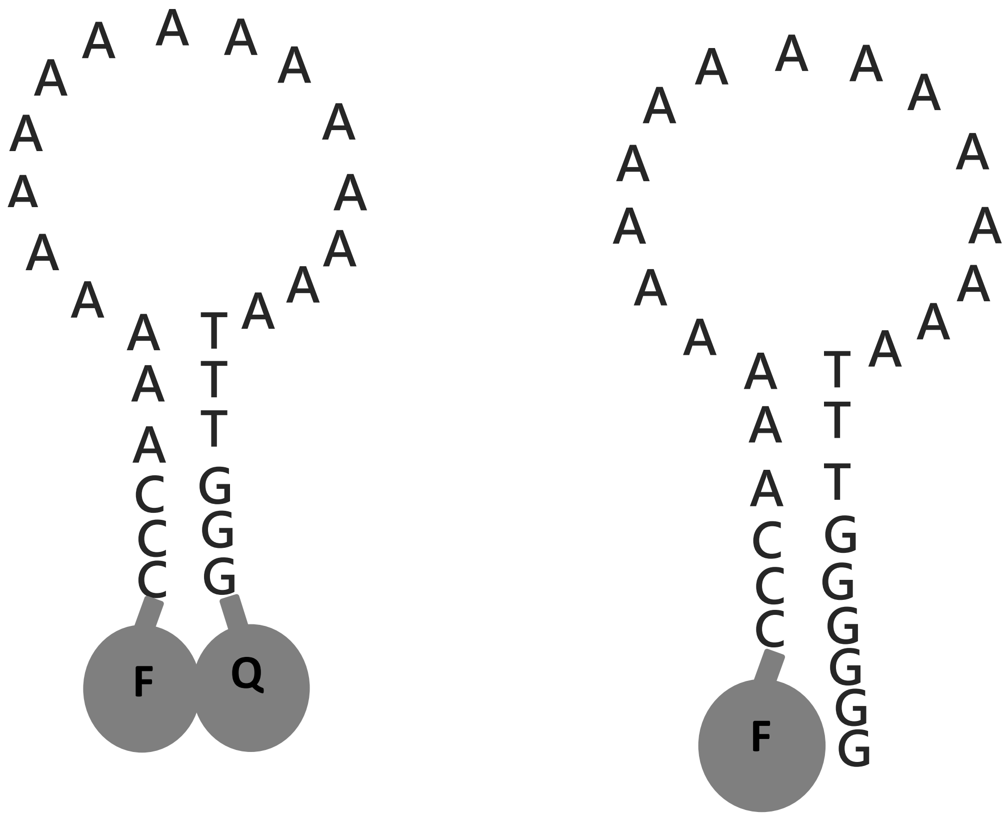

Molecular Becon **Smart Probe**

Figure 1.11. Schematic diagram of the stem-loop structure of the molecular beacon and the smart probe. “F” denotes fluorophore and “Q” denotes quencher.

increased damage while the fluorescence of the unirradiated DNA controls was constant.[125]

These inherent properties make the MBs highly sensitive and very selective probes for DNA damage. However, MBs suffer from some limitations.[138-143] First, they require site-specific labelling of both termini of the hairpin with a fluorophore and a quencher which make their synthesis difficult and expensive.[138,139,141,143] Second, with its two ends occupied, any further modification would require the incorporation of an additional modified nucleotide into the stem.[138,141] In addition, due to incomplete synthesis, the hairpin is only labelled with the fluorophore. Highly sensitive assays are affected by a high background due to unquenched probe molecules.[138,139] Third, in the presence of a mixture of undamaged and damaged DNA, the MB hybridizes only with the undamaged target. Thus, the fluorescence intensity decreases with increasing amounts of damage, providing an inversely proportional signal to the amount of damage, i.e. negative detection of DNA damage. Fourthly, DNA MBs are subjected to endogenous nuclease degradation, non-specific binding by DNA/RNA binding proteins and stem disruption.[142] An attempt to overcome the first and second limitations mentioned above was previously accomplished by our group by using self-quenching smart probes.[126]

1.4.8.3. Smart Probes (SPs)

SPs (Figure 1.11) are hairpin oligonucleotide probe molecules just like MBs and function similarly. Unlike MBs, however, SPs have guanine residues replacing the quencher attached to the other end and the fluorescence quenching of the fluorophores occurs via photoinduced intramolecular electron transfer.[140-143] However, in the presence of the complementary target sequence, the stem unwinds forcing the fluorophore and the guanosine residues far apart, thereby restoring fluorescence. Oladepo et al.[126] demonstrated that SPs have the ability to detect UV-induced DNA damage and single base mismatches. Indeed, SPs are less costly than MBs and allow the introduction of further modification on the free

terminus of the SP. However, SPs suffer from high fluorescence background, in addition to the other MB limitations mentioned above.

1.5. Rational and Scope of the Thesis

The brief reviews in the previous section illustrate that much effort has been focused on developing methods for detecting UV-induced damaged nucleic acids. However, almost all of the proposed methods consist of multi-step procedures, are limited to specific types of damage, require expensive instruments, and/or suffer from a high level of interference. The objective of this thesis is to develop novel, simple, inexpensive, mix-and-read assays for detecting UV-induced nucleic acid damage that will improve on current assays. Assays using hairpin probes have the advantage of hybridization specificity, sensitivity of fluorescence measurements and simplicity of the fast mix-and-read procedure.

Chapters 2 – 6 report the performance of some new hairpin probes designed specially to overcome the mentioned limitations of MBs in order to achieve an inexpensive, sensitive, and specific detection of UV-induced DNA damage. Chapter 2 and 3 introduce two types of backbone modifications of conventional DNA MBs. Locked nucleic acid MBs (LNA MBs), with different numbers of locked nucleotides, are used in Chapter 2 for the detection of UV-induced DNA damage. In Chapter 3, RNA bases are used in the DNA MB at regions complementary to the oligonucleotide target to form the chimeric RNA-DNA MBs (chMBs). In this chapter, the chMB is used to detect single base mismatches in addition to UV-induced DNA damage. These backbone modifications overcame some of the conventional MB limitations but they still obtain a signal that decreases with increasing UV-induced DNA damage. Therefore, in order to overcome this specific limitation, probes discussed in Chapters 4 – 6 were designed.

Chapter 4 describes the use of 2-aminopurine hairpin probes (2AP probe) for the detection of UV-induced DNA damage. 2AP is a fluorescent analogue of adenine which shows no fluorescence for undamaged DNA and fluorescence for

damaged DNA. In Chapter 5, an inexpensive hypochromism probe for UV-induced damage in nucleic acids is introduced. This probe is based upon the decrease in the UV absorbance of DNA associated with the better stacking of purine and pyrimidine residues in double-stranded oligonucleotides than in single-stranded ones. Finally, in Chapter 6 we describe the use of terbium (III) fluorescence in developing a sensitive, selective and inexpensive probe for UV-induced damage in nucleic acids with the aid of a hairpin probe. This research opens up a new route for inexpensive multiplex detection of specific DNA sequences. All the results of Chapters 2 – 6 are summarized and compared in Chapter 7, where future directions are also presented.

1.6. References

1) E. Chargaff, J. Cell. Physiol. 38 (1951) 41-59.
2) E. Chargaff, Experientia 6 (1950) 201–209.
3) J.D. Watson, F.H.C. Crick, Nature 171 (1953) 737-738.
4) K.C. Smith, In The Science of Photobiology, Plenum Press, New York, 1977.
5) D.E. Brash, J.A. Rudolph, J.A. Simon, A. Lin, G.J. McKenna, H.P. Baden, A.J. Halperin, J. Pontén, Proc. Natl. Acad. Sci. U.S.A. 88 (1991) 10124-10128.
6) L. Daya-Grosjean, N. Dumaz, A. Sarasin, J. Photochem. Photobiol. B: Biol. 28 (1995) 115-124.
7) WHO cancer mortality database: http://www-depdb.iarc.fr/who/menu.htm (last accessed on Feb. 6 2013).
8) B.P. Ruzsicska, D.G.E. Lemaire, In CRC Handbook of Organic Photochemistry and Photobiology, W.M. Horspool, P.-S. Song, Ed., CRC Press, New York, 1995, pp 1289.
9) J.E. Cleaver, K.H. Kraemer, Xeroderma pigmentosum, In The Metabolic Basis of Inherited Disease, Vol. II, 6th ed., C.R. Scriver, A.L. Beaudet, W.S. Sly, D. Valle, Eds., McGraw-Hill, New York, 1989, pp 2949.
10) J.E. Cleaver, D.L. Mitchell, Ultraviolet Radiation Carcinogenesis, In Cancer Medicine, 5th ed., J.F. Holland, E. III Frei, R.C.Jr. Bast, D.W. Kufe, D.L.

Morton, R.R. Weichselbaum, Eds.,Williams and Wilkins, Baltimore, 2000, pp 219.

11) J. Knowland, P.J. McHugh, R. Dunford, In Sunscreen Photobiology. Molecular, Cellular and Physiological Aspects, F. P. Gasparo, Ed., Springer, New York, 1997, pp 47.
12) B.S. Martincigh, J.M. Allen, S.K. Allen, In Sunscreen Photobiology. Molecular, Cellular and Physiological Aspects, F.P. Gasparo, Ed., Springer, New York, 1997, pp 11.
13) F. Urbach, Photochem. Photobiol. 50 (1989) 507-513.
14) J. Cadet, P. Vigny, The Photochemistry of Nucleic Acids, In Bioorganic Photochemistry, Vol. 1: Photochemistry and the Nucleic Acids, H. Morrison, Ed., John Wiley & Sons, New York, 1990, pp 1.
15) J.G. Peak, M.J. Peak, Mut. Res. 246 (1991) 187-191.
16) J. Cadet, L. Voituriez, F.E. Hruska, L.-S. Kan, F.A.A. de Leeuw, C. Altona, Can. J. Chem. 63 (1985) 2861-2868.
17) H.Y. You, P.E. Szabo, G.P. Pfeifer, Carcinogenesis 21 (2000) 2113–2117.
18) D.L. Mitchell, J.E. Vaughan, R.S. Nairn, Plasmid 21 (1989) 21–30.
19) M. Protic-Sabljic, K.H. Kraemer, Proc. Natl. Acad. Sci. U.S.A. 82 (1986) 6622–6626.
20) B.A. Donahue, S. Yin, J.S. Taylor, D. Reines, P.C. Hanawalt, Proc. Natl. Acad. Sci. U.S.A. 91 (1994) 8502–8506.
21) A.B. Britt, Plant Physiol. 108 (1995) 891–896.
22) A.B. Britt, Annu. Rev. Plant Physiol. Plant Mol. Biol. 47 (1996) 75–100.
23) T. Douki, J. Cadet, J. Photochem. Photobiol. B: Biol. 15 (1992) 199–213.
24) D.G.E. Lemaire, B.P. Ruzsicska, Biochemistry 32 (1993) 2525–2533.
25) W. Peng, B.R. Shaw, Biochemistry 35 (1996) 10172–10181.
26) A. Sancar, Biochemistry 33 (1994) 2–9.
27) J.-S. Taylor, J. Chem. Ed. 6 (1990) 835-841.
28) G.S. Hwang, J.-K. Kim, B.S. Choi, Eur. J. Biochem. 235 (1996) 359-365.
29) J.-K. Kim, B.S. Choi, Eur. J. Biochem. 228 (1995) 849-854.
30) J.-K. Kim, D. Patel, B.S. Choi, Photochem. Photobiol. 62 (1995) 44-50.

31) Y. Fujiwara, S. Iwai, Biochemistry 36 (1997) 1544-1550.
32) Y.Q. Jing, J.F.L. Kao, J.-S. Taylor, Nucl. Acids Res. 26 (1998) 3845-3853.
33) J.-S. Taylor, M.P. Cohrs, J. Am. Chem. Soc. 109 (1987) 2834–2835.
34) J.-S. Taylor, D.S. Garett, M.P. Cohrs, Biochemistry 27 (1988) 7206-7215.
35) L.-S. Kan, L. Voituriez, J. Cadet, J. Photochem. Photobiol. B: Biol. 12, (1992) 339-357.
36) J.H. Lee, S.H. Bae, B.S. Choi, Proc. Natl. Acad. Sci. U.S.A. 97 (2000) 4591-4596.
37) J. Cadet, E. Sage, T. Douki, Mut. Res. 571 (2005) 3-17.
38) T. Douki, J. Cadet, Biochemistry 40 (2001) 2495–2501.
39) T. Douki, M. Court, S. Sauvaigo, F. Odin, J. Cadet, J. Biol. Chem. 275 (2000) 11678–11685.
40) Y. Barak, O. Cohen-fix, Z. Livneh, J. Biol. Chem. 270 (1995) 24174–24179
41) D.A. Kreutzer, J.M. Essigmann, Proc. Natl. Acad. Sci. U.S.A. 95 (1998), 3578–3582.
42) D.E. Brash, J.A. Rudolph, J.A. Simon, A. Lin, G.J. McKenna, H.P. Baden, A.J. Halperin, J. Ponten, Proc. Natl. Acad. Sci. U.S.A. 88 (1991) 10124-10128.
43) A. Ziegler, D.J. Leffell, S. Kunala, H.W. Sharma, M. Gailani, J.A. Siomon, A.J. Halperin, H.P. Baden, P.E. Shapiro, A.E. Bale, D.E. Brash, Proc. Natl. Acad. Sci. U.S.A. 90 (1993) 4216-4220.
44) S. Kumar, N.D. Sharma, R.J.H. Davies, D.W. Phillipson, J.A. McCloskey Nucl. Acids Res. 15 (1987) 1199–1216.
45) P.H. Clingen, R.J.H. Davies, J. Photochem. Photobiol. B. 38 (1997) 81-87.
46) S. Kumar, P.C. Joshi, N.D. Sharma, S.N. Bose, R.J.H. Davies, N. Takedal, J.A. McCloskey, Nucl. Acids Res. 19 (1991) 2841-2847.
47) T.M.G. Koning, R.J.H. Davies, R. Kaptein, Nucl. Acids Res. 18 (1990) 277–284.
48) X. Zhao, J.-S. Taylor, Nucl. Acids Res. 24 (1996) 1554–1560.
49) N.D. Sharma, R.J.H. Davies, J. Photochem. Photobiol. B: Biol. 3 (1989) 247–258.

50) G.M. Bowden, R.J.H. Davies, Photochem. Photobiol. 66 (1997) 413–417.
51) X. Zhao, J.-S. Taylor, Nucl. Acids Res. 24 (1996) 1561–1565.
52) H. Wei, Q. Cai, M. Lebwohl, Carcinogenesis 19 (1998) 1013–1018.
53) M.S. Stewart, G.S. Cameron, B.C. Pence, J. Invest. Dermatol. 106 (1996) 1086–1089.
54) E. Pelle, X. Huang, T. Mammone, K. Marenus, D. Maes, K. Frenkel, J. Invest. Dermatol. 121 (2003) 177–183.
55) T. Douki, D. Perdiz, P. Grof, Z. Kuluncsics, E. Moustacchi, J. Cadet, E. Sage, Photochem. Photobiol. 70 (1999) 184–190.
56) S.M. Bishop, M. Malone, D. Phillips, A.W. Parker, M.C.R. Symons, J. Chem. Soc. Chem. Commun. 7 (1994) 871–872.
57) T. Mohammad, H. Morrison, J. Am. Chem. Soc. 118 (1996) 1221–1222.
58) H.J. Niggli, P.A. Cerutti, Biochemistry 22 (1983) 1390–1395.
59) J. Cadet, N.E. Gentner, B. Rozga, M.C. Paterson, J. Chromatogr. 280 (1983) 99–108.
60) J. Cadet, M. Berger, Int. J. Rad. Biol. 47 (1985) 127–143.
61) J. Cadet, C. Anselmino, T. Douki, L. Voituriez, J. Photochem. Photobiol. B.: Bio1. 15 (1992) 277-298.
62) T. Douki, L. Voituriez, J. Cadet, Chem. Res. Toxicol. 8 (1995) 244–253.
63) K. Randerath, M.V. Reddy, R.C. Gupta, Proc. Natl. Acad. Sci. U.S.A. 78 (1981) 6126-6129.
64) J. Cadet, M. Weinfeld, Anal. Chem. 65 (1993) 675-682.
65) M. Liuzzi, M. Weinfeld, M.C. Paterson, J. Biol. Chem. 264 (1989) 6355–6363.
66) M. Weinfeld, M. Liuzzi, M.C. Paterson, J. Biol. Chem. 264 (1989) 6364-6370.
67) M. Weinfeld, K- J.M. Soderlind, Biochemistry 30 (1991) 1091-1097.
68) J-F. Mouret, F. Odin, M. Polverelli, J. Cadet, Chem. Res. Toxicol. 3 (1990) 102- 110.
69) T. A. Winters, M. Weinfeld, T.J. Jorgensen, Nucl. Acids Res. 20 (1992) 2573-2580.

70) T. Douki, T. Zalizniak, J. Cadet, Photochem. Photobiol. 66 (1997) 171–179.
71) T. Douki, M. Court, J. Cadet, J. Photochem. Photobiol. B: Biol. 54 (2000) 145–154.
72) R.S. Ramsey, C-H. Ho, Anal. Biochem. 182 (1989) 424-431.
73) I.D. Podmore, M.S. Cooke, K.E. Herbert, J. Lunec, Photochem. Photobiol. 64 (1996) 310-315.
74) J.R. Wagner, C-C. Hu, B.N. Ames, Proc. Natl. Acad. Sci. U.S.A. 89 (1992) 3380-3384.
75) M. Berger, M. de Hazen, A. Nejjari, J. Fournier, J. Gulgnard, H. Pezerat, J. Cadet, Carcinogenesis 14 (1993) 41-46.
76) E. Paleček, F. Jelen, Crit. Rev. Anal. Chem. 3 (2002) 261–270.
77) E. Paleček, M. Fojta, M. Tomschick, J. Wang, Biosens. Bioelectron. 13 (1998) 621–628.
78) M.A. Rahman, N-.H. Kwon, M-.S. Won, E.S. Choe, Y-.B. Shim, Anal. Chem. 77 (2005) 4854–4860.
79) F. Darain, C. Ban, Y-.B. Shim, Biosens. Bioelectron. 20 (2004) 857–863.
80) K. Cahová-Kuchaříková, M. Fojta, T. Mozga, E. Paleček, Anal. Chem. 77 (2005) 2920-2927.
81) T-.Y. Lee, Y-.B. Shim, Anal. Chem. 73 (2001) 5629–5632.
82) M. Fojta, Electroanalysis 14 (2002) 1449-1463.
83) M. Fojta, Collect. Czech. Chem. Commun. 69 (2004) 715-747.
84) E. Paleček, M. Fojta, F. Jelen, V. Vetterl, Electrochemical Analysis of Nucleic Acids. In A.J. Bard, M. Stratsmann, Eds., The Encyclopedia of Electrochemistry, Vol. 9, Bio-electrochemistry, Weinheim, Wiley-VCH, 2002, pp 365.
85) J. Langmaier, Z. Samec, E. Samcova, Electroanalysis 15 (2003) 1555-1560.
86) A.M.O. Brett, J.A.P. Piedade, S.H.P. Serrano, Electroanalysis 12 (2000) 969-973.
87) M. Fafandel, N. Bihari, V. Krajcar, W. Muller, R.K. Zahnc, R. Batel, Sci. Total Environ. 277 (2001) 149-159.

88) V.A. Bespalov, A. Conconi, X. Zhang, D. Fahy, M.J. Smerdon, Environ. Mol. Mutagen. 38 (2001) 166–174.

89) S.E. Freeman, A.D. Blackett, D.C. Monteleone, R.B. Setlow, B.M. Sutherland, J. C. Sutherland, Anal. Biochem. 158 (1986) 119-129.

90) S. Kumari, R.P. Rastogi, K.L. Singh, S.P. Singh, R.P. Sinha, EXCLI Journal 7 (2008) 44-62.

91) S. Tornaletti, D. Rozek, G.P. Pfeifer, Oncogene 8 (1993), 2051–2057.

92) S. Tommasi, M.F. Denissenko, G.P. Pfeifer, Cancer Res. 57 (1997), 4727–4730.

93) R. Drouin, H. Rodriguez, G.P. Holmquist, S.A. Akman, Technologies for DNA Damage and Mutations, G.P. Pfeifer, Ed., Plenum Press, New York 1996, pp 37.

94) Y.H. You, P.E. Szabo, G.P. Pfeifer, Carcinogenesis 21 (2000) 2113–2117.

95) J. Komura, A.D. Riggs, Nucl. Acids. Res. 26 (1998) 1807–1811.

96) P.J. Rochette, N. Bastien, T. Todo, R. Drouin, Photochem. Photobiol. 82 (2006) 1370-1376.

97) A. Karakoula, M.D. Evans, I.D. Podmore, P.E. Hutchinson, J. Lunec, M.S. Cooke, J. Immunol. Meth. 277 (2003) 27–37.

98) G. Wang, L.M. Hallberg, E. Saphier, E.W. Englander. Mut. Res. 433 (1999) 147-157.

99) L. Levine, E.S. Seeman, E. Hammerschlag, H.V. Vunakis, Science 153 (1966) 1666-1667.

100) D.L. Mitchell, J.M. Clarkson, J. Photochem. Photobiol. 40 (1984) 743-748.

101) D.L. Mitchell, J.M. Clarkson, Biochim. Biophys. Acta. 655 (1981) 54–60.

102) T. Mori, M. Nakane, T. Hattori, T. Matsunaga, M. Ihara, O. Nikaido, Photochem. Photobiol. 54 (1991) 225–232.

103) T. Mizuno, T. Matsunaga, M. Ihara, O. Nikaido, Mut. Res. 254 (1991) 175–184.

104) T. Matsunaga, Y. Hatakeyama, M. Ohta, T. Mori, O. Nikaido, Photochem. Photobiol. 57 (1993) 934–940.

105) L. Roza, K.J.M. Van der Wulp, S.J. MacFarlane, P.H.M. Lohman, R.A. Baan Photochem. Photobiol. 48 (1988) 627–634.

106) T. Mori, T. Matsunaga, C-C. Chang, J.E. Trosko, O. Nikaido, Mut. Res. 236 (1990) 99-105.

107) W.H. Jeffrey, P. Aas, M.M. Lyons, R.B. Coffin, R.J. Pledger, D.L. Mitchell, Photochem. Photobiol. 64 (1996) 419-427.

108) R.V. Miller, W. Jeffrey, D. Mitchell, M. Elasri, ASM News 65 (1999) 535-541.

109) D.L. Mitchell, Radioimmunoassay of DNA Damaged by Ultraviolet Light. In Technologies for DNA Damage and Mutations, G.P. Pfeifer, Ed., Plenum Press, New York, 1996, pp 73.

110) D.L. Mitchell, B.S. Rosenstein, Photochem. Photobiol. 45 (1987) 781-786.

111) J. Peccia, M. Hernandez, Appl. Environ. Microbiol. 68 (2002) 2542-2549.

112) A.G. Kriste, B.S. Martinugh, L.F. Salter, J. Photochem. Photobiol. A. 93 (1996) 185-192.

113) A.A. Wani, S.M. D'Ambrosio, N.K. Alvi, Photochem. Photobiol. 46 (1987) 477-482.

114) S. Plaza, A. Boullard, D. Pele, J.J. Cornelis, J. Rommerlaere, P.U. Giacomoni, J. Photochem. Photobiol. 53 (1991) 217-227.

115) S.P. Wallace, B.R. Erlanger, S.M. Beiser, Biochemistry 10 (1971) 679-683.

116) D. Perdiz, P. Gróf, M. Mezzina, O. Nikaido, E. Moustacchi, E. Sage, J. Biol. Chem. 275 (2000) 26732-26742.

117) D.W. Fairbairn, P.L. Olive, K.L. O'Neill, Mut. Res. 339 (1995) 37–59.

118) R.R. Tice, E. Agurell, D. Anderson, B. Burlinson, A. Hartmann, H. Kobayashi, Y. Miyamae, E. Rojas, J.C. Ryu, Y.F. Sasaki, Environ. Mol. Mutagen. 35 (2000) 206–221.

119) M. Lemay, K.A. Wood, Biotechniques 27 (1999) 846–851.

120) L. Marrot, J.P. Belaidi, J.R. Meunier, P. Perez, C. Agapakis-Causse, Photochem. Photobiol. 69 (1999) 686–693.

121) D.B. Yarosh, S. Boumakis, A.B. Brown, M.T. Canning, J.W. Galvin, D.M. Both, E. Kraus, A. O'Connor, D.A. Brown, Methods 28 (2002) 55–62.

122) S. Sauvaigo, C. Serres, N. Signorini, N. Emonet, M.J. Richard, J. Cadet, Anal. Biochem. 259 (1998) 1–7.
123) S. Shaposhnikov, P.D. Thomsen, A.R. Collins, Methods Mol. Biol. 682 (2011) 115-132.
124) S. Shaposhnikov, E. Frengen, A.R. Collins, Mutagenesis 24 (2009) 383-389.
125) S. Yarasi, C. McConachie, G. R. Loppnow, Photochem. Photobiol. 8 (2005) 467-473.
126) S. A. Oladepo, G. R. Loppnow, Anal. Bioanal. Chem. 397 (2010) 2949-2957.
127) A. Rich, I. Tinoco, J. Am. Chem. Soc. 82 (1960) 6409-6411.
128) I. Tinoco, J. Am. Chem. Soc. 82 (1960) 4785-4790.
129) D.A. Skoog, F.J. Holler, S.R. Crouch, In Principles of Instrumental Analysis, Thomson Brooks/Cole, CA, 6th Ed, 2007, pp 1039.
130) J.R. Lakowicz, In Principles of Fluorescence Spectroscopy, Vol. 3, 2006, pp 954.
131) X.C. Le, J.Z. Xing, J. Lee, S.A. Leadon, M. Weinfeld, Science 280 (1998) 1066-1069.
132) X.C. Le, V. Pavski, H. Wang, Can. J. Chem. 83 (2005) 185-194.
133) A. Goulko, PhD thesis, Department of Chemistry, University of Alberta (2011).
134) D.L. Sokol, X. Zhang, P. Lu, A.M. Gewirtz, Proc. Natl. Acad. Sci. U.S.A. 95 (1998) 11538-11543.
135) G. Bonnet, S. Tyagi, A. Libchaber, F.R. Kramer, Proc. Natl. Acad. Sci. U.S.A. 96 (1999) 6171-6176.
136) G. Leone, H. Van-Schijndel, B. Van-Gemen, F.R. Kramer, S.D. Schoen, Nucl. Acids Res. 26 (1998) 2150-2155.
137) S. Tyagi, F.R. Kramer, Nature Biotechnol. 14 (1996) 303-308.
138) K. Stohr, B. Hafner, O. Nolte, J. Wolfrum, M. Sauer, D.-P Herten, Anal. Chem. 77 (2005) 7195-7203.
139) J.P. Knemeyer, N. Marme, M. Sauer, Anal. Chem. 72 (2000) 3717-3724.
140) A. Misra, P. Kumar, K.C. Gupta, Anal. Biochem. 364 (2007) 86-88.

141) T. Heinlein, J.-P. Knemeyer, O. Piestert, M. Sauer, J. Phys. Chem. B. 107 (2003) 7957-7964.
142) Y. Kim, C.J. Yang, W. Tan, Nucl. Acids Res. 35 (2007) 7279-7287.
143) A. Misra, M. Shahid, Bioorg. Med. Chem. 17 (2009) 5826-5833.
144) L. Wang, C.J. Yang, C.D. Medley, S.A. Benner, W. Tan, J. Am. Chem. Soc. 127 (2005) 15664-15665.
145) C.J. Yang, L. Wang, Y. Wu, Y. Kim, C.D. Medley, H. Lin, W. Tan, Nucl. Acids Res. 35 (2007) 4030-4041.
146) Y. Wu, C.J. Yang, L.L. Moroz, W. Tan, Anal. Chem. 80 (2008) 3025-3028.
147) K. Martinez, M.-C. Estevez, Y. Wu, J.A. Phillips, C.D. Medley, W. Tan, Anal. Chem. 81 (2009) 3448-3454.
148) L. Morandi, D. Ferrari, C. Lombardo, A. Pession, G. Tallini, J. Virol. Methods 140 (2007) 148-154.
149) T. Shimayama, F. Nishikawa, S. Nishikawa, K. Taira, Nucl. Acids Res. 21 (1993) 2605–2611.
150) M.C. Rice, K. Czymmek, E.B. Kmiec, Nat. Biotechnol. 19 (2001) 321–326.
151) H.B. Gamper, H. Parekh, M.C. Rice, M. Bruner, H. Youkey, E.B. Kmiec, Nucl. Acids. Res. 28 (2000) 4332–4339.
152) V.W. Coljee, H.L. Murray, W.F. Donahue, K.A. Jarrell, Nat. Biotechnol. 18 (2000) 789–791.
153) J. Rizzo, L.K. Gifford, X. Zhang, A.M. Gewirtz, P. Lu, Mol. Cell. Probes 16 (2002) 277–283.
154) S.M. Elbashir, J. Harborth, W. Lendeckel, A. Yalcin, K. Weber, T. Tuschl, Nature 411 (2001) 494–498.
155) S. Nakano, T. Kanzaki, N. Sugimoto, J. Am. Chem. Soc. 126 (2004) 1088–1095.
156) U. Subuddhi, M. Hogg, L.J. Reha-Krantz, Biochemistry 47 (2008) 6130–6137.
157) D. Tleugabulova, L.J. Reha-Krantz, Biochemistry 46 (2007) 6559 –6569.
158) M.A. O'Neill, J.K. Barton, J. Am. Chem. Soc. 124 (2002) 13053–13066.
159) D.C. Ward, E. Reich, L. Stryer, J. Biol. Chem. 244 (1969) 1228–1237.

160) E.L. Rachofsky, R. Osman, J.B.A. Ros, Biochemistry 40 (2001) 946–956.
161) L.B. Bloom, M.R. Otto, R. Eritja, L.J. Reha-Krantz, M.F. Goodman, J.M. Beechem, Biochemistry 33 (1994) 7576–7685.
162) L.B. Bloom, M.R. Otto, J.M. Beechem, M.F. Goodman, Biochemistry 32 (1993) 11247–11258.
163) L.C. Sowers, G.V. Fazakerley, R. Eritja, B.E. Kaplan, M.F. Goodman, Proc. Natl. Acad. Sci. U.S.A. 83 (1986) 5434–5438.
164) N. Sabbatini, M. Guardigli, J. Lehn, Coord. Chem. Rev. 123 (1993) 201-228.
165) S. Rigault, C. Piguet, G. Bernardinelli, G. Hopfgartner, Angew. Chem. 37 (1998) 169-172.
166) N. Martin, J. Bunzli, V. McKee, C. Piguet, G. Hopfgartner, Inorg. Chem. 37 (1998) 577-589.
167) M. Li, P.R. Selvin, Bioconjug. Chem. 8 (1997) 127-132.
168) S. Ghosh, A. Misra, A. Ozarowski, A. Maki, J. Phys. Chem. B. 107 (2003) 11520-11526.
169) M.J. Belousoff, P. Ung, C.M. Forsyth, Y. Tor, L. Spiccia, B. Graham, J. Am. Chem. Soc. 131 (2009) 1106-1114.
170) M. Lambert, J. Hoerter, M. Pereira, N. Walter, RNA 11 (2005) 1688-1700.

Chapter 2

Locked-Nucleic Acid Hairpin Detection of UV-induced DNA Damage*

2.1. Introduction

Absorption of light by DNA produces molecular-scale lesions in the DNA and RNA, which can subsequently lead to cancer and other diseases[1-4]. Absorption of UVB (290-320 nm) and UVC (200-290 nm) light leads to the formation of thymidine cyclobutyl photodimers (CPD) as the primary photoproduct[5]. Other photoproducts with UV irradiation are pyrimidine pyrimidinone [6-4]-photoproducts, dewar pyrimidinones, and uracil and thymine photohydrates. All these photoproducts are localized on the pyrimidine nucleobases near the C_5=C_6 double bond, opposite to the site of base pairing. Other damage agents, such as oxidative conditions and ionizing radiation, lead to other DNA lesions, such as single- and double-strand breaks, 8-oxoguanosine and other oxidation products, and cross-links.

A number of techniques have been used to detect nucleic acid damage previously, either *in vivo* or *in vitro*. Most of these techniques isolate the DNA, melt it to obtain single-stranded DNA fragments, separate the fragments and detect the lesions.[6-9] Such techniques include gel electrophoresis,[6] capillary electrophoresis,[7] electrochemistry,[7] HPLC,[8] and mass spectrometry.[9] While useful, these techniques are destructive and time-consuming. In addition, the electrophoretic and chromatographic techniques require pre-filtering, which may itself introduce lesions.

Other spectroscopic-based techniques have recently been used to characterize nucleic acid damage. Differences in the fluorescence lifetime of a dye intercalated in undamaged and damaged DNA have been used to detect DNA damage.[10] Fluorescently-labeled antibodies provide an exquisitely selective probe of particular damage photoproducts, such as thymine cyclobutyl photodimers.[11]

*A version of this chapter has been published: A. El-Yazbi, G.R. Loppnow, Can. J. Chem. 89 (2011) 402-408.

Most recently, molecular beacons (MBs) have been used as a broad-spectrum sensor of DNA and RNA damage[12] (A. Mah, S. Yarasi, and G. R. Loppnow, manuscript in preparation). MBs are DNA hairpins labeled with a quencher on one end and a fluorophore on the other. In the hairpin form, the quencher and fluorophore are in close proximity and the fluorescence is quenched. However, in the presence of target DNA or RNA which is complementary to the loop of the molecular beacon, the fluorophore and quencher are separated and the fluorescence is detectable. The inherent sensitivity of fluorescence makes the MBs sensitive probes of nucleic acid damage.

Fluorescently-labeled locked nucleic acid (LNA) hairpins have the potential to detect UV-induced DNA damage. Locked nucleic acids are nucleic acids containing ribonucleosides in which a methylene group connects the $C_{4'}$ and $O_{2'}$ atoms of the ribose sugar, locking it into the 3' endo (North) conformation[13]. This structure allows LNA hairpins to have several advantages such as decreased susceptibility to nuclease digestion and resistance to non-specific protein binding. In addition, the structural resemblance to native nucleic acids imparts LNA hairpins good solubility in physiological conditions and ease of handling. Also, LNA hairpin synthesis is easily automated by conventional phosphoramidite chemistry. Such probes appear to be more selective towards base pair mismatches[13] and have been used to enhance the specificity of probes for fluorescence in-situ hybridization (FISH) assays, DNA microarrays, and real-time polymerase chain reaction (PCR).[14-17] In this chapter, we show that fluorescently-labeled LNA hairpins can indeed detect UV-induced DNA damage, albeit with lower selectivity for damaged DNA than conventional MBs. The results show that the sensitivity of LNA MBs depends on ionic strength, target concentration and the LNA composition of the hairpin. These results are discussed in the context of the conformation dynamics of LNA hairpins.

2.2. Experimental

2.2.1. Materials.

The single-strand oligonucleotide targets and the MBs were obtained from Integrated DNA Technologies Inc. (Coralville, IA, USA) and are listed in Table 2.1. The target oligonucleotides were purified by standard desalting, while the MBs were purified by HPLC. The magnesium chloride ($MgCl_2$) and sodium chloride (NaCl) were both obtained from EMD Chemicals Inc. (Gibbstown, NJ, USA). Tris and ethylenediaminetetraacetic acid (EDTA) were obtained from ICN Biomedicals, (Aurora, OH, USA), and BDH Inc. (Toronto, ON, Canada), respectively. All chemicals were used as received. Nanopure water from a Barnsted Nanopure (Boston, MA, USA) system was used for all solutions. The oligonucleotide samples and MBs were each dissolved in 1 mM EDTA in nanopure water and kept frozen at -20^{o}C until needed.

2.2.2. UV irradiation.

Nitrogen-purged solutions of 4 μM dT_{24} in one of two buffers, either 10 mM Tris, 1 mM EDTA and 3 mM $MgCl_2$ adjusted to pH 7.5 or 20 mM Tris, 1 mM EDTA, 5 mM $MgCl_2$ and 50 mM NaCl adjusted to pH 7.5, were irradiated in sealed, UV-transparent, 1-cm pathlength cuvettes. The cuvettes were placed in a water bath contained also in a UV-transparent water dish. The temperature, which was monitored by means of a Cole-Parmer DiGi-SENSE thermocouple (Niles, IL, USA), was kept constant throughout the irradiation by the water bath. Oligonucleotide samples were irradiated in a Luzchem (Ottawa, ON, Canada) DEV photoreactor chamber with UVC light from lamps emitting principally at 254 nm. The samples were constantly stirred during irradiation and the photoreactor was purged with nitrogen throughout the irradiation to flush out oxygen and any ozone subsequently generated from the UVC lamps. Control samples were handled identically, but were not exposed to UV radiation. The UVC lamps were turned on about 20 minutes before the start of irradiation to stabilize the lamp output.

2.2.3. Absorption and fluorescence measurements.

Absorption spectra were recorded at intervals throughout the irradiation period on a Hewlett-Packard (Sunnyvale, CA USA) 8452A diode array spectrophotometer

by placing the irradiated cuvettes containing the target oligonucleotide solutions directly into the spectrophotometer. For the room-temperature fluorescence measurements, a 20-μL aliquot of each irradiated solution was taken at various time intervals and was later mixed with appropriate amounts of the probe and buffer solution to give final concentrations of 200 nM oligonucleotide and 200 nM probe for the 1 MB : 1 target experiments and final concentrations of 1 μM oligonucleotide target and 200 nM probe for the 1 MB : 5 target experiments. These solutions were then incubated in the dark at room temperature for about 24 hours. Room-temperature fluorescence spectra of 200 μL aliquots of the incubated hybridization mixtures were measured using a Photon Technologies International (Birmingham, NJ, USA) fluorescence system. The spectra were recorded between 500 and 700 nm with excitation at 495 nm. A 10-mm pathlength, Suprasil quartz fluorescence cuvette was used for these measurements.

2.3. Results and Discussion

The design and optimization of MB probes of nucleic acid damage have been described in detail previously.[12] We use the same principles here for designing and optimizing the LNA MBs to ensure that these probes can selectively discriminate single damage sites in oligonucleotides. A representative melting curve of one of the MBs, both alone and in the presence of undamaged target, is shown in Figure 2.1. In the absence of target DNA or RNA, the MB stem is closed and exhibits minimal fluorescence. In the presence of undamaged oligonucleotide, the MB opens and forms a stable target-loop hybrid with maximum fluorescence. Subsequently, the binding should be sufficiently destabilized upon the occurrence of a single damage site such that the hairpin configuration has a much lower melting temperature (i.e. free energy) than the hybridized probe. This condition results in lower fluorescence from the damaged target-loop hybrid and, consequently, a maximum discrimination of damaged ***versus*** undamaged oligonucleotide.

The melting curves (Figure 2.1) show that the MB stem melts at a slightly higher temperature than that of the target-loop hybrid, which is an important

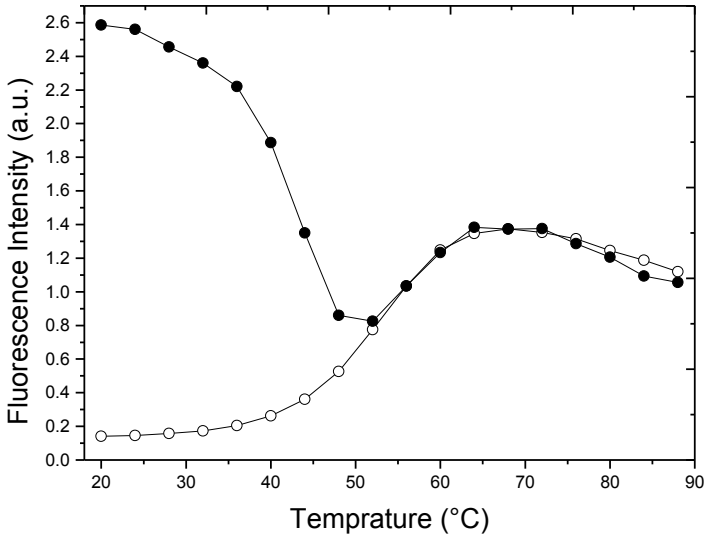

Figure 2.1. Melting curve of 200 nM MB_{26}-5 alone (open circles) and in the presence of 200 nM target dT_{17} (filled circles) in 20 mM Tris buffer containing 1 mM EDTA, 5 mM $MgCl_2$ and 50 mM NaCl. Both curves were generated at a rate of 1.0 ºC/min. This is a representative of the other melting curves of MBs alone and with targets, which showed a similar shape.

Table 2.1. Sequences of the oligonucleotides

Name[a]	Nucleotide Sequence[b]	Melting temperature (°C)			
		MB stem	MB-dT_{24} hybrid	MB-dT_{17} hybrid	MB-rU_{17} hybrid
MB_{33}- 4	5'-(6-FAM)-CCCAAAAAAAAAAAAAA(+A)A(+A)AAA(+A)AA(+A)TTTGGG-(3-DAB)-3'	40.4	38.0	-	-
MB_{33}-0	5'-(6-FAM)-CCCAAAAAAAAAAAAAAAAAAAAAAAAAATTTGGG-(3-DAB)-3'	40.2	36.0	-	-
MB_{26}-4	5'-(6-FAM)-CACAAA AAA A(+A)A (+A)AA A(+A)A A(+A)TTTGTG-(3-BHQ_1)-3'	51.0	-	37.6	32.5
MB_{26}-5	5'-(6-FAM)-CACAAAA(+A)AA(+A)AA(+A)AA(+A)AA(+A)TTTGTG-(3-BHQ_1)-3'	51.8	-	41.8	33.0
MB_{26}-6	5'-(6-FAM)-TCCAAAA(+A)A(+A)A(+A)A(+A)A(+A)A(+A) AATTTGGA-(3-BHQ_1)-3'	54.2	-	43.0	33.9

[a] The subscript represents the total number of bases comprising the oligonucleotide sample and the number at the end represents the number of LNAs in the structure.
[b] '+' denotes the locked nucleotide, 6-FAM is 6-carboxyfluorescein, 3-DAB is 4-(4'-dimethylaminophenylazo)-benzoic acid) and 3-BHQ_1 is the black hole quencher-1.[19] The underlined bases represent the stem of the MB.

criterion for the optimal performance of the MB in the detection of damage.[12] To ensure this criterion is met, we performed thermal denaturation profiles of MBs in equilibrium with their targets and obtained the melting curves for the MBs alone and with the targets. The results are shown in Table 2.1. In all cases, the difference in T_m between the hairpin and hybrid forms of the LNA MBs is similar to the difference in the Tm between the same forms of the non- LNA MB. This result suggests that both probes may have similar selectivity to oligonucleotide damage.[12]

Target dT_{17} and rU_{17} were chosen for this study because of their well known photochemistry. CPDs are the primary form of UV-induced damage in dT_{l7}, in addition to, the formation of small amounts of the pyrimidine-pyrimidinone [6-4] photoproduct.[5,18] In rU_{17} approximately equal amounts of the CPD and photohydrates are formed.[5,18] The quantum yields (Φ) for such processes are Φ = 0.044 for CPD formation in poly-dT, and Φ = 0.012 and Φ = 0.015 for photohydrate and CPD formation, respectively, in poly-rU.[18] Therefore, comparing the MB hybridization with UV-damaged rU_{17} and dT_{17} will allow for a determination of the relative destabilizing effect of CPD and photohydrates on duplex formation. In addition, poly-dT and poly-rU targets exclude complications due to other processes, such as spontaneous depurination due to thermal effects, UV-induced depurination of guanosine residues and UV induced oxidative damage for guanine bases.

The fluorescence of the LNA MBs with targets dT_{17} and rU_{17} which have been irradiated with UVC are shown in Figure 2.2 as a function of irradiation time. As damage accumulates on the target oligonucleotide strand, the MB-target hybrid becomes less stable at the temperature used in the assay, effectively decreasing the fluorescence intensity until the closed, hairpin form is the more stable form of the MB. In Figures 2.2 to 2.5, such a decrease with fluorescence is observed as the irradiation time increases. This result indicates that the MB-target hybrid is becoming less stable than the closed hairpin form of the MB as the irradiation time increases with consequently greater amount of damage to the target

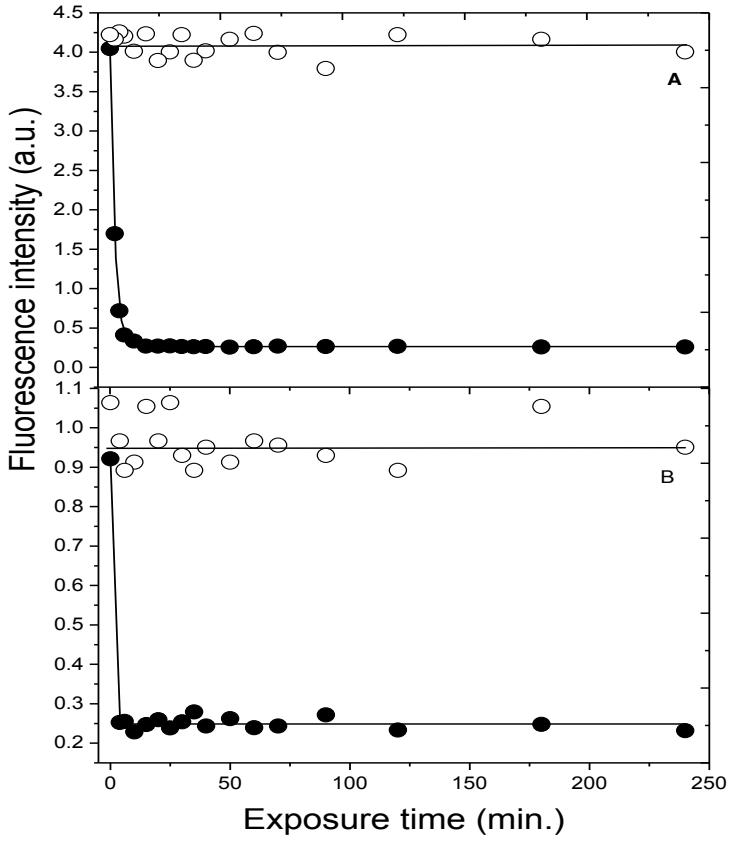

Figure 2.2. Fluorescence intensity at 520 nm as a function of irradiation time for the targets. Only the 200 nM (A) dT_{17} and (B) rU_{17} targets were irradiated (filled circles) and the damage was detected by MB_{26}-5. Aliquots of the irradiated target were mixed with 200 nM MB in buffer containing 200 mM Tris, 5 mM $MgCl_2$, 50 mM NaCl and 1 mM EDTA at pH 7.5 and the fluorescence of this mixture was then measured. The control (open circles) is the unirradiated target sequences hybridized with the MB_{26}-5 in the same buffer. The black, solid line through the irradiated sample points is a single exponential fit to the fluorescence intensity of the irradiated sample with (A) $I_0 = 0.3$, $A = 3.8$ and $\tau = 1.98$ min and (B) $I_0 = 0.2$, $A = 6.7$ and $\tau = 0.79$ min. The straight line through the control sample points is a linear fit drawn by eye.

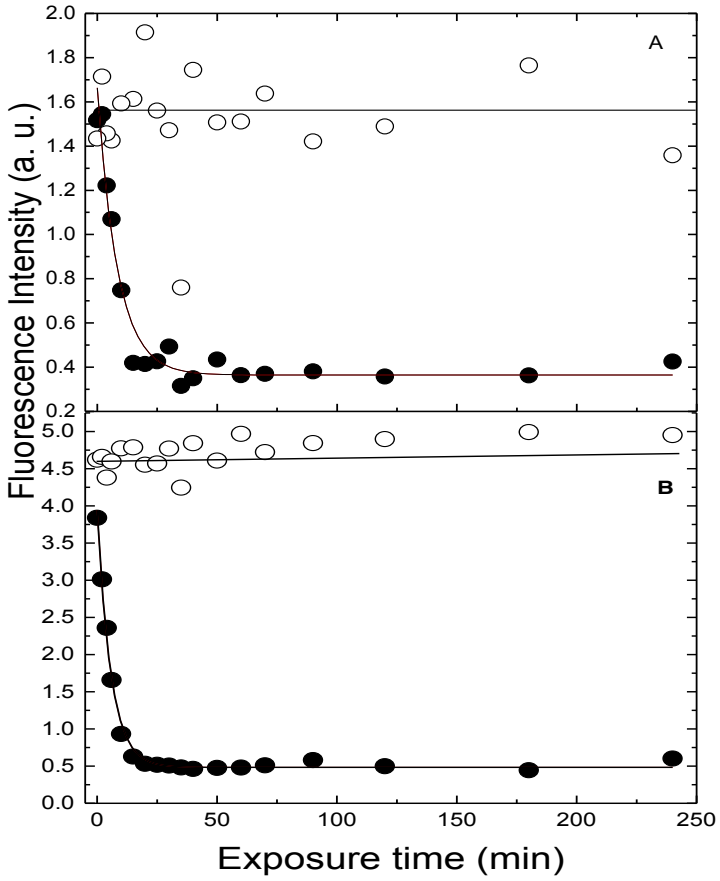

Figure 2.3. Fluorescence intensity at 520 nm as a function of irradiation time for dT_{24} (filled circles). Only the 1 μM dT_{24} target was irradiated and the damage was detected by MB_{33}-4. Aliquots of the irradiated target were mixed with 200 nM MB in buffer containing (A) 10 mM Tris, 3 mM $MgCl_2$ and 1 mM EDTA at pH 7.5 and (B) 20 mM Tris, 50 mM NaCl, 5 mM $MgCl_2$ and 1 mM EDTA at pH 7.5. The fluorescence of this mixture was then measured. The control (open circles) is the unirradiated dT_{24} target sequence hybridized with MB_{33}-4 in the same buffer. The black, solid line through the irradiated sample points is a single exponential fit to the fluorescence intensity of the irradiated sample with (A) $I_0 = 0.4$, $A = 1.3$ and $\tau = 8.4$ min and (B) $I_0 = 0.5$, $A = 3.5$ and $\tau = 5.6$ min. The straight line through the control sample points is a linear fit drawn by eye.

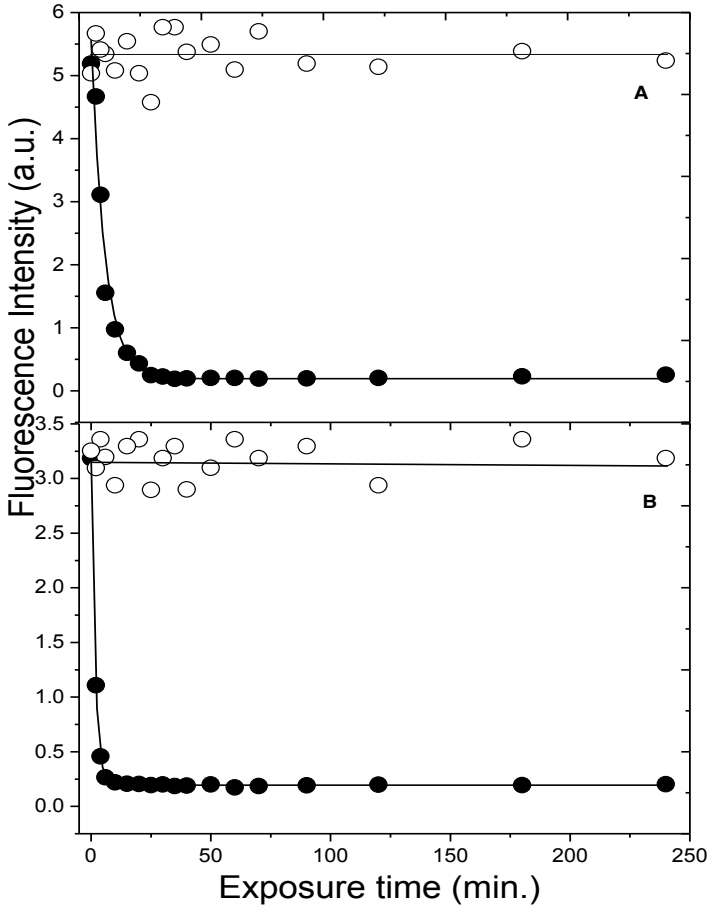

Figure 2.4. Fluorescence intensity at 520 nm as a function of irradiation time for dT_{17} (filled circles). Only (A) 1 μM dT_{17} target and (B) 200 nM dT_{17} target were irradiated and the damage was detected by MB_{26}-4. Aliquots of the irradiated target were mixed with 200 nM MB in buffer containing 20 mM Tris, 5 mM $MgCl_2$, 50 mM NaCl and 1 mM EDTA at pH 7.5 and the fluorescence of this mixture was then measured. The control (open circles) is the unirradiated dT_{17} target sequence hybridized with MB_{26}-4 in the same buffer. The black, solid line through the irradiated sample points is a single exponential fit to the fluorescence intensity of the irradiated sample with (A) $I_0 = 0.2$, $A = 5.4$ and $\tau = 5.79$ min and (B) $I_0 = 0.2$, $A = 2.9$ and $\tau = 1.67$ min. The straight line through the control sample points is a linear fit drawn by eye.

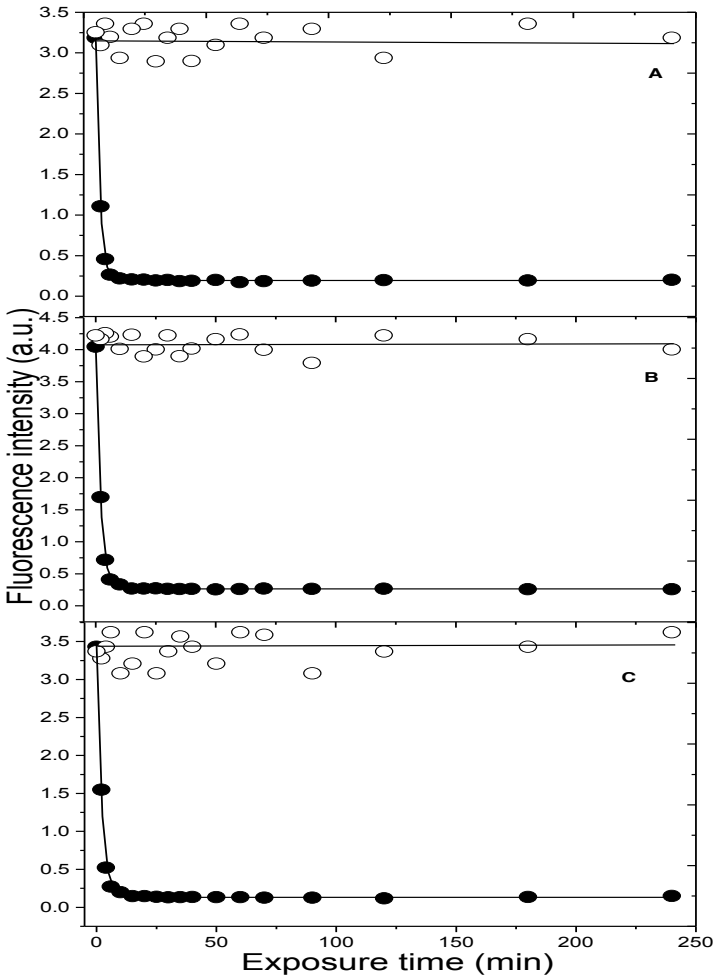

Figure 2.5. Fluorescence intensity at 520 nm as a function of irradiation time for dT_{17}. Only the 200 nM dT_{17} target was irradiated (filled circles) and the damage was detected by (A) MB_{26}-4, (B) MB_{26}-5 and (C) MB_{26}-6. Aliquots of the irradiated target were mixed with 200 nM MB in buffer containing 200 mM Tris, 5 mM $MgCl_2$, 50 mM NaCl and 1 mM EDTA at pH 7.5 and the fluorescence of this mixture was measured. The control (open circles) is the unirradiated dT_{17} target sequence hybridized with the MBs in the same buffer. The black, solid line through the irradiated sample points is a single exponential fit to the fluorescence intensity of the irradiated sample with (A) $I_0 = 0.2$, $A = 2.9$ and $\tau = 1.67$ min, (B) $I_0 = 0.3$, $A = 3.8$ and $\tau = 1.98$ min and (C) $I_0 = 0.1$, $A = 3.3$ and $\tau = 2.13$ min. The straight line through the control sample points is a linear fit drawn by eye.

oligonucleotide strand. This result demonstrates that LNA MBs can detect DNA and RNA damage.

The damage curves shown in Figures 2.2 to 2.5 have been fit with a single exponential function:

$$I = I_o + Ae^{-t/\tau} \qquad (1)$$

where I is the fluorescence intensity at time t, I_0 is the fluorescence intensity at time 0, A is the amplitude, and $e^{-t/\tau}$ is the exponential decay. This fit allows us to determine the rate of decrease of fluorescence intensity with irradiation time. This decay in the fluorescence intensity represents the instability of the damaged target-MB hybrid. Therefore, the faster the rate of fluorescence decays, the more selective the MB is to detect UV-induced oligonucleotide damage, under identical irradiation conditions for the same target. Because all of the target solutions were irradiated under the same conditions, with the same rate of oligonucleotide damage accumulation, the comparison of the rates of fluorescence intensity decrease provides a direct comparison of the selectivity of the different probes to oligonucleotide damage. We studied the effect of ionic strength, target:MB concentration ratios, and the LNA:DNA composition of the MB in order to determine the optimal conditions for the LNA MB to detect UV-damage with high selectivity.

2.3.1. Ionic strength of the medium. As shown previously,[12] MBs detect DNA damage at [Mg^{2+}] of 1 mM or higher. Tan, et al.,[13] have shown that higher ionic strength buffers than that used for MBs may improve the LNA MB detection of single base pair mismatches. Figure 2.3 shows the fluorescence intensity decrease for the LNA MB as a function of target UVC irradiation time at two different conditions, one of low ionic strength, having 1 mM [Mg^{2+}] and the other is of higher ionic strength, incorporating both Na^+ and Mg^{2+} counter ions. Table 2.2 presents the damage constants of the decrease in fluorescence intensity when fit to a single exponential function. Results show that higher ionic strength increases the selectivity of the LNA MB probe to DNA damage (i.e. shows a more rapid decrease in MB fluorescence with irradiation time). With the conditions used here, a 1.5 times higher selectivity to damage is observed than with the lower ionic

Table 2.2. Damage constants of the first-order exponential decay of different samples

Sample	Ratio MB : T	Ionic Strength[a]	Regression coefficient	Damage Constant (min)
MB_{33}-4 + dT_{24}	1 : 5	Low	0.959	8.42
MB_{33}-4 + dT_{24}	1 : 5	High	0.993	5.61
MB_{33}-0 + dT_{24}	1 : 1	Low	0.996	1.34
MB_{26}-4 + dT_{17}	1 : 5	High	0.977	5.79
MB_{26}-4 + dT_{17}	1 : 1	High	1.000	1.67
MB_{26}-5 + dT_{17}	1 : 1	High	0.999	1.98
MB_{26}-6 + dT_{17}	1 : 1	High	0.997	2.13
MB_{26}-4 + rU_{17}	1 : 1	High	0.983	$3x10^{-3}$
MB_{26}-5 + rU_{17}	1 : 1	High	0.993	0.79
MB_{26}-6 + rU_{17}	1 : 1	High	0.997	1.54

[a]Low Ionic Strength: 10 mM Tris + 3 mM $MgCl_2$ + 1 mM EDTA and high ionic strength: 20 mM Tris + 50 mM NaCl + 5 mM $MgCl_2$ + 1 mM EDTA.

strength conditions. This result indicates the importance of the ionic strength in stabilizing the secondary structure of the MB alone and when hybridized with the target.

2.3.2. The oligonucleotide target concentration. In order to study the effect of the target concentration in the presence of the high ionic strength medium on the selectivity of the LNA MBs to detect UV damage, we performed two experiments, one in which the MB_{26}-4 was incubated with UV-damaged dT_{17} target present in a 1:1 concentration ratio and one in which the concentration ratio was 1:5 for the MB : target (Table 2.2). The results are shown in Table 2.2 and Figure 2.4. These results show that high relative target concentration and high ionic strength yield higher damage constants than lower relative target concentrations. This result may suggest the formation of triplexes of two targets and one MB instead of the formation of a duplex hybrid between the target and the MB. Damage to one target of the triplex and subsequent dehybridization would still yield a stable MB-target duplex with high fluorescence. Not until both targets are damaged would the MB form a closed hairpin and exhibit fluorescence quenching. This scheme would yield longer damage constants than a system of only duplexes.

2.3.3. LNA/DNA ratio in the MB design.

Previous studies[14] showed that incorporation of LNA bases in the MB stem sequence significantly increases the stability of the hairpin structure. This increased stability greatly increases the energy barrier of opening the LNA-MB stem and significantly slows down its hybridization kinetics. In this work, we used MBs with LNA bases only in the loops, in different ratios, and stems composed only of DNA bases. This design will allow the study of the effect of LNA bases on the selectivity of the MB to detect UV damage in oligonucleotides and avoid the slow hybridization kinetics of LNA bases in the MB stem.[13] Table 2.1 shows the four MBs used in this experiment, MB_{33}-0 (complement to dT_{24}), MB_{26}-4 (complement to dT_{17}), MB_{26}-5 (complement to dT_{17})and MB_{26}-6 (complement to dT_{17}), with incorporation ratios of LNA bases in the MB loop of 0%, 24% (4/17), 29% (5/17) and 36% (6/17), respectively. After irradiating the target dT_{17} with

UVC light and separately hybridizing aliquots of the damaged target with these four MBs, the results are shown in Figure 2.5 and Table 2.2. It is clear that the damage constants increase with increasing proportion of LNA bases in the loop, reflecting a decrease in selectivity of the LNA MB to detect UV damage with increasing LNA ratio. Similar trends were obtained upon irradiating the rU_{17} target (Table 2.2). However, the damage constants of the single exponential decay fit are much lower for the rU_{17} target than for the dT_{17} one (Figure 2.2). This result agrees with a previously published study[12], which showed that the MB detection of UV-induced damage to poly-rU is much more selective than that to poly-dT, due to a lower overall stability of damaged RNA : DNA hybrids compared to damaged DNA : DNA hybrids.

These results conclusively show that incorporation of LNA bases in the MB loop do not improve the selectivity of the MBs to UVC-induced oligonucleotide damage. This is surprising in light of previous reports of LNA's greater selectivity to single base pair mismatches.[13-16] Indeed, LNAs have been shown to be more sensitive than ssDNA probes in detecting single base pair mismatches.[13-16] However, these previous studies utilized LNA MBs which contained a greater proportion of locked nucleotides, up to a fully modified LNA MB loop.[14] The results presented here suggest that the difference in recognition sites for single base pair mismatches compared to UV-damage products (CPD and photohydrates) in the oligonucleotide target strand is significant enough to preclude the use of LNA MBs for selective detection of DNA damage.

A possible molecular explanation for this difference between damage and mismatch detection by the LNA MBs may lie in differences in the recognition site for single base mismatch (at the site of hydrogen bonding) compared with the recognition site of UV-damage products (at the C_5=C_6 bond, on the opposite side of the molecule from the basepairing site). Although damage is known to disrupt the local DNA structure, such a perturbation may not be as large as the proximal change in hydrogen bonding that occurs upon single base-pair mismatch. Thus, damage may not destabilize the LNA MB as much as single base-pair mismatches. Future experiments should provide a more well-defined model for

the detection of damage by the LNA MB and an explanation for the lower sensitivity of such detection by LNA MBs compared with MBs.

2.4. Conclusion

The results presented in this chapter demonstrate the factors affecting the specificity of LNA MBs to detect UV-induced nucleic acid damage. High ionic strength and low target concentration improves the performance of these MBs in detecting UV-induced damage in dT and rU polynucleotides, as demonstrated by the shorter damage constants. Increasing the LNA ratio in the MB design leads to longer damage constants, reflecting a decrease in the selectivity of these MBs to detect damage. In conclusion, the results presented here show that, although locked nucleic acid (LNA) hairpin probes have greater selectivity to single base pair mismatches than regular molecular beacon (MB) probes, they have lower specificity for detecting nucleic acid damage.

2.5. References

(1) L. Marrot, J.R. Meunier, J. Am. Acad. Dermatol. 58 (2008) S139-S148.

(2) T. Lindahl, Nature 362 (1993) 709-715.

(3) L.J. Marnett, P.C. Burcham, Chem. Res. Toxicol. 6 (1993) 771-785.

(4) B.N. Ames, L.S. Gold, W.C. Willett, Proc. Natl. Acad. Sci. U.S.A. 92 (1995) 5258-5265.

(5) D.L. Mitchell, In CRC Hand Book of Organic Photochemistry and Photobiology, W.M. Horspool, P.-S. Song, Eds., CRC Press, New York, 1995, pp 1326.

(6) M. Weinfeld, K.-J.M. Soderlind, Biochemistry 30 (1991) 1091-1097.

(7) B.B. Haab, R.A. Mathies, Anal. Chem. 67 (1995) 3253-3260.

(8) H. Kaur, B. Halliwell, Biochem. J. 318 (1996) 21-23.

(9) M. Dizdaroglu, Methods Enzymol. 34 (1994) 3-16.

(10) C.C.Trevithick-Sutton, L. Mikelsons, V. Filippenko, J.C. Scaiano, Photochem. Photobiol. 83 (2007) 556-562.

(11) J.Z. Xing, J. Lee, S.A. Leadon, M. Weinfeld, X.C. Le, Methods 22 (2000) 157-163.

(12) S. Yarasi, C. McConachie, G.R. Loppnow, Photochem. Photobiol. 81 (2005) 467-473.

(13) L. Wang, C.J. Yang, C.D. Medley, S.A. Benner, W. Tan, J. Am. Chem. Soc. 127 (2005) 15664-15665.

(14) C.J. Yang, L. Wang, Y. Wu, Y. Kim, C.D. Medley, H. Lin, W. Tan, Nucl. Acids Res. 35 (2007) 4030-4041.

(15) Y. Wu, C.J. Yang, L.L. Moroz, W. Tan, Anal. Chem. 80 (2008) 3025-3028.

(16) K. Martinez, M.-C. Estevez, Y. Wu, J.A. Phillips, C.D. Medley, W. Tan, Anal. Chem. 81 (2009) 3448-3454.

(17) L. Morandi, D. Ferrari, C. Lombardo, A. Pession, G. Tallini, J. Virol. Methods 140 (2007) 148-154.

(18) B.P. Ruzsicska, and D.G.E. Lemaire In CRC Hand Book of Organic Photochemistry and Photobiology, W.M. Horspool, P.-S. Song, Eds., CRC Press, New York, 1995, pp 1289.

(19) http://www.idtdna.com/catalog/Modifications/Modifications.aspx?ProductID=2059

Chapter 3

Chimeric RNA-DNA Molecular Beacons for Quantification of Nucleic Acids, SNPs and Nucleic Acid Damage*

3.1 Introduction

Single nucleotide polymorphisms (SNPs) and nucleic acid damage are two important factors that determine variability and change in the human genome. SNPs are a substitution, insertion, or deletion at a single base position on a DNA strand. There is expected to be, on average, one SNP for every 1000 bases of the human genome.[1] Some variations located in genes are suspected to alter both the protein structure and the expression level. SNPs are the most abundant form of DNA sequence variation in the human genome, and contribute to phenotypic diversity, influencing an individual's anthropometric characteristics, risk of certain disease, and variable response to drugs and the environment.[1] Due to their dense distribution across the genome, SNPs are used as markers in medical diagnosis and in personalized medicine.

Exposure of nucleic acids to a variety of internal and external agents can lead to another source of variability in the genome, damage and mutation. Nucleic acid damage includes genotoxic molecular-scale lesions such as cyclobutane photodimers (CPDs), [6-4] pyrimidine pyrimidinones, dewar pyrimidinones and photohydrates.[2] Other damage includes single- and double-strand breaks, 8-oxoguanosine, other oxidation products, and cross-links. All these damage products lead to miscoding during DNA replication and may result in mutagenesis, carcinogenesis, aging and cell death.[3-6]

The effects of SNPs and nucleic acid damage on the molecular origin of mutagenesis, carcinogenesis[7,8] and the need for a sensitive and precise measurement of SNPs and damaged DNA led to the development of a number of techniques for their detection. These include gel electrophoresis,[9,10] capillary electrophoresis,[11,12,13] electrochemical,[12,13] HPLC,[14] mass spectrometric[15-18] , and

*A version of this chapter has been submitted to Analytical Chemistry

polymerase chain reaction (PCR) amplification[13,19] methods. While useful, these techniques are destructive, elaborate and time-consuming. In addition, electrophoretic and chromatographic techniques need to isolate the probe–target hybrids from an excess of unhybridized probes, which include additional steps that may introduce more lesions.[9]

Other spectroscopic-based techniques have recently been used to characterize nucleic acid damage. Typically, fluorescent methods offer enhanced sensitivity and the potential for use *in situ* or *in vivo*. Differences in the fluorescence lifetime of a dye intercalated in undamaged and damaged DNA have been used to detect DNA damage.[20] Fluorescently-labeled antibodies provide a highly selective probe of particular damage photoproducts, such as thymine cyclobutyl photodimers.[21] More recently, hybridization probes[22-27] have been used to detect single nucleotide polymorphisms (SNPs), gene mutations, and DNA damage. The inherent sensitivity of fluorescence makes these hybridization probes a sensitive tool for the detection of nucleic acid damage.

The most studied hybridization probes are binary probes[24-27] and molecular beacons (MB).[22-23] Binary probes are composed of two single-stranded oligonucleotides complementary to different parts of the oligonucleotide target and are labeled with a fluorophore at the 3′ or 5′ end. After adjacent hybridization of both strands to the complementary oligonucleotide, the labels are close enough to enable either FRET[24] or strong fluorescence quenching[27] to occur. An advantage of binary probes is that they do not yield false positive or nonspecific signals. However, one of their limitations is that the entropy of a binary probe system decreases more when bound to the target (three independent species becoming one hybrid), which reduces the equilibrium stability of the hybrid.[28] Also, the hybridization kinetics of binary probes are slow, because binary probe hybridization depends on the binding of two different components to the target.

Molecular beacons are DNA hairpins labeled with a quencher on one end and a fluorophore on the other end. In the hairpin form, the quencher and fluorophore are in close proximity and the fluorescence is quenched. However, when the MB

hybridizes to a complementary oligonucleotide target, a significant increase in fluorescence is detected. In MBs, the loop sequence is complementary to the target DNA sequence, and the resulting hybridization spatially separates the quencher and the fluorophore. In the presence of a single base mismatch or a single site of damage, the hybrid formed between the probe and the mismatch sequence is less stable, since this target is not perfectly complementary to the loop of the probe. Thus, the observed fluorescence intensity is lower for a sample containing mismatches or damaged DNA bases compared to one containing the perfectly complementary sequences. This inherent signal mechanism allows MBs to function as highly sensitive probes of nucleic acids, with their advantages of simplicity and high specificity. Consequently, a variety of sensitive assays have been developed using MBs constructed from DNA nucleotides to detect nucleic acid damage,[22] SNPs,[29,30] and gene mutations,[31] to quantify the concentration of a target molecule during real-time or quantitative PCR,[32,33] and for intracellular imaging of nucleic acids.[34]

Alternative approaches to DNA-MBs have been developed in which MBs are constructed using modified DNA backbones, such as phosphorothioate, 2′-*O*-methyl RNA bases,[35-37] peptide nucleic acids (PNAs)[38,39] and locked nucleic acids (LNAs).[40] Backbone modifications have several attractive advantages, such as higher binding affinity, increased specificity, faster hybridization kinetics, and fluorescence background suppression, because of a reduction in dynamic opening of the stem.[41] However, there are some disadvantages and limitations, such as the toxicity occasionally associated with phosphorothioate-containing oligonucleotides.[42] 2′-*O*-Methyl modified MBs open up nonspecifically in cells, possibly due to protein binding.[36,37] The neutral PNAs tend to self-aggregate[43] and fold in a way that interferes with duplex formation.[44] PNAs also change their physical properties substantially with small changes in sequence.[45,46] While LNAs have excellent base mismatch discrimination capability,[40] they are less selective in the detection of nucleic acid damage than DNA-MBs as discussed in Chapter 2.

In this chapter we present another type of backbone modification in which a chimeric RNA-DNA MB (chMB) is used for the quantification of base mismatches and UV-induced DNA damage. Recently, chimeric RNA-DNA strands have been widely used in gene targeting,[47] as gene repair materials,[48,49] as PCR primers,[50] as a MB for the detection of ribonuclease activity[51] and as sequence-specific mediators of RNA interference.[52] In each of these applications, the chimeric strand has unique advantages specific to the application. For instance, the DNA in the hybridizing arms in gene targeting enhances the chemical cleavage step, while the RNA loop did not affect its enzymatic activity.[47] Furthermore, an uninterrupted stretch of DNA bases within the chimera is known to be active in sequence alteration while RNA residues aid in complex stability in gene repairing.[49]

The chMB used in this work is designed so that the RNA bases are complementary to the oligonucleotide target, while DNA bases mainly constitute the stem of the MB. Typically, the thermal stability of RNA duplexes and RNA-DNA hybrid duplexes is greater than that of DNA duplexes when their sequences are identical.[53] Because of this, the chMB-DNA hybrid is expected to have a higher fluorescence signal than typical MB-DNA hybrids. The DNA stem is kept in the chMB to provide a reasonable melting temperature that allows the stem to open in the presence of the undamaged oligonucleotide target. To our knowledge, this study represents the first use of chMBs for the quantification of nucleic acids, mismatches and DNA damage. The sensitivity and selectivity of the chMB to nucleic acids, single base mismatch and UVC-induced DNA damage were examined and found to be superior to conventional DNA MBs.

3.2. Experimental

3.2.1. Materials

The single-strand oligonucleotide targets, the chMB and the DNA MB probes (Figure 3.1) were obtained from Integrated DNA Technologies Inc. (Coralville, Iowa). The oligonucleotide targets were purified by standard desalting and the

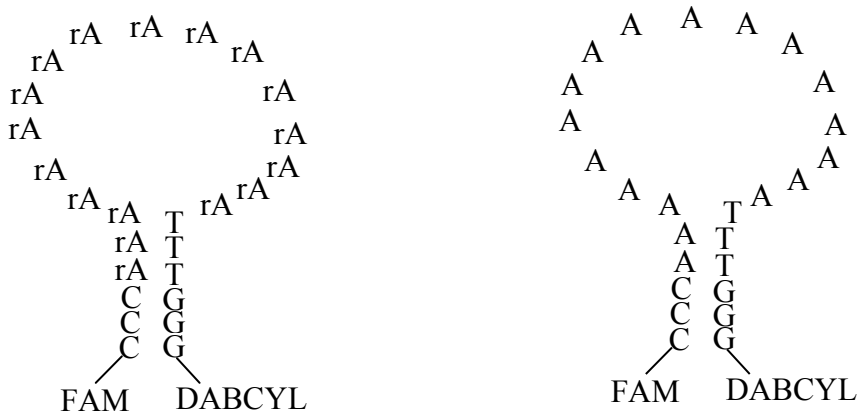

T_{m0}: 3’-TTT TTT TTT TTT TTT TT-5’

T_{m1}: 3’-TTT TTT TTA TTT TTT TT-5’

T_{m12}: 3’-CTC GAA GCT AGG TTA CT-5’

T_{m17}: 3’-AAA AAA AAA AAA AAA AA-5’

Figure 3.1. Sequences of the chimeric RNA-DNA MB (chMB), the DNA MB, the perfect complementary target (T_{m0}), the oligonucleotide target with 1 mismatch (T_{m1}), the target with 12 mismatches (T_{m12}) and the completely non-complementary target (T_{m17}). The underlined bases represent the mismatched bases to either the chMB or DNA MB. “FAM” denotes the 6-carboxyfluorescein fluorophore, “DABCYL” denotes the dabcyl quencher and “r” denotes a ribonucleotide.

probes were purified by HPLC purification. Magnesium chloride ($MgCl_2$) and sodium chloride (NaCl) were obtained from EMD Chemicals Inc. (Gibbstown, New Jersey), Tris was obtained from ICN Biomedicals, (Aurora, Ohio) and ethylenediaminetetraacetic acid (EDTA) was obtained from BDH Inc. (Toronto, Ontario). All chemicals were used as received. Nanopure water from a Barnsted Nanopure (Boston, Massachusetts) system was used for all solutions. The oligonucleotide samples were each dissolved in nanopure water and kept frozen at ~20 °C until needed.

3.2.2. UV Irradiation

Nitrogen-purged solutions of 10 μM dT_{17} were irradiated in sealed, UV-transparent 1 cm path length cuvettes. The cuvettes were placed in a water bath also contained in a UV-transparent water dish. The temperature, which was monitored by means of a Cole-Parmer DiGi-SENSE thermocouple (Niles, Illinois), was kept constant throughout the irradiation by the water bath. Oligonucleotide samples were irradiated in a Luzchem (Ottawa, Ontario) DEV photoreactor chamber with UVC light from lamps emitting principally at 254 nm with an irradiation dose of 75011 mW m^{-2}. The samples were constantly stirred during irradiation, and the photoreactor was purged with nitrogen throughout the irradiation to flush out oxygen and any ozone subsequently generated from the UVC lamps. Control samples were handled identically, but were not exposed to UV radiation. The UVC lamps were turned on ~20 min before the start of irradiation to stabilize the lamp output.

3.2.3. Absorption and fluorescence measurements

Absorption spectra were recorded at intervals throughout the irradiation period on a Hewlett-Packard (Sunnyvale, California) 8452A diode array spectrophotometer by placing the irradiated cuvettes containing the target oligonucleotide solutions directly into the spectrophotometer. For the fluorescence measurements, a 10 μL aliquot of each irradiated solution was taken at various time intervals and was later mixed with appropriate amounts of the probe and buffer solution to give final concentrations of 2 μM oligonucleotide targets and 200 nM MB probe. These

solutions were then incubated in the dark at room temperature for about 24 h. Fluorescence spectra of 100 μL aliquots of the incubated hybridization mixtures were measured using a Photon Technologies International (Birmingham, New Jersey) fluorescence spectrophotometer. The spectra were recorded between 490 and 600 nm with excitation at 480 nm. A 1 cm path length Suprasil quartz fluorescence cuvette was used for these measurements.

For the nucleic acid and mismatch detection, solutions of poly-dT and mismatches (Figure 3.1) were mixed with appropriate amounts of the probe and buffer solution to give final concentrations of 2 μM MB probe and incubated in the dark at the specified temperature for about 24 h. Then the fluorescence measurements were performed as described above.

The chMB was characterized by a thermal denaturation profile experiments, in which temperature-dependent fluorescence measurements were carried out on a buffered 200 nM solution of the MB incubated in the absence or presence of either the target oligonucleotide sequence or the UV-damaged target sequence at 2 μM concentration. The temperature was varied from 20 to 72 °C in 4 °C increments at a heating rate of 1 °C min^{-1} and 5 min settling time for each step of the heating cycle. The reverse was done under the same conditions in order to record the cooling cycle.

3.3. Results and Discussion

The chMB was carefully designed to maximize its performance as a sensitive and specific probe for SNPs and UV-induced nucleic acid damage. This design ensures that the chMB can selectively discriminate single damage sites or mismatches in oligonucleotides. Figure 3.1 demonstrates the structure of the chMB used in this study. The loop region is composed of ribonucleotides and the stem region is composed of six base pairs, of which three nucleotides are ribonucleotides while the rest are 2'-deoxyribonucleotides. The MB is designed such that the oligonucleotide target is complementary to the loop region and three nucleotides in the stem region, to avoid sticky end pairing.[40] The design of the MB maximizes discrimination of damaged ***versus*** undamaged targets, due to the T_m's

of the stem and hybrid; designing the MB to have a T_m for the stem 5 – 10 °C higher than the T_m of the hybrid ensures maximum sensitivity.

3.3.1. Factors affecting the fluorescence of the chMB

3.3.1.1. Effect of Ionic strength

In order to optimize the performance of the chMB, we investigated the effect of ionic strength and temperature on the fluorescence of the chMB Figure 3.2 shows the thermal denaturation profiles of 200 nM chMB and DNA MB alone in different Mg^{2+} and Na^{+} ion concentrations scaled to the fluorescence of the chMB in 3 mM $MgCl_2$ and 20 mM NaCl at 72 °C. The melting curve of the chMB (Figure 3.2A) in the five different concentrations of Mg^{2+} and Na^{+} ions generally shows the same trend, at low temperatures. At low temperatures, the MB acquires the hairpin structure, the fluorophore and the quencher are in close proximity and the fluorescence is quenched. At the melting temperature of the stem, the fluorescence gradually increases with temperature until reaching a plateau, indicating that the distance between the fluorophore and the quencher is constant in the random coil structure.[22] As shown in Figure 3.2A, the fluorescence of the chMB in 3 mM Mg^{2+} increased by 3 times upon increasing the Na^{+} ion concentration from 0 mM to 20 mM. Moreover, the steepness of the slope of the inflection around the melting temperature of the MB stem increased by a factor of 5.4 times. Thus, a Na^{+} ion concentration of 20 mM leads to the highest chMB fluorescence signal.

Likewise, we studied the effect of the Mg^{2+} concentration on the fluorescence of the chMB while keeping the Na^{+} concentration constant at 20 mM. The fluorescence of the chMB (Figure 3.2) decreased by 1.2 times upon increasing the concentration of Mg^{2+} from 3 mM to 5 mM and decreased by 1.6 times when increasing it from 3 mM to 10 mM. In the latter case, the steepness of the slope of the inflection point around the melting temperature decreases by a factor of 2.3 times. Figure 3.2 also shows that high ionic strengths, such as 10 mM $MgCl_2$ and 20 mM NaCl, lead to higher fluorescence levels at low temperatures, reducing the

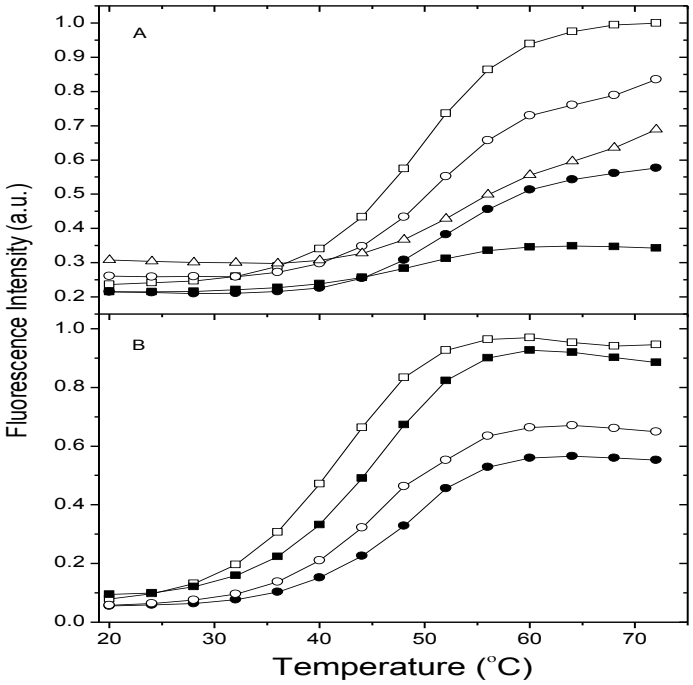

Figure 3.2. Thermal denaturation profiles for (A) the chMB and (B) the DNA MB at different ionic strengths. In both figures are shown the curves for 200 nM MB alone in 3 mM $MgCl_2$ and 0 mM NaCl (filled squares), 5 mM $MgCl_2$ and 0 mM NaCl (filled circles), 10 mM $MgCl_2$ and 20 mM NaCl (open triangles), 5 mM $MgCl_2$ and 20 mM NaCl (open circles) and 3 mM $MgCl_2$ and 20 mM NaCl (open squares). These profiles are scaled to the fluorescence of the MB in 3 mM $MgCl_2$ and 20 mM NaCl at 72 °C. All solutions are in 10 mM Tris buffer and 1 mM EDTA adjusted to pH 7.5. Fluorescence excitation wavelength was 480 nm and the emission was measured at 520 nm. The lines are guides for the eye.

potential dynamic range and sensitivity of the chMB. This result indicates that high ionic strength destabilizes the stem's double-stranded nature, as high Mg^{2+} ion concentration may disrupt the stem hydrogen bonds and therefore affects the hairpin secondary structure of the MB. Similarly, at high temperatures, the chMB exhibits lower fluorescence at high ionic strengths. These results suggest that a buffer containing 3 mM $MgCl_2$ and 20 mM NaCl offers the optimum ionic strength for the chMB to perform efficiently. The DNA MB (Figure 3.2B) shows the same result where 3 mM $MgCl_2$ and 20 mM NaCl offers the optimum ionic strength. The only difference is that in the absence of 20 mM NaCl, 3 mM $MgCl_2$ shows slightly lower fluorescence than in presence of 20 mM NaCl and also is higher than the fluorescence intensity of the DNA MB in 5 mM $MgCl_2$, in the absence and the presence of 20 mM NaCl.

3.3.1.2. Effect of temperature

To study the effect of temperature on the fluorescence of the chMB alone and in the hybrid with the perfectly complementary target, we measured the fluorescence at 520 nm of 200 nM MB alone and in the presence of a 10-fold excess of perfectly complementary oligonucleotide target at temperatures between 20 - 72 $^{\circ}$C. Figure 3.3 shows the thermal denaturation profile of the chMB alone and in the hybrid with undamaged target, both of which show the expected profile. At low temperatures, the MB alone acquires the hairpin structure, the fluorophore and the quencher are in close proximity and the fluorescence is quenched. At the melting temperature of the stem, the fluorescence gradually increases with temperature until reaching a plateau, indicating that the distance between the fluorophore and the quencher is constant in the random coil structure.[22] For the chMB-target hybrid, the fluorophore and the quencher are far apart and maximum fluorescence is observed at low temperatures. At higher temperatures, the hybrid melts and the chMB re-forms the hairpin, leading to a decrease in fluorescence. At temperatures higher than the stem melting temperature (~48 $^{\circ}$C), the chMB again forms a random coil and the fluorescence shows the same trend as the chMB alone.

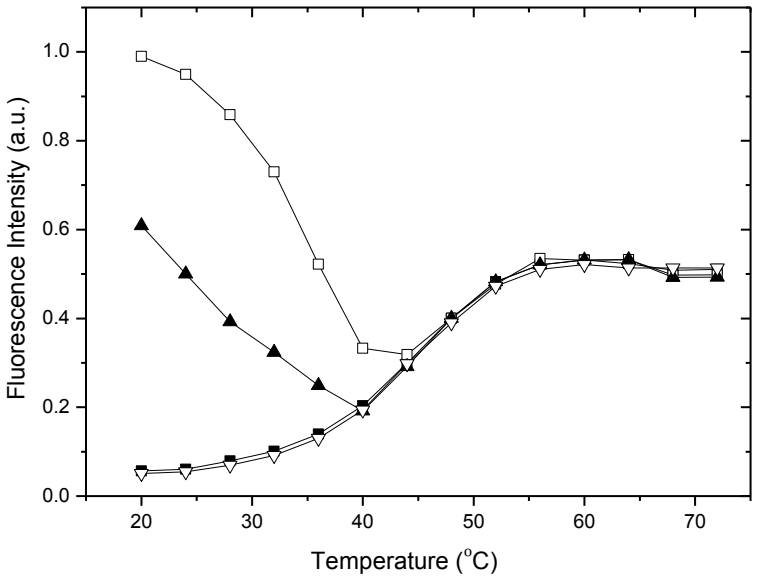

Figure 3.3. Thermal denaturation profiles for 200 nM chMB alone (filled squares), in the presence of a 10-fold excess of perfectly complementary oligonucleotide target sequence (open squares), and in the presence of a 10-fold excess of the UV-irradiated oligonucleotide target sequence for 1 min (filled triangles), and for 10 min (open triangles). These profiles are scaled to the fluorescence of the MB - perfectly complementary oligonucleotide target hybrid at 20 °C. The lines are guides for the eye.

3.3.2. Nucleic acid detection by the chMB

Fluorescence measurements were performed to test the sensitivity of the chMB to detect DNA and to compare it to the DNA MB. The DNA MB (Figure 3.1) used in this study was designed to the same sequence as the chMB, with 2'-deoxyribonucleotides comprising the whole loop and stem of the MB. Figure 3.4 shows the fluorescence of the chMB and DNA MB with varying concentrations of the perfectly complementary oligonucleotide target. Note that the response of the DNA MB at all target concentrations is lower than that from the chMB. However, at zero target concentration, the emission of the chMB is slightly lower than that of the DNA MB, lowering the fluorescence background and increasing the sensitivity of the chMB to detect the oligonucleotide target. This can be attributed to the three RNA nucleotides present in one side of the stem of the chMB (Figure 3.1), resulting in an increase of the chMB stem stability compared to the DNA MB. Because of this higher stability, the quenching is enhanced between the fluorescein fluorophore and the dabcyl quencher. When titrated with target oligonucleotide, both the chMB and the DNA MB hybridize with the target and their fluorescence intensities increase with increasing target concentration. After 1.0 equivalent of the target was added to the chMB and the DNA MB solutions, i.e., at 2 μM target concentration, higher target concentrations produce no change in the fluorescence intensity (Figure 3.4).

Table 3.1 shows the analytical parameters for the quantification of oligonucleotide target by chMB and DNA MB. The table shows that the chMB has a larger linear dynamic range. The sensitivity of the chMB is 1.8 times higher than that of the DNA MB and the LOD and LOQ for the chMB are 5.6 times lower than those for the DNA MB. These results suggest that the chMB may be a more sensitive and selective probe of DNA damage.

Table 3.1. Analytical parameters for the quantification of different oligonucleotides with chMB and DNA MB

Parameter[a]	Undamaged oligonucleotides		Mismatched oligonucleotide[b]		Damaged oligonucleotides[c]	
	DNA MB	**chMB**	**DNA MB**	**chMB**	**DNA MB**	**chMB**
Linear Dynamic Range (μM)	0.40 – 2.00	0.00 – 2.00	1.10 – 2.00	0.00 – 2.00	2.60 – 4.50	0.00 – 2.50
R^2	0.995	0.998	0.973	0.981	0.995	0.996
Sensitivity (cps M^{-1})	5.19×10^{11}	9.43×10^{11}	8.62×10^{11}	1.22×10^{12}	9.54×10^{11}	1.47×10^{12}
LOD (nM)	76.0	13.5	45.8	10.4	41.4	8.64
LOQ (nM)	253	45.0	153	34.6	138	28.8

For the determination of the blank standard deviation, 20 solutions of the MB hairpin alone were used. The standard deviations of these measurements were 0.4 $\times 10^4$ cps and 1.3$\times 10^4$ cps for the chMB and the DNA MB, respectively. [a]In this table, linear dynamic range is the concentration range corresponding to the linear region in the calibration curve, R^2 is the linear regression coefficient squared, sensitivity is the slope of the calibration curve, LOD is the limit of detection and is 3 times the standard deviation of the blank divided by the sensitivity, and LOQ is the limit of quantification and is 3.3 times the LOD. [b]The mismatched oligonucleotides are oligonucleotides with one mismatch. [c]The damaged oligonucleotides are oligonucleotides damaged with UVC light.

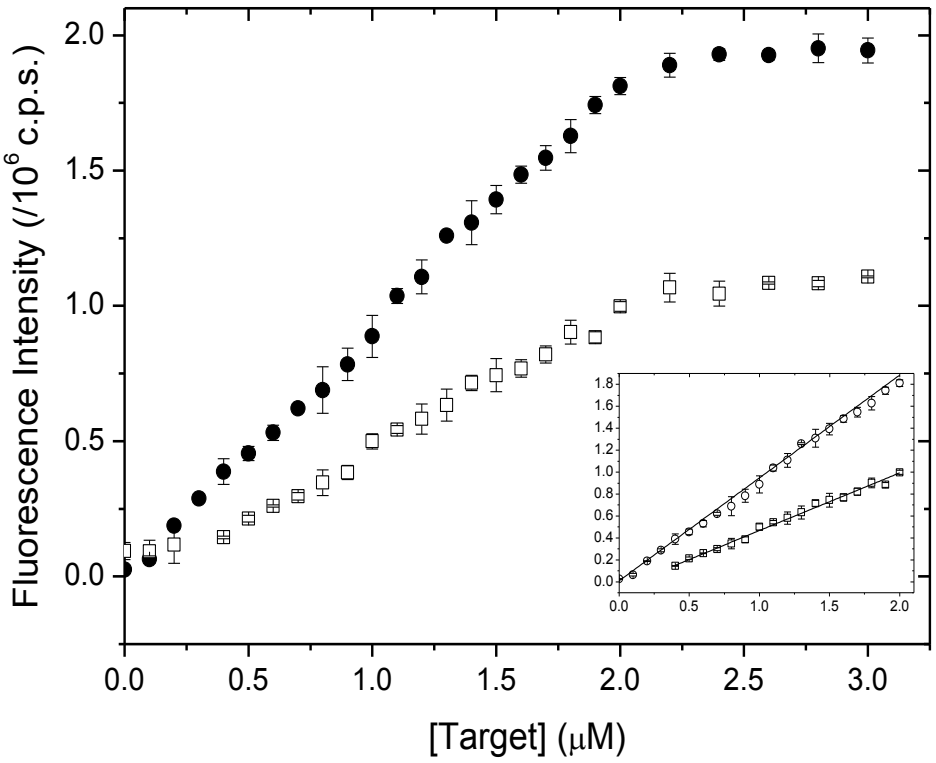

Figure 3.4. Calibration curve for the detection of undamaged poly-dT_{17} target by 2 μM chMB (filled circles) and 2 μM DNA MB (open squares). Inset shows the fit to the linear portions of the calibration curves and has the same axes labels as the main graph. Fit parameters are shown in Table 3.1. Each data point is an average of three replicate measurements and the error bars correspond to the standard deviation of each measurement. "c.p.s." denotes counts per second.

3.3.3. ChMB Selectivity and Sensitivity for SNPs

To examine the selectivity of the chMB, it was hybridized with the perfect complement (T_{m0}), an oligonucleotide target containing 1 mismatch (T_{m1}), one containing 12 mismatches (T_{m12}) and one that is completely non-complementary to the chMB (T_{m17}, Figure 3.1). The DNA MB was also hybridized with the same targets in order to compare its selectivity to the chMB. Figure 3.5 shows the fluorescence measurements of these solutions. The fluorescence of the chMB-T_{m0} hybrid shows the highest fluorescence signal of all chMB hybrids, i.e. the fluorescence signal of chMB completely dies to the background level with the $T_{m1,}$ T_{m12} and T_{m17} hybrids. This result demonstrates the high selectivity of the chMB to a single base mismatch; the chMB acquires the hairpin structure for all mismatches. On the other hand, the DNA MB-T_{m0} shows slightly higher fluorescence than the DNA MB-T_{m1} while the fluorescence completely drops to background level for the DNA MB hybrids with T_{m12} and T_{m17}. This indicates that the DNA MB is less selective to a single base mismatch compared to the chMB. Also, the fluorescence intensity of the chMB alone is much lower than that of the DNA MB alone, consistent with Figure 3.4.

To understand the difference in selectivity between the chMB and the DNA MB, we measured the fluorescence at 520 nm of 200 nM chMB and DNA MB alone and in the presence of a 10-fold excess of T_{m0} and T_{m1} at temperatures between 20 - 72 $^{\circ}$C. Figure 3.6 shows the thermal denaturation profiles of the chMB and DNA MB alone and hybridized with T_{m0} and T_{m1}. Solutions containing the chMB and DNA MB alone and the chMB-T_{m0} and DNA MB-T_{m0} hybrids show the expected profile. At low temperatures, the MB alone acquires the hairpin structure, the fluorophore and the quencher are in close proximity and the fluorescence is quenched. At the melting temperature of the stem, the fluorescence gradually increases with temperature until reaching a plateau, indicating that the distance between the fluorophore and the quencher is constant in the random coil structure.[22] For the chMB-target hybrid, the fluorophore and

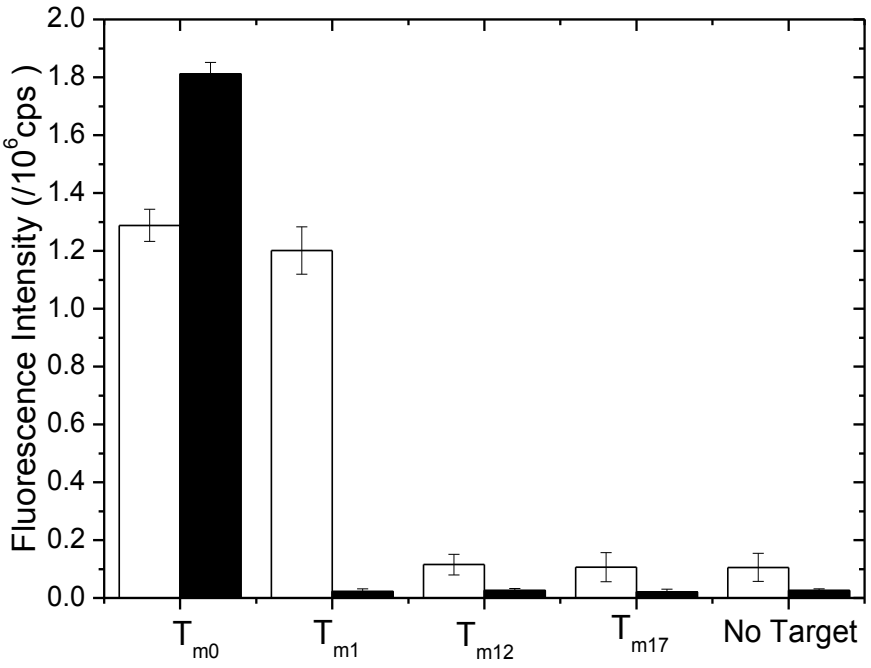

Figure 3.5. Fluorescence intensity at 520 nm of 200 nM of DNA MB (white bars) and chMB (black bars) hybridized at 20°C with a 10-fold excess of the respective oligonucleotide targets (Figure 3.1). "No target" represents the fluorescence intensity of the chMB or DNA MB alone.

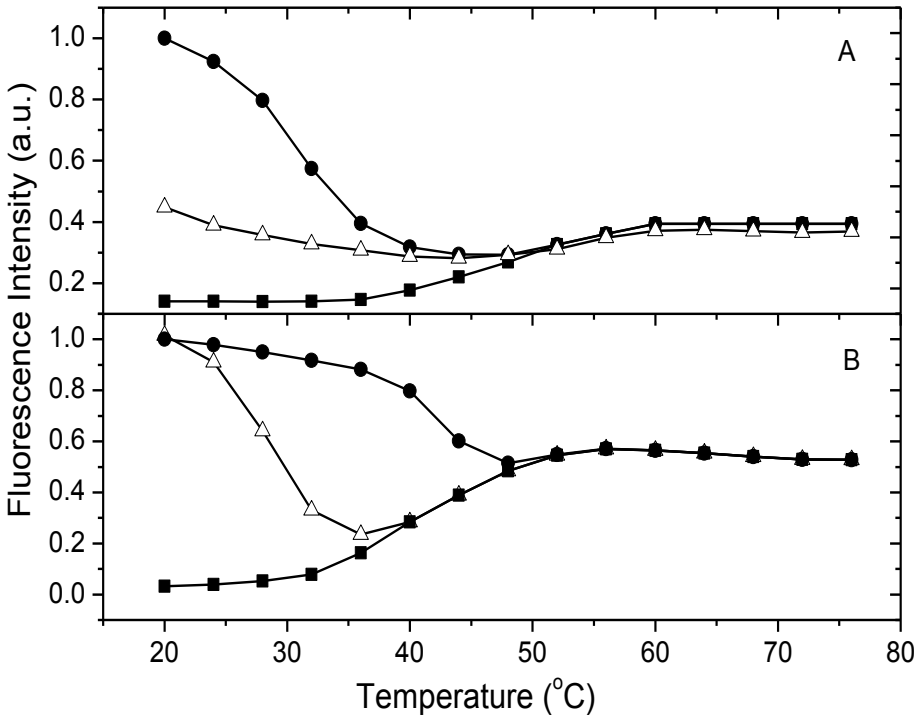

Figure 3.6. Thermal denaturation profiles for the (A) chMB and (B) DNA MB. In both figures are shown the curves for 200 nM MB alone (filled squares), 200 nM MB in the presence of a 10-fold excess of perfectly complementary oligonucleotide target sequence (filled circles), and 200 nM MB in the presence of a 10-fold excess of the oligonucleotide target with 1 mismatch (open triangles). These profiles are scaled to the fluorescence of the MB - perfectly complementary oligonucleotide target hybrid at 20 °C.

the quencher are far apart and maximum fluorescence is observed at low temperatures. At higher temperatures, the hybrid melts and the chMB re-forms the hairpin, leading to a decrease in fluorescence. At temperatures higher than the stem melting temperature (~48 °C), the chMB again forms a random coil and the fluorescence shows the same trend as the chMB alone. The chMB-T_{m1} hybrid (Figure 3.6A) shows a lower room-temperature fluorescence intensity than that of the chMB-T_{m0} hybrid, and closer to the fluorescence of the chMB alone, due to the incomplete hybridization between the chMB and T_{m1}. Also, the melting temperature of the hybrid has decreased from ~30 °C for the chMB-T_{m0} hybrid to <25 °C for the chMB-T_{m1} hybrid, consistent with the latter's lower stability. The DNA MB-T_{m1} hybrid (Figure 3.6B) exhibits approximately the same fluorescence intensity as the DNA MB-T_{m0} hybrid at 20 °C, but lower fluorescence intensity at higher temperatures. Similar to the chMB, the melting temperature of the DNA MB-T_{m1} hybrid has decreased from ~40 °C for the DNA MB-T_{m0} hybrid to ~30 °C for the DNA MB-T_{m1} hybrid. As shown in Figure 3.6, the maximum discrimination between the perfectly complementary and the single mismatch targets hybridized with the chMB is ~20 °C, while for the DNA MB, it is ~30 °C. Therefore, we have chosen 20 and 30 °C hybridization temperatures for the quantification of single base mismatches with the chMB and DNA MB, respectively.

In order to also check the sensitivity of the chMB and DNA MB to detect single base mismatch in the presence of perfectly complementary targets, we measured the fluorescence intensity as a function of the T_{m1} : T_{m0} concentration ratio at a total target concentration equal to either the chMB or DNA MB concentration. This experiment measured the ability of the probes to detect a mismatched strand within a solution of perfectly complementary strands. Figure 3.7 shows the resulting calibration curves obtained. Consistent with Figure 3.4, the chMB fluorescence decreases linearly with increasing T_{m1} concentration, and the decrease starts immediately. The fluorescence intensity for both the chMB and

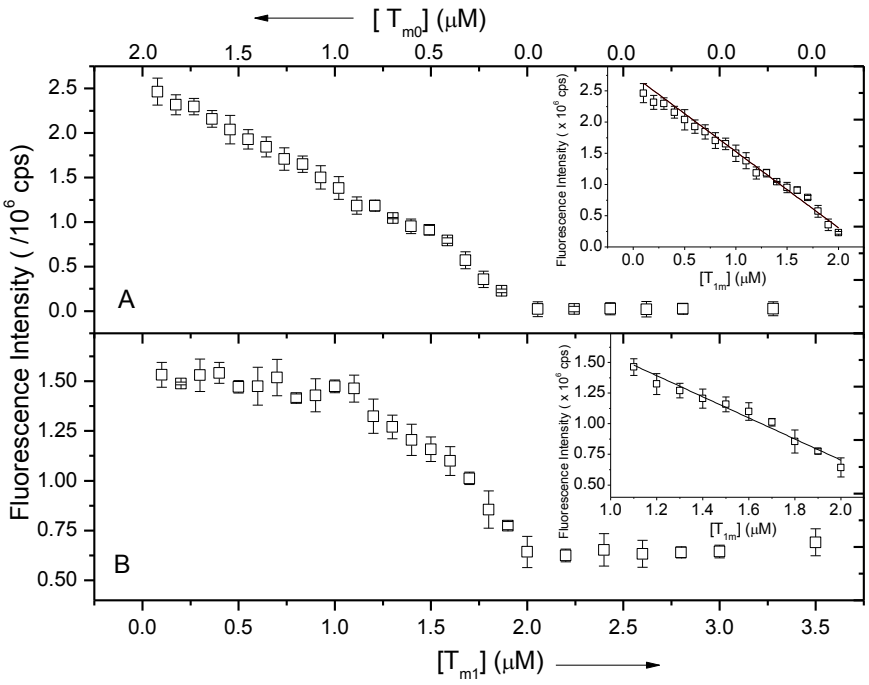

Figure 3.7. Calibration curve of the detection of target by 2.0 μM chMB (A) hybridized at 20 °C and 2.0 μM DNA MB (B)hybridized at 30 °C as a function of $[T_{m0}]$ (upper axis) and $[T_{m1}]$ (lower axis). Insets show the fit to the linear portions of the calibration curves. Note that at $[T_{m1}] > 2.0$ μM, no additional T_{m0} is added. Each data point is an average of three replicate measurements and the error bars correspond to the standard deviation of the measurements.

DNA MB decreases to a plateau at 2.0 μM T_{m1} target concentration, comparable to the background fluorescence of the respective quenched MB. For the DNA MB (Figure 3.7B), any decrease in fluorescence signal requires a minimum of 1.1 μM concentration of the T_{m1} target. The constant fluorescence signal of the DNA MB over the range of 0 – 1.1 μM of the T_{m1} target concentration can be attributed to the lower selectivity of the DNA MB to single base mismatch as discussed before. Also, the DNA MB exhibits a 5 times higher background fluorescence than the chMB, consistent with Figure 3.5.

Table 3.1 shows the parameters for the quantification of the single base mismatch from Figure 3.7. The calibration curve for the chMB shows a larger linear dynamic range than the DNA MB (Figure 3.7). The sensitivity of detection also is larger by a factor of ~1.4 for the chMB, leading to a lower limit of detection (LOD) and limit of quantification (LOQ) by 4.4 times. It is worth mentioning that the values recorded in Table 3.1 for the LOD and LOQ for DNA MB detection of single base mismatches are obtained by using the standard deviation of the blank measurements and the sensitivity of the method, while the LOD and LOQ will be practically limited to ~1.1 μM (Figure 3.7B) due to the unvarying fluorescence signal of the DNA MB at low mismatch concentrations. Using the values in Table 3.1 and Figure 3.7, we calculate that a single base mismatch within 3300 perfectly matched bases can be detected by the chMB.

3.3.4. Detection of UV-induced photoproducts with the chMB

In characterizing the chMB for the detection of DNA damage, T_{m0} was used here because of its well-known photochemistry. In this target, the CPD is the major photoproduct formed after UV irradiation, with smaller amounts of the [6-4] pyrimidine pyrimidinone and the Dewar pyrimidinone photoproducts.[2] Furthermore, it has been reported that a tripyrimidine stretch represents a hot spot for UV-induced DNA damage.[54] The 260 nm absorption band of T_{m0} gradually bleaches with increasing irradiation time, indicating photoproduct formation and loss of the C_5=C_6, yielding an independent spectroscopic marker for DNA

damage. Thus, the loss of the 260 nm absorption band can be directly related to the concentration of the photoproducts formed.

In order to optimize the hybridization temperature as a step to enhance the selectivity and sensitivity of the MB for UV-induced DNA damage, we measured the thermal denaturation profile of the hybrids of the chMB and the oligonucleotide target subjected to UVC light for 1 min and 10 min. The thermal denaturation profile of the hybrid between the chMB and the oligonucleotide target subjected to UVC light for 1 min is shown in Figure 3.3, where it shows lower fluorescence intensity than that of the hybrid between the chMB and the undamaged target. The fluorescence is much lower for the hybrid of the target exposed to UV light for 10 min having a thermal denaturation profile similar to that of the chMB alone (Figure 3.3). This can be attributed to that most of the oligonucleotide targets are damaged with this exposure time and most of the chMBs are in the hairpin structure. As shown in Figure 3.3, the maximum discrimination in the fluorescence between the undamaged and damaged targets hybridized with the chMB occurs at 20 $^{\circ}$C. Therefore, we have chosen this hybridization temperature for detecting the formation of the UV-induced photoproducts.

The T_{m0} oligonucleotide target was irradiated at constant temperature, and the resultant damage was detected by UV-Vis absorption measurements of the irradiated and control samples. Figure 3.8 shows a plot of the absorbance of the oligonucleotide target as a function of irradiation time with UVC light. The 260 nm $\pi\pi^*$ absorption band decreases with time. This result is expected and indicates UV-induced damage to the oligonucleotides with the consequent loss of the C_5=C_6 bond in all photoproducts formed. This decrease in absorbance is not observed in the unirradiated controls, demonstrating that the absorption change arises from irradiation of the samples and subsequent photochemistry rather than any other effect.

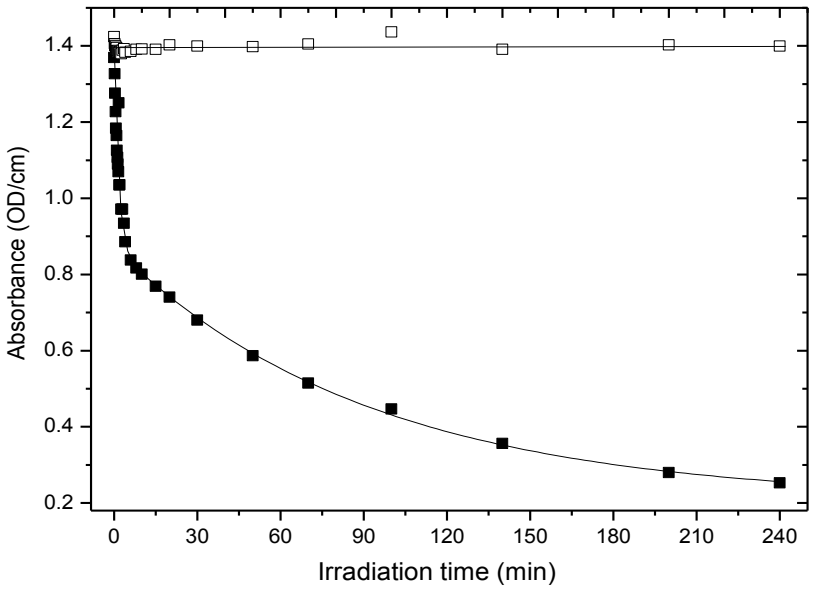

Figure 3.8 Absorbance of 10 μM irradiated T_{m0} target (filled squares) and unirradiated T_{m0} control (open squares) monitored at 260 nm as a function of irradiation time. The solid line through the absorbance points (filled squares) is the least-squares fit to an offset, double exponential function, $A = A_0 + A_1 e^{t/\tau 1} + A_2 e^{t/\tau 2}$, where the absorbance damage constants are 6.08 ± 0.07 min (τ_1) and 91.8 ± 2.0 min (τ_2), and the amplitudes are $A_1 = 0.52 \pm 0.01$ and $A_2 = 0.66 \pm 0.02$. The offset (A_o) is 0.21 ± 0.02. The control points (filled circles) are fit to a straight line with zero slope by eye.

In order to further examine the selectivity of the chMB in more detail and compare it to the DNA MB, the plot of T_{m0} absorbance as a function of irradiation time (Figure 3.8) was fit to a double-exponential function while the fluorescence curves (Figure 3.9) are fit to a single exponential function. This decay in the absorbance represents the formation of thymine photoproducts containing saturated C_5-C_6 bonds, and can be correlated to the concentration of the damage products. The decrease in the fluorescence intensity represents the decreased stability of the damaged target-MB hybrid. Therefore, the faster the fluorescence intensity decreases, the more selective the MB is at detecting UV-induced oligonucleotide damage under identical irradiation conditions for the same target. The damage constants obtained by fitting these fluorescence and absorbance damage curves are shown in Table 3.2 for both the chMB and DNA MB. It is clear from Table 3.2 that the rate of decrease in absorbance is slower than the rate of decrease in fluorescence intensity for both the chMB and DNA MB. This result indicates the lower selectivity of the absorbance measurement compared to the fluorescence measurement for detecting damage. Table 3.2 also shows that the damage constant of the chMB is 6 times faster than that of the DNA MB and 9-10 times faster than the fastest absorption damage constant. This allows the chMB to have superior selectivity for detection of UV damage in nucleic acids compared to absorption and the DNA MB methods.

In order to check the sensitivity of the chMB for damage detection, we used the UV absorbance measurements as a function of UV irradiation time to quantify the amount of UV damage and to develop calibration curves of the UV-induced photoproducts detected by the chMB and DNA MB. The procedure and calculation of the photoproducts concentration from the absorbance measurements of the irradiated solutions will be presented in details in Chapter 4 on page 104. Figure 3.10 shows the calibration curve obtained upon plotting the chMB and DNA MB fluorescence intensity as a function of the calculated concentration of the photoproducts. At high damage concentrations, the hybrids formed between

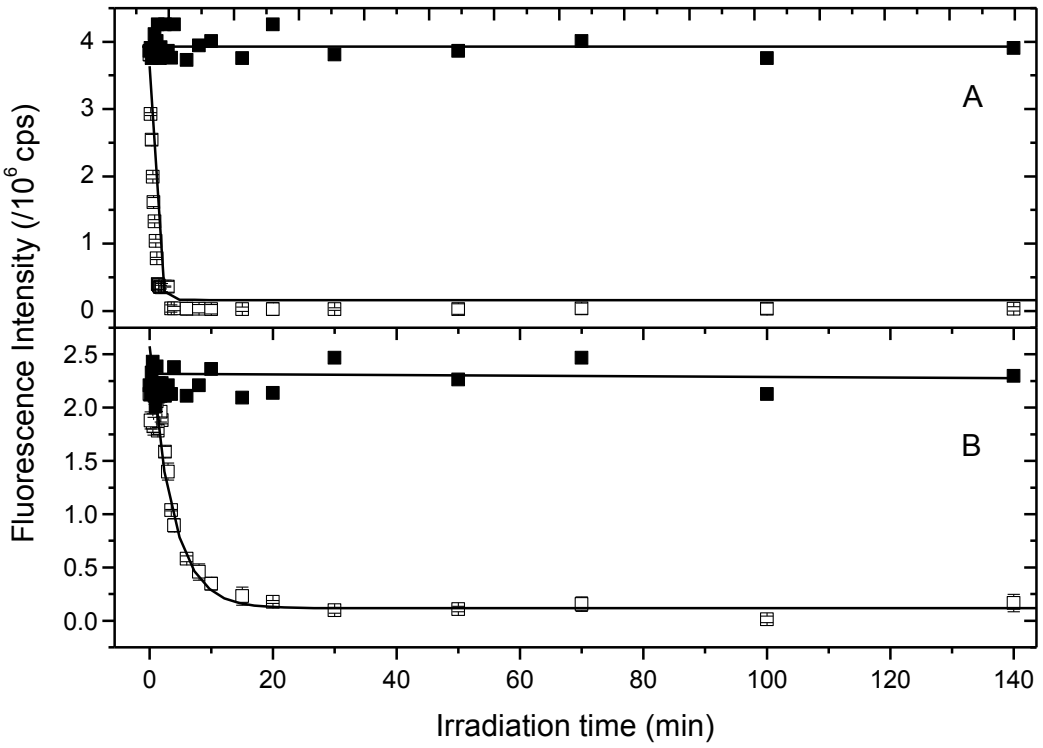

Figure 3.9. Fluorescence intensity as a function of irradiation time for oligonucleotide target (open squares) and unirradiated target control (filled squares) detected by the chMB (A) and DNA MB (B). Only the 2 μM T_{m0} target was irradiated. Aliquots of the irradiated target were mixed with 200 nM MB (10 mM Tris, 3 mM $MgCl_2$, 20 mM NaCl, 1 mM EDTA, pH 7.5) and the fluorescence at 520 nm of these mixtures were then measured. The solid line through the irradiated sample points (open squares) is a single exponential fit to the equation $I_F = I_{F,0} + A\ e^{-t/\tau}$ where $\tau = 0.62 \pm 0.02$ min, $I_{F,0} = 0.16 \pm 0.02 \times 10^6$, and $A = 3.5 \pm 0.1 \times 10^6$ for the chMB (A), and $\tau = 3.59 \pm 0.2$ min, $I_{F,0} = 0.12 \pm 0.04 \times 10^6$, and $A = 2.5 \pm 0.1 \times 10^6$ for the DNA MB (B). The control points (filled squares) are fit to straight lines of zero slope by eye.

Table 3.2. Damage constants of the different DNA damage assay methods.

Method	Damage constant (min)[a]
chMB fluorescence	$\tau = 0.62 \pm 0.02$
DNA MB fluorescence	$\tau = 3.6 \pm 0.20$
Absorbance	$\tau_1 = 6.1 \pm 0.07$
	$\tau_2 = 92 \pm 2.00$

[a]The damage constants (τ) were obtained from the exponential fits in Figure 3.9.

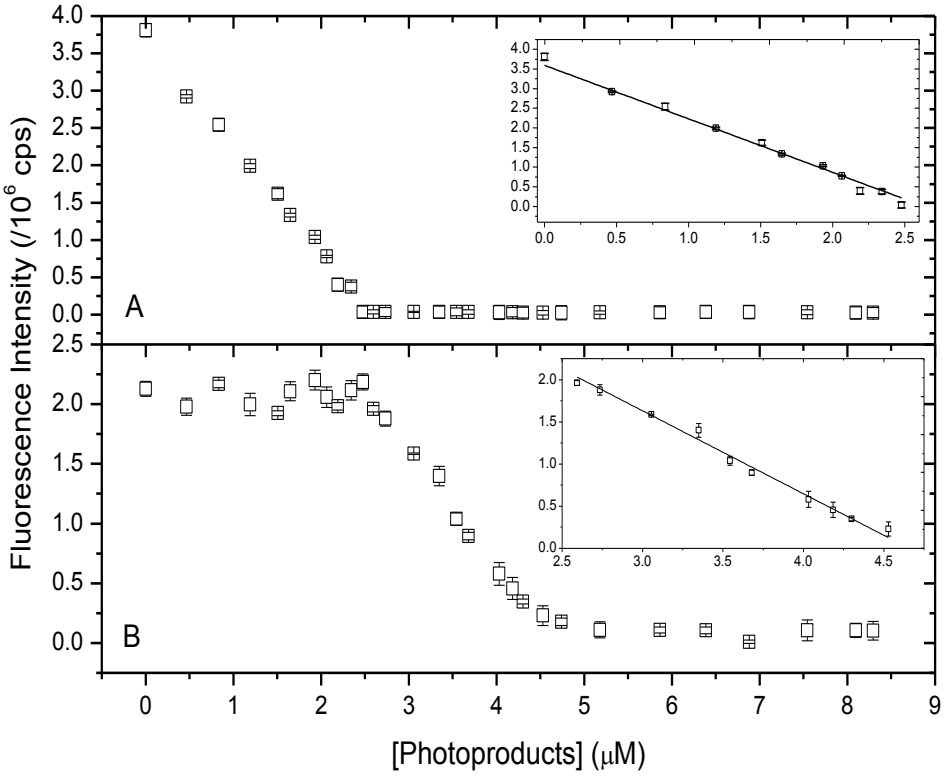

Figure 3.10. Calibration curve of DNA photodamage formed upon UV irradiation of the T_{m0} target for the (A) chMB and (B) DNA MB. The inset shows the fit to the linear portions of the calibration curves. Each data point is an average of three replicate measurements and the error bars correspond to the standard deviation of the measurements.

the MBs and the damaged strands are completely unstable, and the MBs acquire the hairpin structure with quenched fluorescence. Additional formation of photoproducts cannot lead to any more dehybridization, so the fluorescence signal remains constant at a minimum value. Consistent with Figures 3.4 and 3.9, the chMB fluorescence decreases immediately as the photoproducts concentration increases, while the DNA MB (Figure 3.10B) fluorescence signal requires a 2.6 μM concentration of the photoproducts before decreasing. The DNA MB shows even lower selectivity for the detection of DNA damage compared to detecting mismatches (Figure 3.7B).

Table 3.1 shows the parameters for the quantification of UV-induced DNA damage from Figure 3.10. The calibration curve for chMB shows a larger linear dynamic range than that of DNA MB (Figure 3.10). The sensitivity of detection also is larger by a factor of ~1.5 for the chMB, leading to a lower limit of detection (LOD) and limit of quantification (LOQ) by 5 times. It is worth mentioning that values recorded in Table 3.1 for the LOD and LOQ for the DNA MB method for the detection of DNA damage were obtained by using the standard deviation of the blank measurements and the sensitivity of the method, while the LOD and LOQ will be practically limited to ~2.6 μM (Figure 3.10B) due to the unvarying fluorescence signal of the DNA MB at low photoproduct concentrations. From this data, we calculate that the chMB can detect one damage site in the presence of ~4000 undamaged sites.

These results conclusively show that the chMB is a sensitive tool for the detection of nucleic acids and can be applied in the detection and quantification of single-stranded DNA, single base mismatches and UV-induced DNA damage. The RNA nucleotides incorporated in the MB loop increased the stability of the hybrids formed between the chMB and the oligonucleotide targets compared to that of the DNA MB, allowing the chMB to have superior sensitivity and selectivity compared to the DNA MB. The chMB represents a promising tool for various bioanalytical applications.

3.4. Conclusion

In summary, the assay reported here uses RNA nucleotides in the design of a chimeric RNA-DNA MB as a fluorescence sensor for the detection and quantification of nucleic acids, single base mismatches, and UV-induced nucleic acid damage by taking advantage of the increased stability of the RNA-DNA hybrids over the DNA-DNA hybrids. This method proves to have good sensitivity and selectivity for UVC-induced nucleic acid damage and is superior to the DNA MB.

3.5. References

1) D.M. Jordan, V.E. Ramensky, S.R. Sunyaev, Curr. Opin. Struct. Biol. 20 (2010) 342–350.
2) B.P. Ruzsicska, D.G.E. Lemaire, In DNA Photochemistry, CRC Handbook of Organic Photochemistry and Photobiology, P.-S. Horspool, W.M. Song, Eds., CRC Press, New York (1995) pp 1289.
3) L. Marrot, J. R. Meunier, J. Am. Acad. Dermatol. 58 (2008) S139 – S148.
4) T. Lindahl, Nature 362 (1993) 709 -715.
5) L.J. Marnett, B.C. Burcham, Chem. Res. Toxicol. 6 (1993) 771- 785.
6) B.N. Ames, L.S. Gold, W.C. Willett, Proc. Natl. Acad. Sci. U.S.A. 92 (1995) 5258 - 5265.
7) Z.E. Sauna, C. Kimchi-Sarfaty, Nature Rev. Genet. 12 (2011) 683-691.
8) P.J. Rochette, J.P. Therrien, R. Drouin, D. Perdiz, N. Bastien, E.A. Drobetsky, E. Sage, Nucl. Acids Res. 31 (2003) 2786–2794.
9) M. Weinfeld, K.-J. M. Soderlind, Biochemistry 30 (1991) 1091-1097.
10) A. Bromberg, E.C. Jensen, J. Kim, Y.K. Jung, R.A. Mathies, Anal. Chem. 84 (2012) 963–970.
11) X.C. Le, J.Z. Xing, J. Lee, S.A. Leadon, M. Weinfeld, Science 280 (1998) 1066-1069.
12) J. Wang, G. Rivas, M. Ozsoz, D.H. Grant, X. Cai, C. Parrado, Anal. Chem. 69 (1997) 1457-1460.

13) K. Kerman, M. Vestergaard, N. Nagatani, Y. Takamura, E. Tamiya, Anal. Chem. 78 (2006) 2182–2189.
14) H. Kaur, B. Halliwell, Biochem. J. 318 (1996) 21-23.
15) T. Douki, M. Court, S. Sauvaigo, F. Odin, J. Cadet, J. Biol. Chem. 275 (2000) 11678-11685.
16) T. Douki, J. Cadet, Biochemistry 40 (2001) 2495-2501.
17) J.-L. Ravanat, T. Douki, J. Cadet, J. Photochem. Photobiol. B: Biol. 63 (2001) 88-102.
18) F. Totsingan, S. Rossi, R. Corradini, T. Tedeschi, S. Sforza, A. Juris, E. Scaravelli, R. Marchelli, Org. Biomol. Chem. 6 (2008) 1232-1237.
19) A. Kumar, M.B. Tyagi, P.N. Jha, Biochem. Biophys. Res. Commun. 318 (2004) 1025-1030.
20) C.C. Trevithick-Sutton, L. Mikelsons, V. Filippenko, J.C. Scaiano, Photochem. Photobiol. 83 (2007) 556-562.
21) J.Z. Xing, J. Lee, S.A. Leadon, M. Weinfeld, X.C. Le, Methods 22 (2000) 157-163.
22) S. Yarasi, C. McConachie, G.R. Loppnow, Photochem. Photobiol. 81 (2005) 467-473.
23) S.A. Oladepo, G.R. Loppnow, Anal. Bioanal. Chem. 397 (2010) 2949-2957.
24) S.A.E. Marras, F. R. Kramer, S. Tyagi, Nucl. Acids Res. 30 (2002) 122.
25) A.A. Martí, X. Li, S. Jockusch, N. Stevens, Z. Li, B. Raveendra, S. Kalachikov, I. Morozova, J.J. Russo, D.L. Akins, J. Ju, N.J. Turro, Tetrahedron 63 (2007) 3591–3600.
26) C. Liu, L. Wang, W. Jiang, Talanta 81 (2001) 597–601.
27) M.J. Heller, L.E. Morrison, W.D. Prevatt, C. Akin, European Patent Application 70 (1983) 685.
28) L.E. Morrison, L.M. Stols, Biochemistry 32 (1993) 3095–3104.
29) J-L. Mergny, A.S. Boutorine, T. Garestier, F. Belloc, M. Rougée, N.V. Bulychev, A.A. Koshkin, J. Bourson, A.V. Lebedev, B. Valeur, N.T. Thuong, C. Hèléne, Nucl. Acids Res. 22 (1994) 920–928.
30) S.A.E. Marras, S. Tyagi, F.R. Kramer, Clin. Chim. Acta 363 (2006) 48–60.

31) X.H. Peng, Z.H. Cao, J.T. Xia, G.W. Carlson, M.M. Lewis, W.C. Wood, L. Yang, Cancer Res. 65 (2005) 1909–1917.

32) Y. Sei-Iida, H. Koshimoto, S. Kondo, A. Tsuji, Nucl. Acids Res. 28 (2000) e59.

33) S. Sandhya, W. Chen, A. Mulchandani, Anal. Chim. Acta 614 (2008) 208–212.

34) C.J. Yang, C.D. Medley, W.H. Tan, Curr. Pharm. Biotechnol. 6 (2005) 445–452.

35) M.M. Mhlanga, D.Y. Vargas, C.W. Fung, F.R. Kramer, S. Tyagi, Nucl. Acids Res. 33 (2005) 1902-1912.

36) C. Molenaar, S.A. Marras, J.C.M. Slats, J.C. Truffert, M. Lemaitre, A.K. Raap, R.W. Dirks, H.J. Tanke, Nucl. Acids Res. 29 (2001) 89-90.

37) A. Tsourkas, M.A. Behlke, G. Bao, Nucl. Acids Res. 30 (2002) 5168-5174.

38) H. Kuhn, V.V. Demidov, B.D. Gildea, M.J. Fiandaca, J.C. Coull, M.D. Frank-Kamenetskii, Anti. Nucl. Acid Drug Dev. 11 (2001) 265-270.

39) K. Petersen, U. Vogel, E. Rockenbauer, K.V. Nielsen, S. Kolvraa, L. Bolund, B. Nexo, Mol. Cell. Probes 18 (2004) 117-122.

40) C.J. Yang, L. Wang, Y. Wu, Y. Kim, C.D. Medley, H. Lin, W.H. Tan, Nucl. Acids Res. 35 (2007) 4030-4041.

41) J. Perlette, W.H. Tan, Anal. Chem. 73 (2001) 5544–5550.

42) D.A. Braasch, D.R. Corey, Chem. Biol. 8 (2001) 1-7.

43) M. Egholm, P.E. Nielsen, O. Buchardt, R.H. Berg, J. Am. Chem. Soc. 114 (1992) 9677-9678.

44) K.L. Dueholm, M. Egholm, C. Behrens, L. Christensen, H.F. Hansen, T. Vulpius, K.H. Petersen, R.H. Berg, P.E. Nielsen, J. Org. Chem. 59 (1994) 5767-5773.

45) F. Bergmann, W. Bannwarth, S. Tam, Tetrahedron Lett. 36 (1995) 6823-6826.

46) B.D. Gildea, S. Casey, J. MacNeill, H. Perry-O'Keefe, D. Sorensen, J.M. Coull, Tetrahedron Lett. 39 (1998) 7255-7258.

47) T. Shimayama, F. Nishikawa, S. Nishikawa, K. Taira, Nucl. Acids Res. 21 (1993) 2605-2611.

48) M.C. Rice, K. Czymmek, E.B. Kmiec, Nat. Biotechnol. 19 (2001) 321-326.

49) H.B. Gamper, H. Parekh, M.C. Rice, M. Bruner, H. Youkey, E.B. Kmiec, Nucl. Acids Res. 28 (2000) 4332-4339.

50) V.W. Coljee, H.L. Murray, W.F. Donahue, K.A. Jarrell, Nat. Biotechnol. 18 (2000) 789-791.

51) J. Rizzo, L.K. Gifford, X. Zhang, A.M. Gewirtz, P. Lu, Mol. Cell. Probes 16 (2002) 277-283.

52) S.M. Elbashir, J. Harborth, W. Lendeckel, A. Yalcin, K. Weber, T. Tuschl, Nature 411 (2001) 494-498.

53) S. Nakano, T. Kanzaki, N. Sugimoto, J. Am. Chem. Soc. 126 (2004) 1088-1095.

54) M. Weinfeld, M. Liuzzi, M.C. Paterson, Biol. Chem. 264 (1989) 6364-6370.

Chapter 4

2-Aminopurine hairpin probes for the detection of UV-Induced DNA Damage*

4.1. Introduction

Absorption of solar UV radiation by DNA gives rise to photochemical products such as cyclobutane pyrimidine dimers (CPDs), [6-4] pyrimidine-pyrimidinones, dewar pyrimidinones photoproducts and uracil and thymine photohydrates.[1-3] Other damage agents, such as oxidative conditions and ionizing radiation, lead to other DNA lesions, such as single- and double-strand breaks, 8-oxoguanosine and other oxidation products, and cross-links. All these damage products have been implicated in mutagenesis, carcinogenesis and cell death.[4-7]

The sensitive and precise measurement of DNA damage is essential for understanding the lethal and mutagenic effects of UV-induced DNA photoproducts.[3] A number of techniques have been used to detect nucleic acid damage. These include gel electrophoresis,[8] capillary electrophoresis,[9,10] electrochemical,[9-10] HPLC ,[12] mass spectrometric[13-15] and polymerase chain reaction (PCR) amplification[16] methods. While useful, these techniques are destructive and time-consuming. In addition, electrophoretic and chromatographic techniques need to isolate the probe–target hybrids from an excess of unhybridized probes, which include extra steps that may introduce additional lesions.[8]

Other spectroscopic-based techniques have recently been used to characterize nucleic acid damage. Typically, fluorescent methods offer enhanced sensitivity and the potential for use *in situ* or *in vivo*. Differences in the fluorescence lifetime of a dye intercalated in undamaged and damaged DNA have been used to detect

*A version of this chapter has been published: A.F. El-Yazbi, G.R. Loppnow, Anal. Chim. Acta. 726 (2012) 44-49.

DNA damage.[17] Fluorescently-labeled antibodies provide a highly selective probe of particular damage photoproducts, such as thymine cyclobutyl photodimers.[18] More recently, molecular beacons (MBs) have been used for broad-spectrum detection of DNA and RNA damage[3,19] as discussed in Chapters 2 and 3. The inherent sensitivity of fluorescence makes the MBs sensitive probes of nucleic acid damage.

However, despite the wide applications and the exquisite sensitivity and selectivity of MBs, they have some limitations.[20-25] For instance, MBs require site-specific labeling of each terminus of the hairpin with a fluorophore and a quencher, respectively. This dual labeling makes their synthesis and purification difficult and expensive.[20,21,23,25] Since the two termini of the hairpin are already occupied by the donor and acceptor, any further modification, for example, for attachment to a solid support, would require the incorporation of an additional modified nucleotide into the stem.[20,23] Furthermore, due to incomplete attachment of the quencher, some hairpins may only be labeled with the fluorophore. In this case, highly sensitive assays would be affected by a high background due to unquenchable probe molecules.[7,8] Even for those probes that are dually labeled, the sensitivity of the hairpin probe could be detrimentally affected by inefficient FRET, leading to high background signals. Finally, in the presence of a mixture of the undamaged and the damaged target DNA of sequences complementary to the MB loop, the MB hybridizes with the undamaged target. The hybrid formed between the MB and the damaged DNA is destabilized by the damage and the MB will preferentially acquire the hairpin structure, where the fluorophore and the quencher are in close proximity. Thus, the fluorescence intensity decreases with increasing amounts of damage, providing an inversely proportional signal to the amount of damage i.e. negative detection of damage.

The main focus of this chapter is to design a probe in which a fluorescent signal is directly proportional to the amount of DNA damage. Here, we report the incorporation of 2-aminopurine (2AP), a fluorescent base analog of adenine, into a hairpin for detecting DNA damage. This base analogue has been extensively

used in studying protein-DNA interactions and conformational changes during DNA replication,[26-28] and has two useful features. Unlike natural bases, 2AP is fluorescent under normal physiological conditions, and its fluorescence is strongly dependent upon its local environment. While the 2AP base or nucleotide in solution is highly fluorescent, its fluorescence is somewhat quenched in single stranded DNA and highly quenched in double strands, due to base stacking interactions.[29-32] The other desirable feature of 2AP is that it is an excellent analog of adenine, since 2AP forms a Watson–Crick base pair with thymine (T) with minimal disruption of structure.[33] In this work, in order to obtain a detectable fluorescent signal that increases directly with DNA damage, a 2AP hairpin probe (Figure 4.1) is designed. The probe forms a hybrid with the undamaged target and the fluorescence is significantly quenched. Because of the instability of the hybrid formed with the damaged targets, the 2AP hairpins will preferentially acquire the hairpin structure, emitting maximum fluorescence. Thus, the more damaged DNA targets there are in solution, the more 2AP probes will be in the hairpin structure and the higher the fluorescence intensity will be. To our knowledge this study represents the first time 2AP nucleotides have been used to probe nucleic acid damage. Probes with one or two 2AP nucleotides in the loop region were examined in an effort to increase the sensitivity and selectivity of the detection of UV damage comparable to that of the MB probes.

4.2. Experimental

4.2.1. Materials

The single-strand dT_{17} oligonucleotide target, the 2AP hairpin probes and the MB probe (Figure 4.1) were obtained from Integrated DNA Technologies Inc. (Coralville, Iowa) and were purified by standard desalting. The magnesium chloride ($MgCl_2$) and sodium chloride (NaCl) were obtained from EMD Chemicals Inc. (Gibbstown, New Jersey), Tris was obtained from ICN Biomedicals, (Aurora, Ohio) and ethylenediaminetetraacetic acid (EDTA) was obtained from BDH Inc. (Toronto, Ontario), respectively. All chemicals were used as received. Nanopure water from a Barnsted Nanopure (Boston,

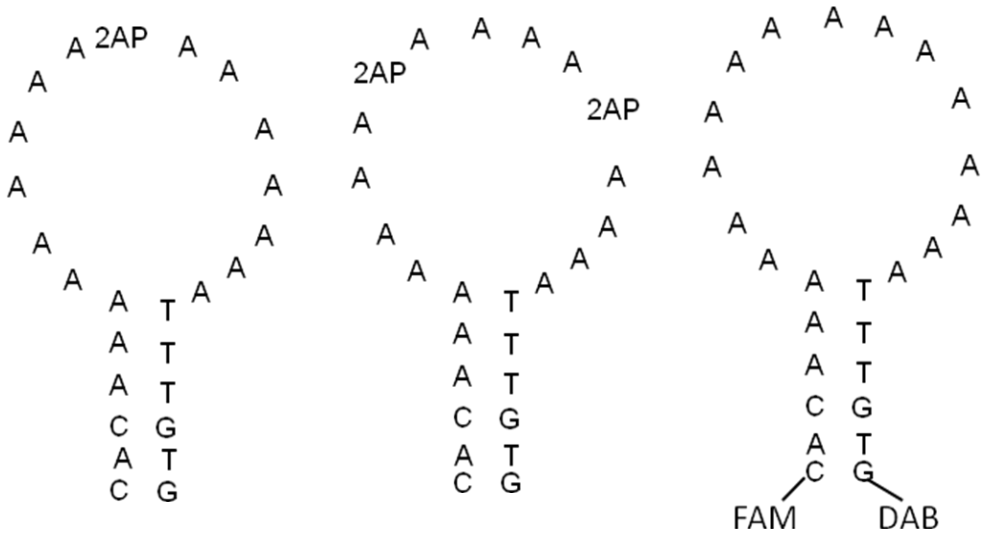

(a) (b) (c)

$2AP^1$ hp probe $2AP^2$ hp probe MB hp probe

Figure 4.1. Sequences of the 2AP hp probes with one 2AP nucleotide (a) $2AP^1$ and two 2AP nucleotides (b) $2AP^2$ in the loop. (c) Sequence of the MB hairpin probe. "2AP" denotes the 2AP nucleotide, "FAM" denotes the 6-carboxyfluorescein fluorophore, and "DAB" denotes the DABCYL quencher.

Massachusetts) system was used for all solutions. The oligonucleotide samples were each dissolved in nanopure water and kept frozen at –20 °C until needed.

4.2.2. UV Irradiation

Nitrogen-purged solutions of 10 μM dT_{17} were irradiated in sealed, UV-transparent 1 cm path length cuvettes. The cuvettes were placed in a water bath also contained in a UV-transparent water dish. The temperature, which was monitored by means of a Cole-Parmer DiGi-SENSE thermocouple (Niles, Illinois), was kept constant throughout the irradiation by the water bath. Oligonucleotide samples were irradiated in a Luzchem (Ottawa, Ontario) DEV photoreactor chamber with UVC light from lamps emitting principally at 254 nm with an irradiation dose of 75011 mW m^{-2}. The samples were constantly stirred during irradiation, and the photoreactor was purged with nitrogen throughout the irradiation to flush out oxygen and any ozone subsequently generated from the UVC lamps. Control samples were handled identically, but were not exposed to UV radiation. The UVC lamps were turned on ~20 min before the start of irradiation to stabilize the lamp output.

4.2.3. Absorption and fluorescence measurements

Absorption spectra were recorded at intervals throughout the irradiation period on a Hewlett-Packard (Sunnyvale, California) 8452A diode array spectrophotometer by placing the irradiated cuvettes containing the target oligonucleotide solutions directly into the spectrophotometer. For the fluorescence measurements, a 10 μL aliquot of each irradiated solution was taken at various time intervals and was later mixed with appropriate amounts of the probe and buffer solution (20 mM Tris, 1 mM EDTA, 3 mM $MgCl_2$, 50 mM NaCl, pH 7.5) to give final concentrations of 1 μM oligonucleotide target and 200 nM 2AP hairpin probe. These solutions were then incubated in the dark at room temperature for about 24 h. Fluorescence spectra of 100 μL aliquots of the incubated hybridization mixtures were measured using a Photon Technologies International (Birmingham, New Jersey) fluorescence system. The spectra were recorded between 310 and

550 nm with excitation at 305 nm. A 1 cm path length Suprasil quartz fluorescence cuvette was used for these measurements.

The 2AP hairpin probe was characterized by a thermal denaturation profile experiment, in which temperature-dependent fluorescence measurements were carried out on a buffered 200 nM solution of the 2AP hairpin probe incubated in the absence or presence of either the target oligonucleotide sequence or the UV-damaged target sequence at 2 μM concentration. The temperature was varied from 10 to 82 °C in 4 °C increments at a heating rate of 1 °C min^{-1} and 5 min settling time for each step of the heating cycle. The reverse was done under the same conditions in order to record the cooling cycle.

4.3. Results and Discussion

The 2AP hairpin was carefully designed to maximize its performance as a sensitive and specific probe to UV-induced nucleic acid damage. This design ensures that the probe can selectively discriminate single damage sites in oligonucleotides. Figure 4.1 demonstrates the structure of the 2AP hairpin probe used in this study. It is composed of a loop region that contains one or two 2AP nucleotides and a stem region composed of six base pairs. The probe is designed such that the oligonucleotide target is complementary to the loop region and three nucleotides in the stem region to avoid sticky end pairing.[34] The design of the probe maximized discrimination of damaged ***versus*** undamaged targets.

4.3.1. Factors affecting 2AP fluorescence

In order to optimize the performance of the 2AP hairpin probe, we studied two factors that are known to affect the 2AP fluorescence.[35,36] We investigated the effect of Mg^{2+} concentration and temperature on the fluorescence of the 2AP in single and double stranded DNA. Figure 4.2 shows the effect of the Mg^{2+} concentration on the fluorescence of 200 nM 2AP hairpin probe alone (single stranded form) and in the presence of undamaged target. When normalized to the fluorescence of the 2AP hairpin probe alone in 1 mM $MgCl_2$, the 2AP hairpin probe at higher Mg^{2+} concentrations show fluorescence that is enhanced by ~1.3

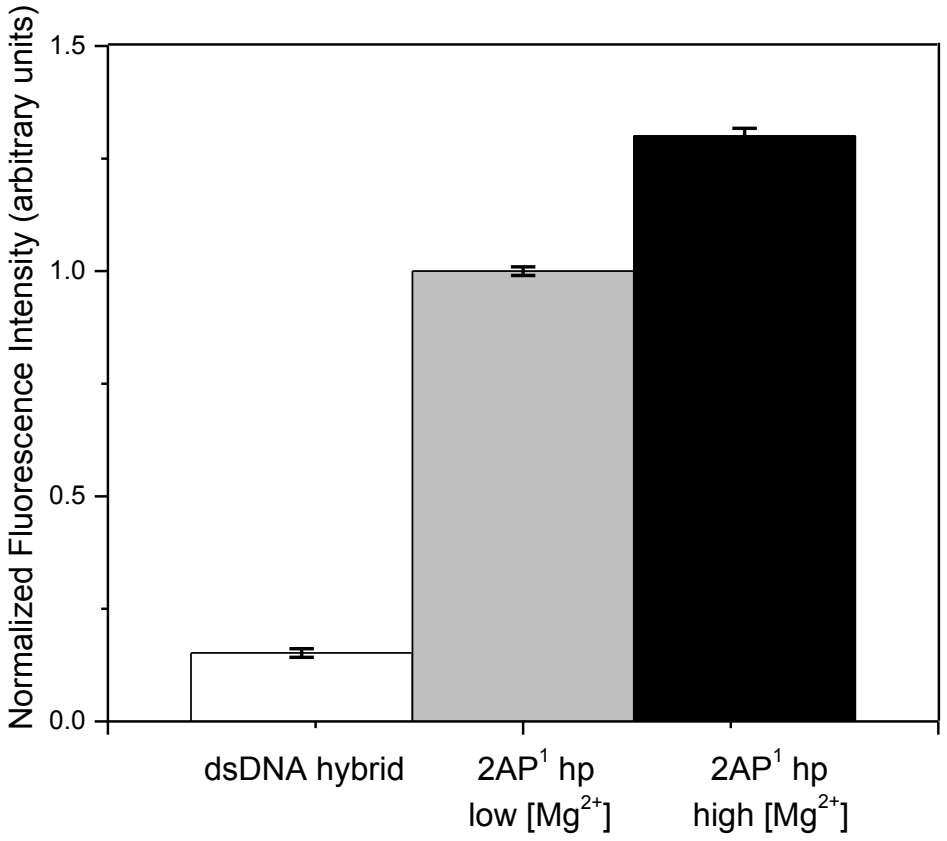

Figure 4.2. Normalized fluorescence intensity at 370 nm of 200 nM $2AP^1$ hairpin probe hybridized with a 10-fold excess of the perfectly complementary oligonucleotide target sequence in 0 to 5 mM $MgCl_2$ (white bar), $2AP^1$ hairpin probe alone in 0 to 1 mM $MgCl_2$ (light gray bar) and in 2 to 5 mM $MgCl_2$ (black bar). All solutions are in 20 mM Tris buffer, 50 mM NaCl and 1mM EDTA adjusted to pH 7.5. Fluorescence excitation wavelength was 305 nm and the spectra were recorded at room temperature.

times. The fluorescence of the duplex hybrid is much lower than in either of the 2AP probes alone and is unaffected by Mg^{2+} concentrations between 0 and 5 mM. Also, Figure 4.3 shows that the fluorescence of 2AP in the hairpin probe is 9 times higher than its fluorescence in the duplex form. As a result, we chose to use 3 mM $MgCl_2$ to benefit from the higher dynamic range and to ensure that there is maximum discrimination between the 2AP hairpin probe in the free form and in the hybrid form with the undamaged target.

To study the effect of temperature on the fluorescence of the 2AP nucleotide in the hairpin probe and in the hybrid with the undamaged target, we measured the fluorescence at 370 nm of 200 nM 2AP hairpin probe alone and in the presence of a 10-fold excess of perfectly complementary oligonucleotide target at temperatures between 10 - 82 $^{\circ}$C. Figure 4.4 shows that the fluorescence of the 2AP hairpin probe alone decreases exponentially with increasing temperature. The lack of a well-defined transition in this melting curve at the stem melting temperature suggests that the 2AP fluorescence is only sensitive to local structure, which is not perturbed in the hairpin-to-random coil transition. For the double-stranded hybrid, the fluorescence of 2AP is quenched at low temperatures and the 2AP fluorescence increases as the temperature increases, i.e. as the hybrid melts. At temperatures greater than 45 $^{\circ}$C, the fluorescence of 2AP in the hybrid essentially overlaps with the 2AP fluorescence of the hairpin probe, as expected. These results suggest that the solution of the hybrid at temperatures above 45 $^{\circ}$C contains the 2AP probe in the random coil structure and not in the double-stranded hybrid structure.

It is worth mentioning here that the trend shown in the thermal denaturation profile for the 2AP hairpin probe alone and in the presence of the target is different from the one expected from MB probes of damage.[3,19,34] At low temperatures, the MB alone exists in the hairpin structure, in which the quencher and the fluorophore are in close proximity and the fluorescence is quenched. At the melting temperature of the stem, the fluorescence will gradually increase with temperature until reaching a plateau, indicating that the distance between the

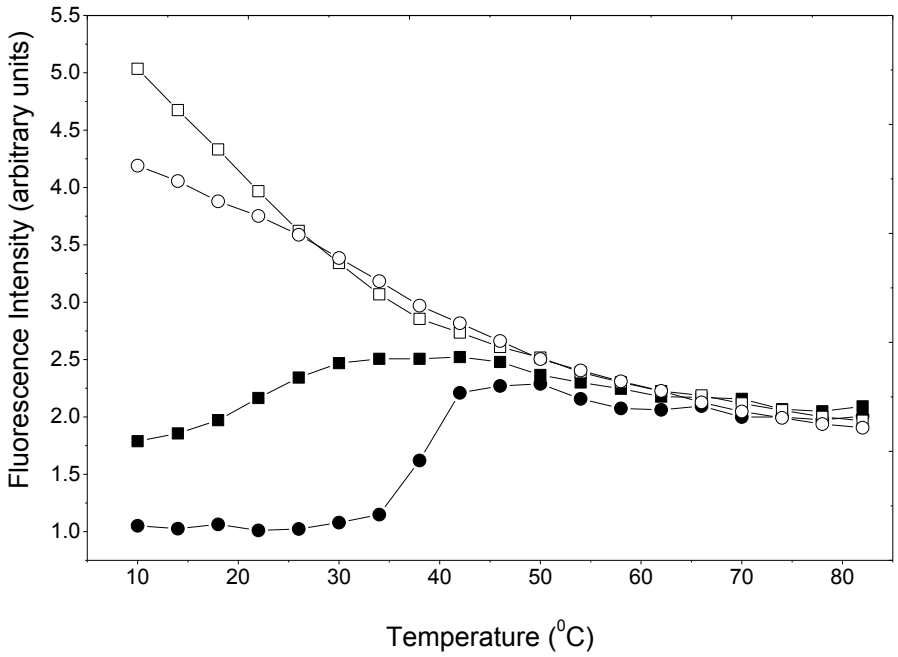

Figure 4.3. Thermal denaturation curves for 200 nM 2AP[1] hairpin probe alone (open squares), 200 nM 2AP[1] hairpin probe in the presence of a 10-fold excess of perfectly complementary oligonucleotide target sequence (filled circles), and 200 nM 2AP[1] hairpin probe in the presence of a 10-fold excess of the UV-irradiated oligonucleotide target sequence for 4 min (filled squares), and for 50 min (open circles). The lines are guides for the eye.

fluorophore and the quencher is constant in the random coil structure.[3] In solutions containing the MB-target hybrid, at low temperatures, the fluorophore and the quencher are far apart and maximum fluorescence is observed. At higher temperatures, the hybrid will melt and the MB will re-form the hairpin, leading to a decrease in fluorescence. At temperatures higher than the stem melting temperature, the MB again forms a random coil and the fluorescence shows the same trend as the MB probe alone.

It is clear that the thermal denaturation profile of the target-2AP hairpin probe hybrid shows an opposite trend to that of the MB probe and this is what allows the 2AP fluorescence signal to increase with increasing damage to the target. This result is demonstrated in Figure 4.3, where the hybrid between the 2AP probe and the oligonucleotide target subjected to UVC light for 4 min shows higher fluorescence intensity than that of the hybrid between the 2AP hairpin and the healthy target. The fluorescence is even higher for the hybrid of the target exposed to UV light for 50 min. Because this last thermal denaturation profile is very close to that of the 2AP probe alone, most of the oligonucleotide targets are damaged with this exposure time and most of the 2AP probes are in the hairpin structure.

As shown in Figure 4.3, there is good discrimination in the fluorescence between the healthy and damaged targets hybridized with the 2AP probe at 20 $^{\circ}$C. Therefore, we have chosen this hybridization temperature for detecting the formation of the UV-induced photoproducts. While the fluorescence at 10 $^{\circ}$C shows a slightly higher discrimination than that at 20 $^{\circ}$C, we chose the 20 $^{\circ}$C temperature as it is much easier to keep the fluorimeter fixed at this temperature.

4.3.2. Detection of UV-induced photoproducts with the 2AP hairpin probes

The target used in this study is dT_{17} because of its well known photochemistry. In this target, CPD is the major photoproduct formed after UV-irradiation, with small amounts of the [6-4] pyrimidine-pyrimidinone and the dewar pyrimidinone photoproducts.[1] Also, the 260 nm absorption band of dT_{17} gradually bleaches with

increasing irradiation time, indicating photoproduct formation and loss of the C_5=C_6 bond.

Similar to Chapter 3, in order to confirm that the change in signal is due to UV-induced damage and not due to any other effect, the dT_{17} oligonucleotide target was irradiated at constant temperature, and the resultant damage was detected by UV-Vis absorption measurements of the irradiated and control samples. Figure 4.4 shows a plot of the absorbance of the oligonucleotide target as a function of irradiation time with UVC light. The 260 nm absorption band, which represents the ππ* transitions of the nucleobases, is seen to decrease with time. This result is expected and indicates UV-induced damage to the oligonucleotides with the consequent loss of the C_5=C_6 bond in all photoproducts formed. This decrease in absorbance is not observed in the unirradiated controls. Therefore, the absorption changes arise from irradiation of the samples and subsequent photochemistry rather than any other effect.

In order to investigate the sensitivity and selectivity of the 2AP probe to detect nucleic acid damage, we measured the fluorescence of aliquots of the irradiated target samples after incubation for 24 h with two 2AP hairpin probes (Figure 4.5), one which has a single 2AP nucleotide ($2AP^1$ probe) and another with two 2AP nucleotides ($2AP^2$ probes) in the loop region of the hairpin probe (Figure 4.1). Aliquots of unirradiated samples of these solutions were also incubated with the 2AP probes as controls. It should be noted that the 2AP probes were not irradiated; they were only incubated with aliquots of irradiated oligonucleotide solutions, as well as their unirradiated controls. The solutions were excited at 305 nm and the fluorescence was recorded at 370 nm. As shown in Figure 4.5, the fluorescence from both 2AP probes increases with UV irradiation and continues to increase with increasing irradiation until it reaches a plateau corresponding to the fluorescence of the unhybridized 2AP hairpin probe. This plateau is reached within the first 10 min of irradiation. This indicates that after 10 min irradiation,

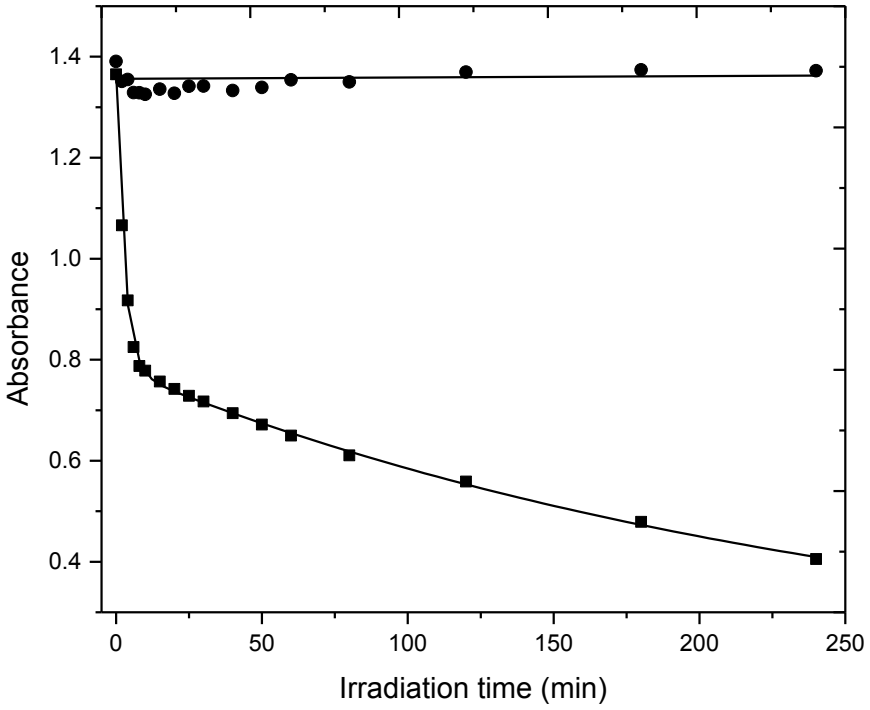

Figure 4.4. Normalized absorbance of 10 μM irradiated target (filled squares) and unirradiated target control (filled circles) monitored at 266 nm as a function of irradiation time. The solid line through the absorbance points (filled squares) is the least-squares fit to an offset, double-exponential function, $A = A_0 + a_1 e^{t/\tau 1} + a_2 e^{t/\tau 2}$, where the absorbance damage constants are 5.77 ± 0.1 min (τ_1) and 81.8 ± 2 min (τ_2), and the amplitudes are $a_1 = 0.51 \pm 0.01$ min^{-1} and $a_2 = 0.41 \pm 0.01$ min^{-1}. The offset (A_o) is 0.09± 0.01. The control points (filled circles) are fit by eye.

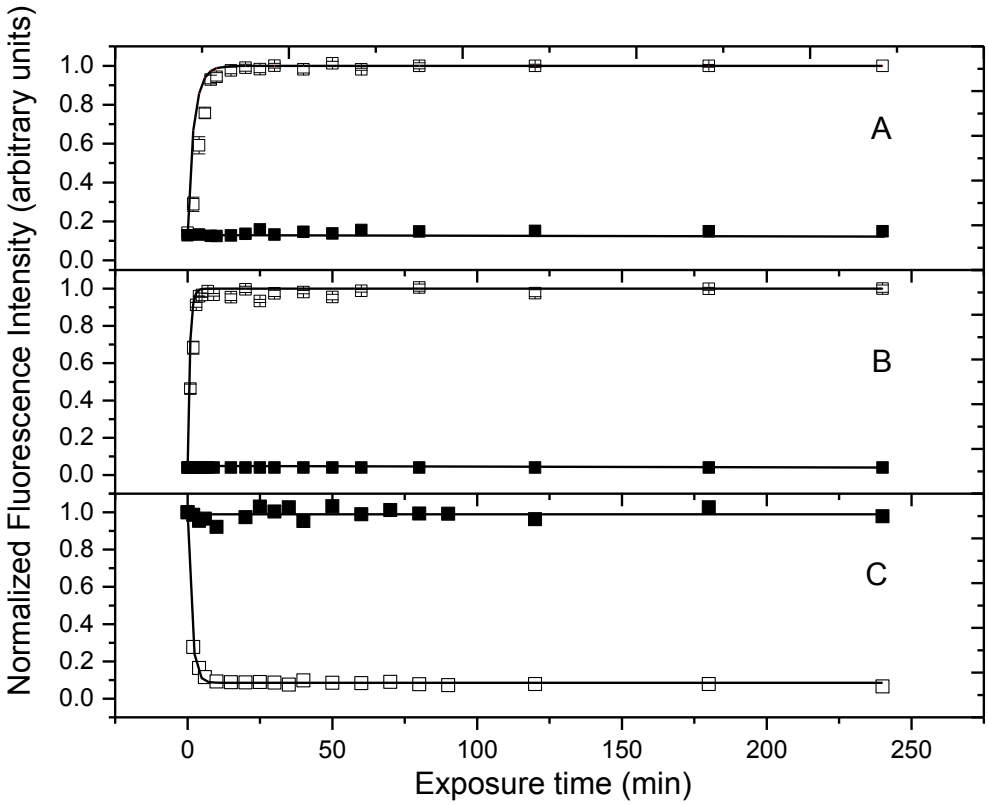

Figure 4.5. Normalized fluorescence intensity as a function of irradiation time for the oligonucleotide target (open squares) and unirradiated target control (filled squares). Only the 1 μM poly dT_{17} target was irradiated and the damage was detected by the $2AP^1$ hairpin probe (A), $2AP^2$ hairpin probe (B) and MB probe (C). Aliquots of the irradiated target were mixed with 200 nM probe (20 mM Tris, 3 mM $MgCl_2$, 50 mM NaCl, 1 mM EDTA, pH 7.5), and the fluorescence of these mixtures were then measured. The 2AP hairpin probes were excited at 305 nm and the fluorescence emission was monitored at 370 nm, while the MB probe was excited at 495 nm and the fluorescence emission was monitored at 520 nm. The solid line through the irradiated sample fluorescence points (open squares) is a single exponential fit. The 2AP probe fluorescence is fit by $I_F = I_{F,0} + a\,(1 - e^{-t/\tau})$, where (A) $I_{F,0} = 0.18 \pm 0.01$, $a = 0.77 \pm 0.01$, and $\tau = 4.31 \pm 0.2$ min, and (B) $I_{F,0} = 0.09 \pm 0.01$, $a = 0.91 \pm 0.01$, and $\tau = 0.80 \pm 0.01$ min. The MB fluorescence decay (C) is fit by $I_F = I_{F,0} + a\,e^{-t/\tau}$ where $\tau = 1.34 \pm 0.1$ min, $I_{F,0} = 0.08 \pm 0.01$, and $a = 0.91 \pm 0.01$, The controls (filled squares) are fitted by eye.

the entire oligonucleotide target is damaged, the entire 2AP probe is in the hairpin form, and the probes exhibit their maximum fluorescence signal.

The plot of absorbance as a function of irradiation time for oligonucleotide target (Figure 4.4) was fit to a double-exponential function while the fluorescence curves (Figure 4.5) are fit to a single exponential function. This decay in the absorbance represents the formation of thymine photoproducts containing saturated C_5-C_6 bonds, and can be correlated to the concentration of the damage products (see below). The increase in the fluorescence intensity represents the decreased stability of the damaged target-2AP hybrid. Therefore, the faster the fluorescence intensity increases, the more selective the probe is at detecting UV-induced oligonucleotide damage under identical irradiation conditions for the same target.

This method for the detection of UV-induced nucleic acid damage by the 2AP hairpin probes was compared to the MB probes capability to detect UV-induced damage. The MB probe (Figure 4.1) used in this study was designed to the same sequence as the 2AP probe, with an adenine base replacing the 2AP base. In addition, a FAM fluorophore was attached to the 5'- end and a DABCYL quencher was attached to the 3'-end. As explained previously, the fluorescence is quenched in the hairpin position when the FAM and DABCYL are in close proximity, and the fluorescence intensity is high in the presence of complementary target when the MB forms a hybrid with the target. As damage accumulates on the target strand, the MB-target hybrid becomes less stable, effectively decreasing the fluorescence intensity until the closed, hairpin form is the more stable form of the MB. This trend is shown in Figure 4.5C, in which the MB fluorescence intensity decreases with longer irradiation time until reaching a constant minimum corresponding to the fluorescence of the MB in the hairpin structure. The fluorescence curve was fit to a single exponential function, as before. The damage constants obtained by the 3 probes are shown in Table 4.1 for both the MB and 2AP hairpin methods for detecting DNA damage. It is clear

Table 4.1. Damage constants of the irradiation experiments

Method[a]	***Damage constant (min)***
2AP1 probe	4.31 ± 0.2
2AP2 probe	0.80 ± 0.02
MB probe	1.34 ± 0.1
Absorbance	τ_1 = 5.77 ± 0.1
	τ_2 = 81.8 ± 2

[a]The damage constants (τ) represent the fluorescence decay or the absorbance decay with increasing irradiation time.

from Table 4.1 that the rate of absorption decay is slower than the rate of the increase of the 2AP fluorescence and the rate of decrease of the MB fluorescence. This indicates the lower selectivity of the absorbance measurements.[19] Table 4.1 also shows that the $2AP^1$ hairpin probe has damage constant slightly higher than that of the MB probe which indicates that it has lower selectivity to detect DNA damage. However, upon addition of another 2AP nucleotide in the hairpin loop, the damage constant decreases by 5 times (Table 4.1). This indicates an increase in the selectivity of damage detection. This allows the $2AP^2$ probe to have superior selectivity for detection of UV damage in nucleic acids compared to absorption and the MB probe.

In order to check the effect of the second 2AP nucleotide on the sensitivity of the 2AP probe for damage detection, we used the UV absorbance measurements as a function of UV irradiation time to quantify the amount of UV damage and to develop calibration curves for the 2AP hairpin probes. Formation of a single CPD in dT_{17} results in the bleaching of two thymine nucleobases due to the loss of the C_5=C_6 absorbance in the two thymine bases.[1] However, the formation of a single [6,4] photoproduct or a dewar pyrimidinone photoproduct is accompanied by the loss of only one of the C_5=C_6 bond of the two thymine bases forming the photoproduct.[1] Therefore, in order to deduce the concentration of the photoproducts formed upon irradiation at different time intervals from the absorbance measurements, a weighted average of the photoproducts must be estimated. The weighted average was calculated using the percentage of CPD (77%), [6-4] pyrimidine-pyrimidinone (20%) and dewar pyrimidinone (0.8%) photoproducts formed upon UVC irradiation.[1] Figure 4.6 shows the calibration curve obtained upon plotting the 2AP fluorescence intensity as a function of the total concentration of the photoproducts calculated for both the $2AP^1$ and $2AP^2$ probes. The fluorescence at zero concentration of the photoproducts represents the background level corresponding to the quenched fluorescence of the 2AP hairpin probe when it is completely hybridized with the healthy target. At high damage concentrations, the hybrid formed between the 2AP hairpin probe and the

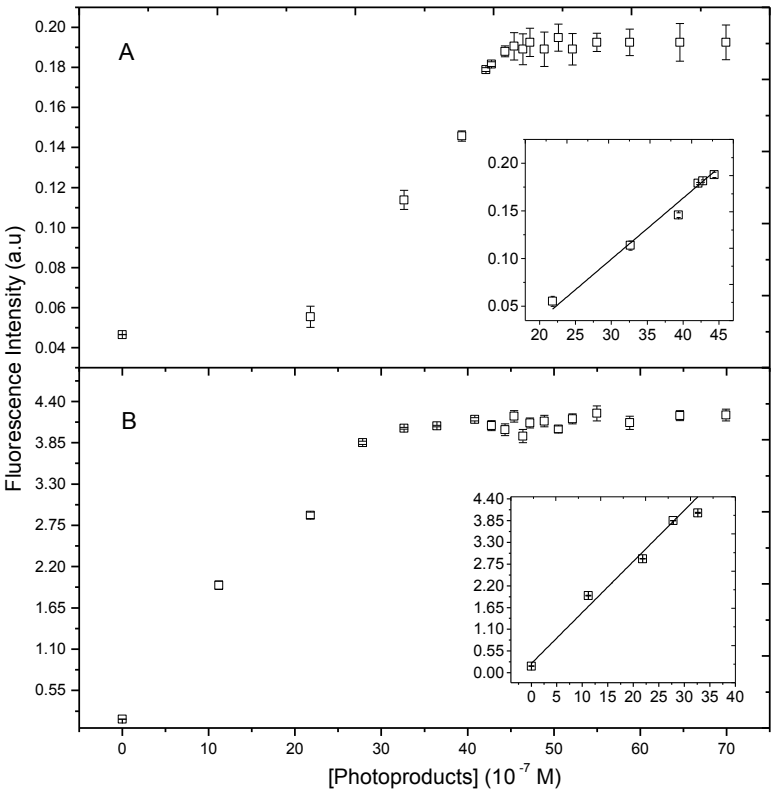

Figure 4.6. Calibration curve of DNA photodamage formed upon UV irradiation of the poly dT_{17} target for the (A) $2AP^1$ and (B) $2AP^2$ probes. Inset shows the fit to the linear portions of the calibration curves. Each data point is an average of three replicate measurements and the error bars correspond to the relative standard deviation of the measurements.

Table 4.2. Analytical parameters for the quantification of UV-induced DNA damage by the two 2AP probes

Parameter[a]	**2AP[1] probe**	**2AP[2] probe**
Linear Dynamic Range	2.0 – 4.5 μM	0 – 3.5 μM
R^2	0.988	0.982
Sensitivity	6.3×10^8 M^{-1}	1.2×10^{10} M^{-1}
LOD	960 nM	17.2 nM
LOQ	3197 nM	57.23 nM

The blank used is the 2AP hairpin probes hybridized with the undamaged target. 20 blank solutions were used, with excitation at 305 nm and the fluorescence emission was measured at 370 nm. The standard deviations of these measurements were obtained and were used in the calculation of LOD and LOQ.

[a]In this table, Linear Dynamic Range is the concentration range corresponding to the linear region in the calibration curve, R^2 is the linear regression coefficient squared, Sensitivity is the slope of the calibration curve, LOD is the limit of detection and is 3 times the standard deviation of the blank divided by the sensitivity, LOQ is the limit of quantification and is 10 times the standard deviation of the blank divided by the sensitivity.

damaged strand is completely unstable, and the 2AP probe acquires the hairpin structure with maximum fluorescence. Additional formation of photoproducts does not lead to any more dehybridization, so the fluorescence signal shows saturation-like behaviour.

Table 4.2 shows the parameters for the quantification of UV-induced DNA damage from Figure 4.6. The calibration curve for the $2AP^2$ probe shows a larger linear dynamic range than the $2AP^1$ probe (Figure 4.6). The sensitivity of detection also increases by 2 orders of magnitude for the $2AP^2$ probe and this leads to a higher signal-to-noise ratio with a lower limit of detection (LOD) and limit of quantitation (LOQ) by 50 times.

These results conclusively show that the 2AP hairpin probe is a sensitive tool to detect UVC-induced oligonucleotide damage. The more 2AP nucleotides incorporated in the probe, the more the sensitivity and selectivity of the 2AP probes appears to be enhanced, allowing these probes to have superior selectivity compared to the MB probes. The 2AP hairpin probes also have the advantages of being easier to synthesize. The 2AP hairpin probe represents a promising tool in the design of biosensors for the *in vivo* detection of nucleic acid damage.

4.4. Conclusion

In summary, the assay reported here uses 2AP nucleotides in the design of a hairpin probe as a fluorescence sensor for the quantification of UVC-induced nucleic acid damage, by taking advantage of the unique quenching of 2AP fluorescence intensity in dsDNA. The fluorescence sensor shows good sensitivity and selectivity for UVC-induced nucleic acid damage. Moreover, the addition of a second 2AP nucleotide in the loop region of the probe significantly increases the sensitivity and decreases the LOD to detect UVC-induced DNA damage.

4.5. References

1) B.P. Ruzsicska, D.G.E. Lemaire, In DNA Photochemistry, CRC Handbook of Organic Photochemistry and Photobiology, P.-S. Horspool, W.M. Song, Eds., CRC Press, New York (1995) pp 1289.
2) D.M. Wagner, G.R. Loppnow, Spectrum 17 (2004) 26-29.
3) S. Yarasi, C. McConachie, G.R. Loppnow, Photochem. Photobiol. 81 (2005) 467-473.
4) L. Marrot, J.R. Meunier, J. Am. Acad. Dermatol. 58 (2008) S139 – S148.
5) T. Lindahl, Nature 362 (1993) 709 -715.
6) L.J. Marnett, P.C. Burcham, Chem. Res. Toxicol. 6 (1993) 771- 785.
7) B.N. Ames, L.S. Gold, W.C. Willett, Proc. Natl. Acad. Sci. U.S.A. 92 (1995) 5258 - 5265.
8) M. Weinfeld, K.-J.M. Soderlind, Biochemistry 30 (1991) 1091-1097.
9) B.B. Haab, R.A. Mathies, Anal. Chem. 67 (1995) 3253-3260.
10) X.C. Le, J.Z. Xing, J. Lee, S.A. Leadon, M. Weinfeld, Science 280 (1998) 1066-1069.
11) J. Wang, G. Rivas, M. Ozsoz, D.H. Grant, X. Cai, C. Parrado, Anal. Chem. 69 (1997) 1457-1460.
12) H. Kaur, B. Halliwell, Biochem. J. 318 (1996) 21-23.
13) T. Douki, M. Court, S. Sauvaigo, F. Odin, J. Cadet, J. Biol. Chem. 275 (2000) 11678-11685.
14) T. Douki, J. Cadet, Biochemistry 40 (2001) 2495-2501.
15) J.-L. Ravanat, T. Douki, J. Cadet, J. Photochem. Photobiol. B: Biol. 63 (2001) 88-102.
16) A. Kumar, M.B. Tyagi, P.N. Jha, Biochem. Biophys. Res. Commun. 318 (2004) 1025-1030.
17) C.C. Trevithick-Sutton, L. Mikelsons, V. Filippenko, J.C. Scaiano, Photochem. Photobiol. 83 (2007) 556-562.
18) J.Z. Xing, J. Lee, S.A. Leadon, M. Weinfeld, X.C. Le, Methods 22 (2000) 157-163.
19) S.A. Oladepo, G.R. Loppnow, Anal. Bioanal. Chem. 397 (2010) 2949-2957.

20) K. Stohr, B. Hafner, O. Nolte, J. Wolfrum, M. Sauer, D.-P. Herten, Anal. Chem. 77 (2005) 7195-7203.
21) J.-P. Knemeyer, N. Marme, M. Sauer, Anal. Chem. 72 (2000) 3717-3724.
22) A. Misra, P. Kumar, K.C. Gupta, Anal. Biochem. 364 (2007) 86-88.
23) T. Heinlein, J.-P. Knemeyer, O. Piestert, M. Sauer, J. Phys. Chem. B 107 (2003) 7957-7964.
24) Y. Kim, C.J. Yang, W. Tan, Nucl. Acids Res. 35 (2007) 7279-7287.
25) A. Misra, M. Shahid, Bioorg. Med. Chem. 17 (2009) 5826-5833.
26) U. Subuddhi, M. Hogg, L.J. Reha-Krantz, Biochemistry 47 (2008) 6130-6137.
27) D. Tleugabulova, L.J. Reha-Krantz, Biochemistry 46 (2007) 6559-6569.
28) M.A. O'Neill, J.K. Barton, J. Am. Chem. Soc. 124 (2002) 13053-13066.
29) D.C. Ward, E. Reich, L. Stryer, J. Biol. Chem. 244 (1969) 1228 –1237.
30) E.L. Rachofsky, R. Osman, J.B.A. Ros, Biochemistry 40 (2001) 946 – 956.
31) L.B. Bloom, M.R. Otto, R. Eritja, L.J. Reha-Krantz, M.F. Goodman, J.M. Beechem, Biochemistry 33 (1994) 7576 –7685.
32) L.B. Bloom, M.R. Otto, J.M. Beechem, M.F. Goodman, Biochemistry 32 (1993) 11247 –11258.
33) L.C. Sowers, G.V. Fazakerley, R. Eritja, B.E. Kaplan, M.F. Goodman, Proc. Natl. Acad. Sci. U.S.A. 83 (1986) 5434–5438.
34) C.J. Yang, L. Wang, Y. Wu, Y. Kim, C.D. Medley, H. Lin, W.H. Tan, Nucl. Acids Res. 35 (2007) 4030-4041.
35) C.R. Guest, R.A. Hochstrasser, L.C. Sowers, D.P. Millar, Biochemistry 30 (1991) 3271-3279.
36) E.L. Rachofsky, E. Seibert, J.T. Stivers, R. Osman, J.B.A. Ros, Biochemistry 40 (2001) 957-967.

Chapter 5

A Selective, Inexpensive Probe for UV-Induced Damage in Nucleic Acids*

5.1. Introduction

Absorption of solar UV radiation by DNA gives rise to photochemical products such as cyclobutane pyrimidine dimers (CPDs), [6-4] pyrimidine pyrimidinones, dewar pyrimidinones, and uracil and thymine photohydrates.[1-3] Other damage agents, such as oxidative conditions and ionizing radiation, lead to other DNA lesions, such as single- and double-strand breaks, 8-oxoguanosine and cross-links. All these damage products have been implicated in mutagenesis, carcinogenesis and cell death.[4-7]

The precise measurement of DNA damage is essential for understanding the lethal and mutagenic effects of UV-induced DNA photoproducts.[3] A number of techniques have been used to detect nucleic acid damage. These include gel electrophoresis,[8] capillary electrophoresis,[9,10] electrochemical,[9,11] HPLC,[12] mass spectrometric[13-15] and polymerase chain reaction (PCR) amplification[16] methods. While useful, these techniques are destructive and time-consuming. In addition, electrophoretic and chromatographic techniques need to isolate the probe–target hybrids from an excess of unhybridized probes, which include extra steps that may introduce additional lesions.[8]

Other spectroscopic techniques have recently been used to characterize nucleic acid damage. Typically, fluorescent methods offer enhanced sensitivity and the potential for use *in situ* or *in vivo*. Differences in the fluorescence lifetime of a dye intercalated in undamaged and damaged DNA have been used to detect DNA damage.[17] Fluorescently-labeled antibodies provide a highly selective probe of specific damage photoproducts, such as thymine cyclobutane pyrimidine

---

*A version of this chapter has been published: A.F. El-Yazbi, G.R. Loppnow, Canadian Journal of Chemistry, published on the web 10 December 2012, 10.1139/cjc-2012-0417.

photodimers.[18] More recently, molecular beacons (MBs) have been used for broad-spectrum detection of DNA and RNA damage.[3,19] The inherent sensitivity of fluorescence makes the MBs sensitive probes of nucleic acid damage. However, despite the wide applications and the exquisite sensitivity and selectivity of MBs, they have some limitations.[20-25] For instance, MBs require site-specific labeling of each terminus of the hairpin with a fluorophore and a quencher, respectively. This dual labeling makes their synthesis and purification difficult and expensive.[20,21,23,25] Since the two termini of the hairpin are already occupied by the donor and acceptor, any further modification - for example, for attachment to a solid support - would require the incorporation of an additional modified nucleotide into the stem.[20,23] Furthermore, due to incomplete attachment of the quencher, some hairpins may only be labeled with the fluorophore. In this case, highly sensitive assays would be affected by a high background due to unquenchable probe molecules.[7,8] Finally, in the presence of a mixture of undamaged and damaged DNA, the MB hybridizes only with the undamaged target. Thus, the fluorescence intensity decreases with increasing amounts of damage, providing an inversely proportional signal to the amount of damage, i.e. negative detection of DNA damage.

The main focus of this work is to design an inexpensive alternative to MB probes, in which the produced signal is directly proportional to the amount of DNA damage (positive detection of DNA damage). We have previously reported a method for the positive detection of DNA damage using a 2-aminopurine (2AP) hairpin probe as discussed in Chapter 4. Using 2AP hairpins to detect damage offers high sensitivity and selectivity, and they have overcome most of the MB probe limitations. However, the 2AP hairpin probes are expensive, especially with an increasing number of 2AP nucleobases incorporated in the probe. In this chapter, we will present a less expensive alternative for the positive detection of DNA damage based on a hybridization assay coupled with the hypochromic effect.

The hypochromic effect is a well known phenomenon in nucleic acids. [26,27] It is the lowering of the absorbance in the ultraviolet absorption spectrum which is associated with the better stacking of purine and pyrimidine residues in double-stranded oligonucleotides compared to single-stranded ones. Measurements of hypochromism have been used frequently to study the secondary structure of polynucleotides[28,29] and the stability of naturally occurring and synthetic DNA structures.[30] In this work, a detectable signal is obtained which increases directly with increasing DNA damage by using a hairpin probe (Figure 5.1). The probe forms a hybrid with the undamaged target and the absorbance signal is significantly decreased. Because of the increased instability of the hybrid when damaged, the probe will preferentially dehybridize from the target and acquire the hairpin structure, increasing the concentration of single stranded damaged target and increasing the absorbance signal. Thus, the more damaged targets in the solution, the lower the number of double-stranded hybrids and the higher the absorbance signal.

The target oligonucleotide used in this study is dT_{17} because of its well-known photochemistry. In this target, CPD is the major photoproduct formed after UV-irradiation, with small amounts of the [6-4] pyrimidine pyrimidinone and the dewar pyrimidinone photoproducts.[1] Also, the 260 nm absorbance band of dT_{17} gradually bleaches with increasing irradiation time, indicating photoproduct formation and loss of the C_5=C_6 bond yielding an independent spectroscopic marker for DNA damage. Thus, the loss of the 260 nm absorbance band can be directly related to the concentration of the photoproducts formed. Furthermore, it has been reported that a tripyrimidine stretch represents a hot spot for UV-induced DNA damage.[32] To our knowledge, this study represents the first time DNA hypochromism is used to probe nucleic acid damage. The performance of the DNA hypochromism probe to detect UV-induced DNA damage was examined and compared to DNA MBs.

5.2. Experimental

5.2.1. Materials

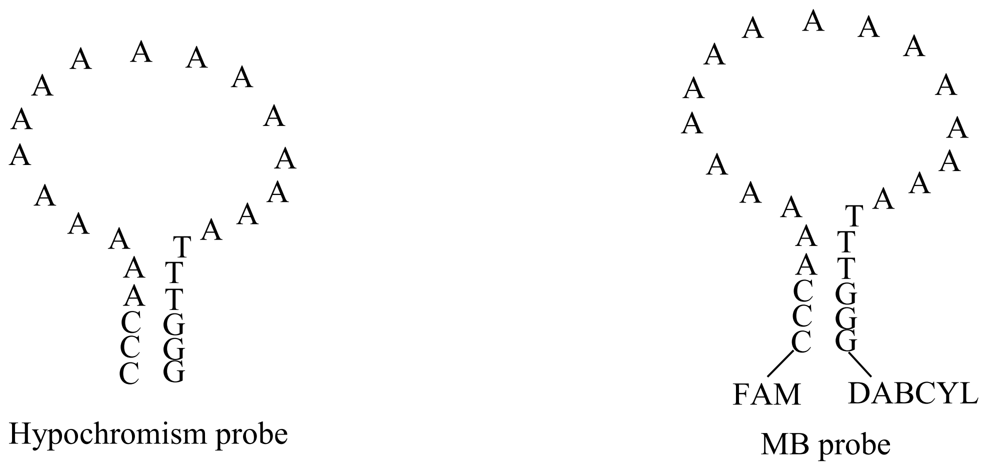

Figure 5.1. Sequences of the hypochromism hairpin and MB probes. “FAM” denotes the 6-carboxyfluorescein fluorophore, and “DAB” denotes the DBCYL quencher.

The single-strand dT_{17} oligonucleotide target, the hypochromism hairpin probe and the MB probe (Figure 5.1) were obtained from Integrated DNA Technologies Inc. (Coralville, Iowa) and purified by standard desalting. The MB was further purified with HPLC. The magnesium chloride ($MgCl_2$) and sodium chloride (NaCl) were obtained from EMD Chemicals Inc. (Gibbstown, New Jersey), Tris was obtained from ICN Biomedicals, (Aurora, Ohio) and ethylenediaminetetraacetic acid (EDTA) was obtained from BDH Inc. (Toronto, Ontario). All chemicals were used as received. Nanopure water from a Barnsted Nanopure (Boston, Massachusetts) system was used for all solutions. The oligonucleotide samples were each dissolved in nanopure water and kept frozen at –20 °C until needed.

5.2.2. UV-Irradiation

Nitrogen-purged solutions of 10 μM dT_{17} were irradiated in sealed, UV-transparent 1 cm path length cuvettes. The cuvettes were placed in a water bath also contained in a UV-transparent water dish. The temperature, which was monitored by means of a Cole-Parmer DiGi-SENSE thermocouple (Niles, Illinois), was kept constant throughout the irradiation by the water bath. Oligonucleotide samples were irradiated in a Luzchem (Ottawa, Ontario) DEV photoreactor chamber with UVC light from lamps emitting principally at 254 nm with a power density of 75 W m^{-2}. The samples were constantly stirred during irradiation, and the photoreactor was purged with nitrogen throughout the irradiation to flush out oxygen and any ozone subsequently generated from the UVC lamps. Control samples were handled identically, but were not exposed to UV radiation. The UVC lamps were turned on ~20 min before the start of irradiation to stabilize the lamp output.

5.2.3. Absorbance and fluorescence measurements

Absorption spectra were recorded at intervals throughout the irradiation period on a Hewlett-Packard (Sunnyvale, California) 8452A diode array spectrophotometer by placing the irradiated cuvettes containing the target oligonucleotide solutions directly into the spectrophotometer. For the hypochromism measurements, a 50

μL aliquot of each irradiated solution was taken at various time intervals and was later mixed with an equimolar amount of the hypochromism hairpin probe. Then, buffer solution (20 mM Tris, 1 mM EDTA, 3 mM $MgCl_2$, 50 mM NaCl, pH 7.5) was added to have a total volume of 100 μL. The 260 nm absorption maxima were recorded for aliquots at different time intervals. For the fluorescence measurements, a 10 μL aliquot of each irradiated solution was taken at various time intervals and was later mixed with an appropriate amount of the MB probe and buffer solution to give final concentrations of 1 μM oligonucleotide target and 200 nM MB probe. These solutions were then incubated in the dark at room temperature for about 24 h. Fluorescence spectra of 100 μL aliquots of the incubated hybridization mixtures were measured using a Photon Technologies International (Birmingham, New Jersey) fluorescence system. The spectra were recorded between 500 and 700 nm with excitation at 490 nm. A 1 cm path length Suprasil quartz fluorescence cuvette was used for these measurements.

The hypochromism probe was characterized by a thermal denaturation profile experiment in which temperature-dependent absorbance measurements were carried out on a buffered 200 nM solution of the hairpin probe incubated in the presence of an equimolar amount of the target oligonucleotide sequence. The temperature was varied from 20 to 72 °C in 4 °C increments at a heating rate of 1 °C min^{-1} and 5 min settling time for each step of the heating cycle.

5.3. Results and Discussion

The hypochromism hairpin probe was carefully designed to maximize its performance as a sensitive and specific probe to UV-induced nucleic acid damage. Figure 5.1 shows the structure of the hypochromism hairpin probe used in this study. The probe is designed such that the oligonucleotide target is complementary to the loop region and three nucleotides in the stem region to avoid sticky end pairing.[31] The design of the hypochromism probe maximizes discrimination of damaged *versus* undamaged targets, due to the T_m's of the stem and hybrid; designing the probe to have a T_m for the stem 5 – 10 °C higher than the T_m of the hybrid ensures maximum sensitivity.[19]

Figure 5.2 shows the effect of temperature and damage on the 260 nm absorbance of the oligonucleotide target-hairpin hybrid. The absorbance of the undamaged double-stranded hybrid is initially constant with increasing temperature. At temperatures close to the melting temperature of the hybrid, the absorbance starts to increase with increasing temperature as the hybrid melts. At temperatures greater than 60 $^{\circ}$C, the absorbance is constant again at a maximum. These results suggest that the hybrid has melted at temperatures above 60 $^{\circ}$C.

It is worth mentioning here that the trend shown in the thermal denaturation profile for the hypochromism hairpin probe in the presence of the target is different from the one expected from MB probes of damage.[3,19,31] At low temperatures, the fluorophore and the quencher in solutions containing the MB-target hybrid are far apart and maximum fluorescence is observed. At higher temperatures, the hybrid will melt and the MB will re-form the hairpin, leading to a decrease in fluorescence. It is clear that the thermal denaturation profile of the hybrid of the target with the hypochromism probe shows an opposite trend to that with the MB probe and this is what allows the hypochromism signal to increase with increasing damage to the target.

Figure 5.2 also shows the absorbance as a function of temperature for a hybrid of the hypochromism hairpin probe and a UV-damaged oligonucleotide strand. Here, the hybrid between the hypochromism hairpin probe and the UV-damaged oligonucleotide target shows a higher absorbance than that of the hybrid between the hypochromism hairpin and the healthy target at low temperatures. In addition, the melting temperature of the damaged oligonucleotide hybrid (~42 °C) is less than the melting temperature of the undamaged oligonucleotide hybrid (~46 °C). As shown in Figure 5.2, there is good discrimination in the absorbance between the undamaged and damaged targets hybridized with the hypochromism probe at 20 $^{\circ}$C. Therefore, we have chosen this hybridization temperature for detecting the formation of the UV-induced photoproducts.

Similar to Chapters 3 and 4, in order to confirm that the DNA damage is induced by UV light only and not by any other damaging factors, the dT_{17}

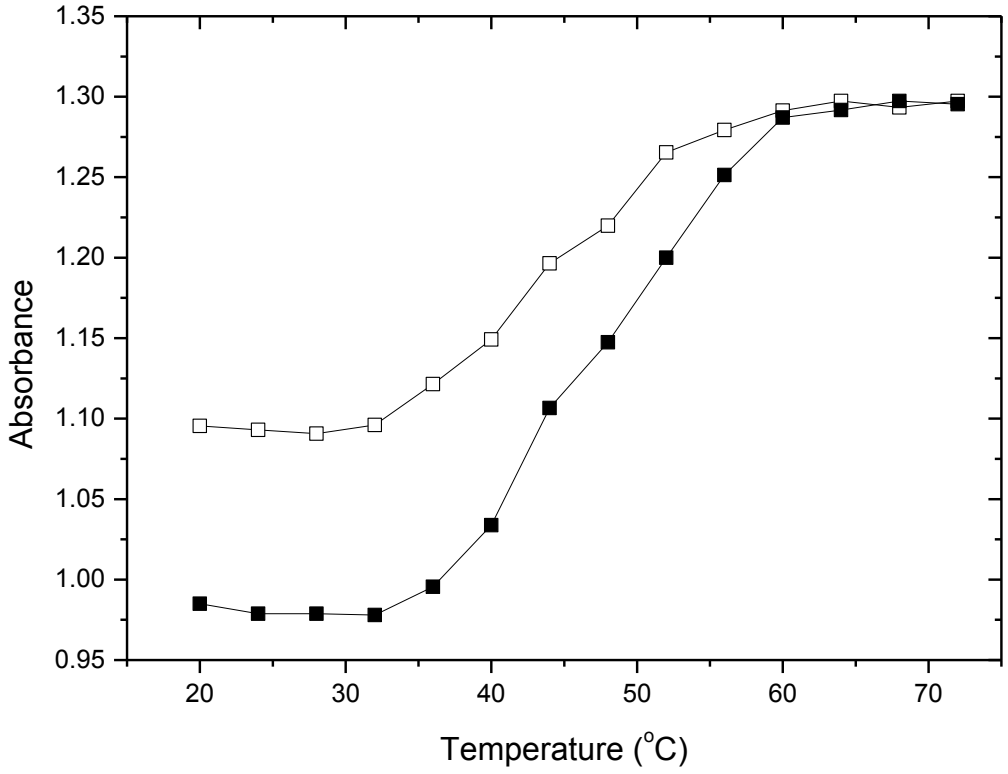

Figure 5.2. Thermal denaturation curves for 200 nM hypochromism hairpin probe in the presence of an equimolar amount of the perfectly complementary undamaged oligonucleotide target sequence (filled squares), and 200 nM hypochromism hairpin probe in the presence of an equimolar amount of the UV-irradiated oligonucleotide target sequence for 5 min (open squares) in 1 cm cuvettes. The lines are guides for the eye.

oligonucleotide target was irradiated at constant temperature, and the resultant damage was detected by UV-Vis absorbance measurements of the irradiated and control samples. Figure 5.3 shows a plot of the absorbance of the oligonucleotide target as a function of irradiation time with UVC light. The 260 nm absorption band, which represents the $\pi\pi^*$ transitions of the nucleobases, is seen to decrease with time. This result is expected and indicates UV-induced damage to the oligonucleotides with the consequent loss of the C_5=C_6 bond in all photoproducts formed. This decrease in absorbance is not observed in the unirradiated controls, demonstrating that the absorbance changes arise from irradiation of the samples and subsequent photochemistry rather than any other effect.

In order to investigate the sensitivity and selectivity of the hypochromism probe to detect nucleic acid damage, we measured the absorbance of aliquots of the irradiated target samples after incubation for 24 hrs. with the hairpin probe (Figure 5.4A). Aliquots of unirradiated samples of these solutions were also incubated with the probe as controls. It should be noted that the probe solution was not irradiated; it was only incubated with aliquots of irradiated oligonucleotide solutions, as well as their unirradiated controls. As shown in Figure 5.4A, the absorbance signal increases with UV irradiation and continues to increase with increasing irradiation until it reaches a plateau corresponding to the absorbance of the damaged target and unhybridized hairpin probe. This plateau is reached within the first 5 min of irradiation. This indicates that after 5 min irradiation, all of the hypochromism probes are in the hairpin form, and the solutions exhibit their maximum absorbance signal.

The plot of absorbance as a function of irradiation time for the oligonucleotide target (Figure 5.3) was fit to a double-exponential function while the hypochromism plot (Figure 5.4A) was fit to a single exponential growth function. For the absorbance (Figure 5.3), this decay represents the formation of thymine photoproducts containing saturated C_5-C_6 bonds and can be correlated to the concentration of the damage products. The increase in the absorbance signal in the

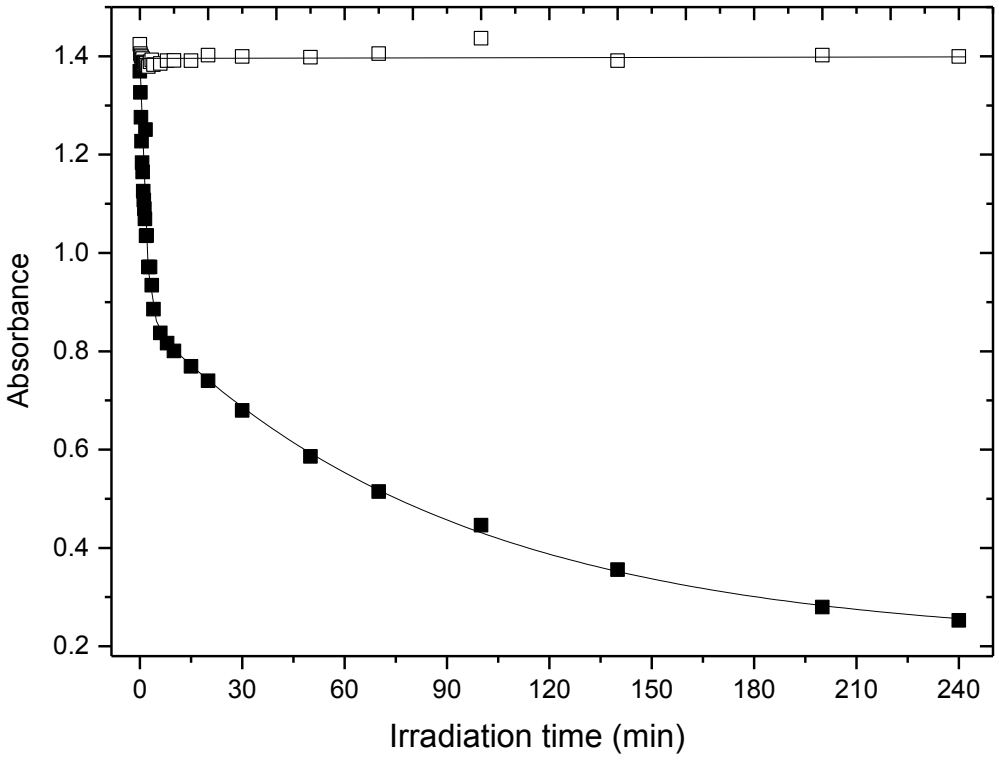

Figure 5.3. Absorbance of 10 μM irradiated target (filled squares) and unirradiated control (open squares) monitored at 260 nm as a function of irradiation time in 1 cm cuvettes. The solid line through the absorbance points (filled squares) is the least-squares fit to an offset, double exponential function, $A = A_0 + A_1e^{-t/\tau1} + A_2e^{-t/\tau2}$, where the absorbance damage constants are 6.31 ± 0.04 min (τ_1) and 94.8 ± 1.3 min (τ_2), and the amplitudes are $A_1 = 0.48 \pm 0.01$ and $A_2 = 0.70 \pm 0.01$. The offset (A_o) is 0.23 ± 0.03. The control points (open squares) are fit to a straight line with zero slope by eye.

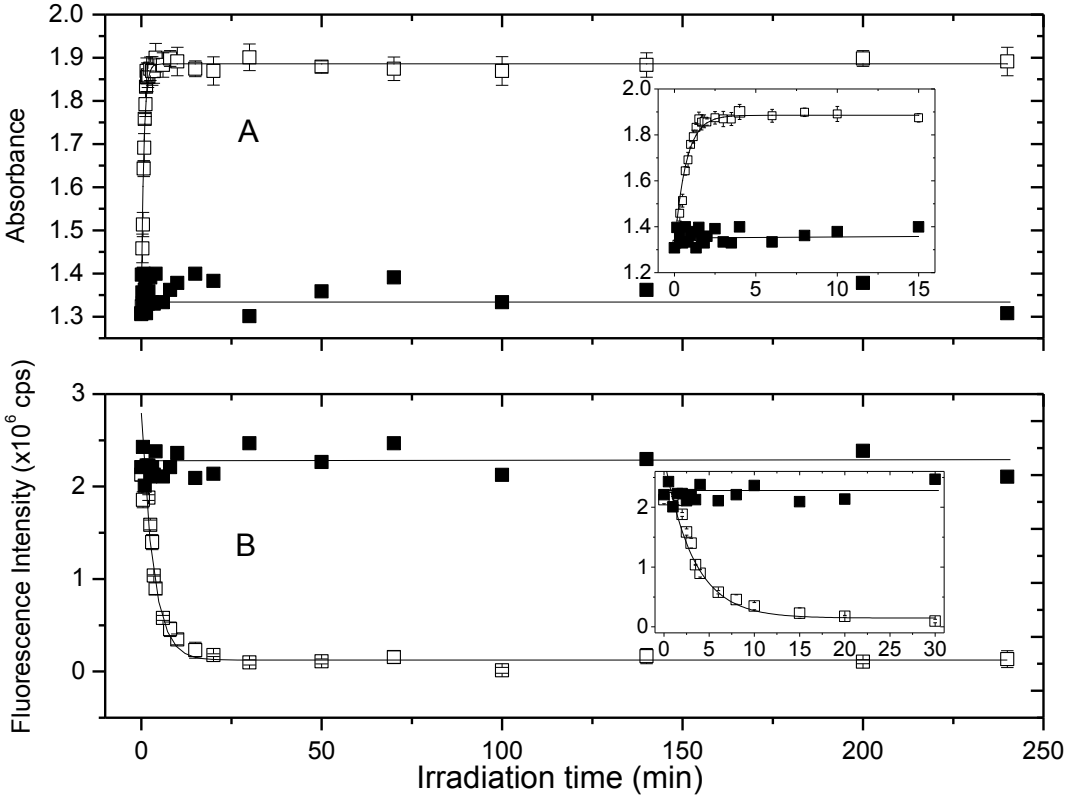

Figure 5.4. Absorbance at 260 nm of the hypochromism hairpin probe (A) and fluorescence intensity at 520 nm of the DNA MB (B) as a function of irradiation time for the oligonucleotide targets (open squares) and unirradiated target controls (filled squares) in 1 cm cuvettes. Only the 10 μM target was irradiated. Aliquots of the irradiated target were mixed with equimolar amounts of both probes (10 mM Tris, 3 mM $MgCl_2$, 20 mM NaCl, 1 mM EDTA, pH 7.5). The solid line through the irradiated sample points (open squares) is a single exponential fit. The hypochromism probe absorbance (A) is fit by $A_t = A_0 + a\,(1 - e^{-t/\tau})$, where $A_0 = 1.3 \pm 0.01$, $a = 0.58 \pm 0.02$, and $\tau = 1.02 \pm 0.01$ min. The MB fluorescence decay (B) is fit by $I_F = I_{F,0} + a\,e^{-t/\tau}$ where $I_{F,0} = 0.12 \pm 0.04 \times 10^6$, and $a = 2.5 \pm 0.1 \times 10^6$, $\tau = 3.59 \pm 0.2$ min. The control points (filled squares) are fit to straight lines of zero slopes by eye. Inset shows the absorbance at 260 nm of the hypochromism hairpin probe for the first 15 min of irradiation and the fluorescence intensity at 520 nm of the DNA MB for the first 30 min of irradiation.

hypochromism plot (Figure 5.4A) represents the decreased stability of the damaged target-hairpin hybrid. Therefore, the faster the absorbance signal increases, the more selective the probe is at detecting UV-induced oligonucleotide damage under identical irradiation conditions for the same target. This method for the detection of UV-induced nucleic acid damage by the hypochromism probe was compared to the MB probe's ability to detect UV-induced damage. The MB probe (Figure 5.1) used in this study was designed to the same sequence as the hypochromism probe. In addition, a FAM fluorophore was attached to the 5'- end and a DABCYL quencher was attached to the 3'-end. As explained above, the fluorescence is quenched in the hairpin position when the FAM and DABCYL are in close proximity, and the fluorescence intensity is high in the presence of complementary target when the MB forms a hybrid with the target. As damage accumulates on the target strand, the MB-target hybrid becomes less stable, effectively decreasing the fluorescence intensity until the closed, hairpin form is the more stable form of the MB. This trend is shown in Figure 5.4B, in which the MB fluorescence intensity decreases with longer irradiation time until reaching a constant minimum corresponding to the fluorescence of the MB in the hairpin structure. The fluorescence curve was fit to a single exponential decay function. The damage constants obtained by the two probes are shown in Table 5.1 for the absorbance, MB and hypochromism probe methods for detecting DNA damage. The ideal probe would detect damage at the rate it is being formed, but the reality is that probes may not be sensitive to a single lesion. The damage constant reflects the instability of the damaged target-probe hybrid. The lower (faster) the damage constant, the more selective the probe is at detecting UV-induced DNA damage, to the limit of the target damage rate. It is clear from Table 5.1 that the rate of absorbance decay is slower than the rate of the increase of the absorbance in the hypochromism plot and the rate of decrease of the MB fluorescence. This indicates the lower selectivity of the absorbance measurements.[19] Table 5.1 also shows that the hypochromism hairpin probe has a lower damage constant than that of the MB probe, which indicates that it has a higher selectivity to detect DNA damage. This allows the hypochromism probe to have superior selectivity

Table 5.1. Damage constants of the different DNA damage assay methods.

Method	Damage constant (min)[a]
Hypochromism Probe	$\tau = 1.02 \pm 0.02$
DNA MB fluorescence	$\tau = 3.59 \pm 0.2$
Absorbance	$\tau_1 = 6.31 \pm 0.04$
	$\tau_2 = 94.8 \pm 1.3$

[a]The damage constants (τ) were obtained from the fits in Figures 5.3 and 5.4.

for detection of UV damage in nucleic acids compared to absorbance and the MB probe.

In order to check the sensitivity of the hypochromism probe for damage detection, we used the UV absorbance measurements as a function of UV irradiation time to quantify the amount of UV damage and to develop calibration curves for the hypochromism probe. The procedure and calculation of the photoproduct concentrations from the absorbance of the irradiated solutions have been explained previously in Chapter 4. Figure 5.5 shows the calibration curve obtained upon plotting the hypochromism absorbance signal as a function of the total concentration of the photoproducts calculated for both the hypochromism and the fluorescence signal for the MB probes (Figure 5.5B). The signal at zero concentration of the photoproducts represents the background level corresponding to the highest hypochromism (least absorbance) of the probe when it is completely hybridized with the undamaged target. At photoproduct concentrations higher than 0.5 μM, the hybrid formed between the probe and the damaged strand is completely unstable, and the probe acquires the hairpin structure and is not hybridized with the damaged target giving maximum absorbance. Additional formation of photoproducts does not lead to any more unhybridization, so the absorbance signal shows saturation-like behaviour. For the DNA MB (Figure 5.5B), any decrease in fluorescence signal requires a minimum of 2.6 μM concentration of the photoproducts. The constant fluorescence signal of the DNA MB over the range of 0 – 2.6 μM of the photoproducts concentration can be attributed to the lower selectivity of the DNA MB to UV-induced DNA damage as discussed before. At high photoproduct concentrations, the hybrid formed between the DNA MB and the damaged strand is completely unstable, and the DNA MB preferentially acquires the hairpin structure where the fluorophore and the quencher are in close proximity and the fluorescence is the lowest. Any further damage doesn't lead to any additional decrease in fluorescence and the signal remains constant showing a saturation-like behaviour.

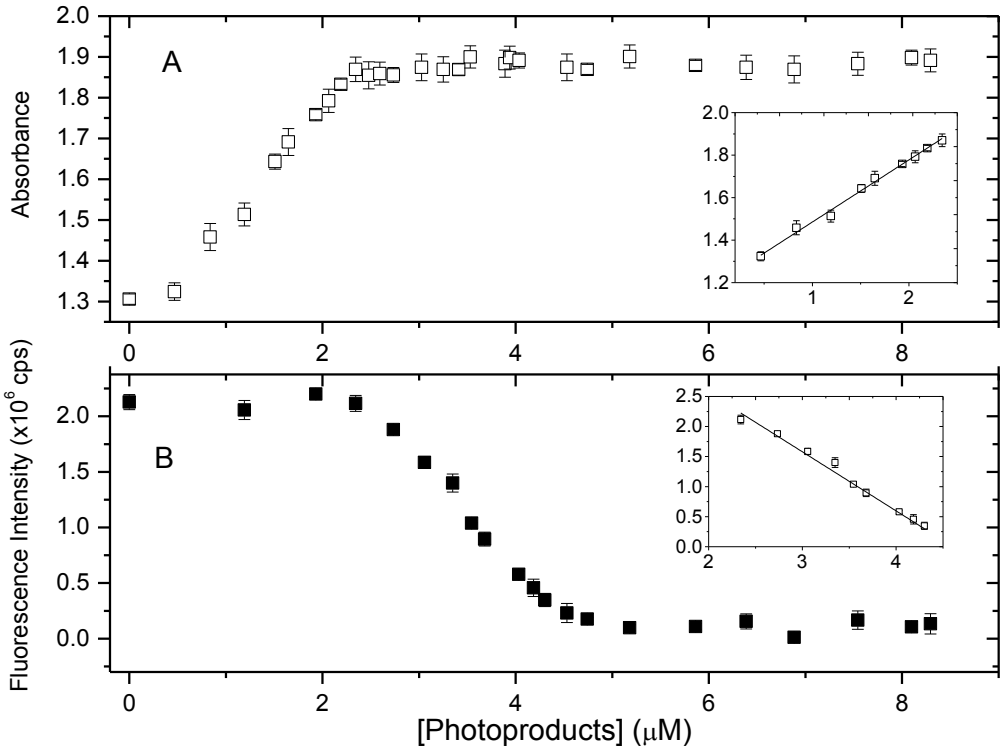

Figure 5.5. Calibration curve of DNA photodamage formed upon UV irradiation of the poly dT_{17} target for the (A) hypochromism hairpin probe and (B) MB probe. Inset shows the fit to the linear portions of the calibration curves. Each data point is an average of three replicate measurements and the error bars correspond to the relative standard deviation of the measurements. Solutions were measures in 1 cm cuvettes.

Table 5.2 shows the parameters for the quantification of UV-induced DNA damage from Figure 5.5. The calibration curve for the hypochromism probe shows a similar linear dynamic range to the MB probe (Figure 5.5) taking into account the threshold response of 0.5 μM. On the other hand, the DNA MB requires concentrations of 2.6 μM or more to show any fluorescence response to the photoproducts formed. While the hypochromism probe has higher selectivity than the MB probe, the sensitivity of detection, calculated as the slope of the calibration curve (Figure 5.5), is 6 orders of magnitude higher for the MB probe than the hypochromism probe. This large difference in sensitivity can be attributed to the 6 order of magnitude difference between the fluorescence scale of the MB probe and the absorbance scale of the hypochromism probe. The MB probe has a limit of detection (LOD) and limit of quantitation (LOQ) lower by only 8 times than the hypochromism probe, though, since the LOD and LOQ correct for the higher deviations in the blank. These lower LOD and LOQ are due to the intrinsically higher sensitivity of the zero-background fluorescence detection. It is worth mentioning that the values recorded in Table 5.2 for the LOD and LOQ for the hypochromism probe and DNA MB detection of the UV-induced photoproducts are obtained by using the standard deviation of the blank measurements and the sensitivity of the method, while the LOD and LOQ will be practically limited to ~0.5 and ~2.6 μM, respectively (Figure 5.5B) due to the threshold shown at low photoproducts concentrations. From this data, upon multiplying the concentration of the irradiated DNA target by the number of nucleotides forming the DNA target and dividing by the LOD, we are able to calculate that the hypochromism probe can detect one damage site in the presence of ~260 undamaged sites, compared to one damage site in the presence of ~2060 undamaged site with the MB probe. This again confirms the higher sensitivity of the MB probe over the hypochromism probe.

These results conclusively show that the hypochromism probe has superior selectivity to detect UVC-induced oligonucleotide damage over the DNA MB. Although its sensitivity is not as good as DNA MB probes, being 10 times

Table 5.2. Analytical parameters for the quantification of UV-induced DNA damage with the hypochromism probe and DNA MB.

Parameter[a]	Hypochromism probe	DNA MB
Linear Dynamic Range	0.5 – 2.1 μM	2.60 – 4.50 μM
R^2	0.994	0.995
Sensitivity	2.9×10^5 M^{-1}	9.54×10^{11} cps M^{-1}
LOD	325.5 nM	41.4 nM
LOQ	1085 nM	138 nM

For the determination of the blank standard deviation, 20 solutions of the MB hairpin alone were used. The standard deviations of these measurements were 3.1×10^{-2} and 1.3×10^4 cps for the hypochromism hairpin probe and the DNA MB, respectively. [a]In this table, linear dynamic range is the concentration range corresponding to the linear region in the calibration curve, R^2 is the linear regression coefficient squared, sensitivity is the slope of the calibration curve, LOD is the limit of detection and is 3 times the standard deviation of the blank divided by the sensitivity, and LOQ is the limit of quantification and is 3.3 times the LOD.

cheaper than MB probes makes it an attractive tool for the high throughput qualitative analysis of DNA damage. For in vivo applications, samples will have mixtures of single- and double-stranded DNA of different lengths. Therefore the absorbance signal will not be specific to the hypochromism probe/target signal. This limits that use of this probe to the less complex in vitro techniques.

5.4. Conclusion

In summary, the assay reported here uses the hypochromism phenomenon to design a probe for the detection of UVC-induced nucleic acid damage, by taking advantage of the hypochromic effect occurring in dsDNA. The hypochromism probe shows better selectivity for UVC-induced nucleic acid damage than MBs, but with lower sensitivity. Moreover, it is cheap, simple and easy to synthesize which introduces a new probe for the qualitative detection of UVC-induced DNA damage.

5.5. References

1) B.P. Ruzsicska, D.G.E. Lemaire, In DNA Photochemistry, CRC Handbook of Organic Photochemistry and Photobiology, P.-S. Horspool, W.M. Song, Eds., CRC Press, New York (1995) pp 1289.
2) D.M. Wagner, G.R. Loppnow, Spectrum 17 (2004) 26.
3) S. Yarasi, C. McConachie, G.R. Loppnow, Photochem. Photobiol. 81 (2005) 467-473.
4) L. Marrot, J.R. Meunier, J. Am. Acad. Dermatol. 58 (2008) S139-S148.
5) T. Lindahl, Nature 362 (1993) 709-715.
6) L.J. Marnett, P.C. Burcham, Chem. Res. Toxicol. 6 (1993) 771-785.
7) B.N. Ames, L.S. Gold, W.C. Willett, Proc. Natl. Acad. Sci. U.S.A. 92 (1995) 5258-5265.
8) M. Weinfeld, K.-J.M. Soderlind, Biochemistry 30 (1991) 1091-1097.
9) B.B. Haab, R.A. Mathies, Anal. Chem. 67 (1995) 3253-3260.
10) X.C. Le, J.Z. Xing, J. Lee, S.A. Leadon, M. Weinfeld, Science 280 (1998) 1066-1069.
11) J. Wang, G. Rivas, M. Ozsoz, D.H. Grant, X. Cai, C. Parrado, Anal. Chem. 69 (1997) 1457-1460.

12) H. Kaur, B. Halliwell, Biochem. J. 318 (1996) 21-23.
13) T. Douki, M. Court, S. Sauvaigo, F.Odin, J. Cadet, J. Biol. Chem. 275 (2000) 11678-11685.
14) T. Douki, J. Cadet, Biochemistry 40 (2001) 2495-2501.
15) J.-L. Ravanat, T. Douki, J. Cadet, J. Photochem. Photobiol. B: Biol. 63 (2001) 88-102.
16) A. Kumar, M.B. Tyagi, P.N. Jha, Biochem. Biophys. Res. Commun. 318 (2004) 1025-1030.
17) C.C. Trevithick-Sutton, L. Mikelsons, V. Filippenko, J.C. Scaiano, Photochem. Photobiol. 83 (2007) 556-562.
18) J.Z. Xing, J. Lee, S.A. Leadon, M. Weinfeld, X.C. Le, Methods 22 (2000) 157-163.
19) S.A. Oladepo, G.R. Loppnow, Anal. Bioanal. Chem. 397 (2010) 2949-2957.
20) K. Stohr, B. Hafner, O. Nolte, J. Wolfrum, M. Sauer, D.-P. Herten, Anal. Chem. 77 (2005) 7195-7203.
21) J.-P. Knemeyer, N. Marme, M. Sauer, Anal. Chem. 72 (2000) 3717-3724.
22) A. Misra, P. Kumar, K.C. Gupta, Anal. Biochem. 364 (2007) 86-88.
23) T. Heinlein, J.-P. Knemeyer, O. Piestert, M. Sauer, J. Phys. Chem. B 107 (2003) 7957-7964.
24) Y. Kim, C.J. Yang, W.H. Tan, Nucl. Acids Res. 35 (2007) 7279-7287.
25) A. Misra, M. Shahid, Bioorg. Med. Chem. 17 (2009) 5826-5833.
26) A. Rich, I. Tinoco, J. Am. Chem. Soc. 82 (1960) 6409-6410.
27) I. Tinoco, J. Am. Chem. Soc. 82 (1960) 4785-4790.
28) R. Haschemeyer, B. Singer, H. Fraenkel-Conrat, Proc. Natl. Acad. Sci. U.S.A. 45 (1959) 313-319.
29) A. Rich, Nature 181 (1958) 521-525.
30) T. Hill, J. Chem. Phys. 30 (1959) 383-387.
31) C.J. Yang, L. Wang, Y. Wu, Y. Kim, C.D. Medley, H. Lin, W.H. Tan, Nucl. Acids Res. 35 (2007) 4030-4041.
32) M. Weinfeld, M. Liuzzi, M.C. Paterson, J. Biol. Chem. 264 (1989) 6364-6370.

Chapter 6

Terbium Fluorescence as a Sensitive, Inexpensive Probe for UV-induced Damage in Nucleic Acids*

6.1. Introduction

Exposure of nucleic acids to solar UV radiation gives rise to a wide range of photochemical products such as cyclobutane pyrimidine dimers (CPDs), [6-4] pyrimidine-pyrimidinones, dewar pyrimidinone photoproducts and uracil and thymine photohydrates.[1,2] On the other hand, free radicals, such as reactive oxygen species, leads to oxidation products, such as 8-oxoguanosine and photohydrates. Other damage agents, such as reactive chemicals and ionizing radiation, lead to other DNA lesions, such as single- and double-strand breaks, adducts, and cross-links. All these damage products lead to miscoding during DNA replication and may result in mutagenesis, carcinogenesis and cell death.[3-6]

Fluorescent methods have been shown to be superior for detecting DNA damage over previous destructive, time-consuming techniques such as gel electrophoresis,[7] capillary electrophoresis,[8,9] electrochemical,[9,10] HPLC,[11] mass spectrometric[12-14] and polymerase chain reaction (PCR) amplification[15] methods. Fluorescent probes offer enhanced sensitivity and the potential for use *in situ* or *in vivo*. Differences in the fluorescence lifetime of a dye intercalated in undamaged and damaged DNA have also been used to detect DNA damage.[16] Fluorescently-labeled antibodies provide a highly selective probe of particular damage photoproducts, such as thymine cyclobutyl photodimers.[17]

The use of fluorescent nucleic acid probes, such as molecular beacons (MBs) and smart probes, have become powerful tools for application in detection of nucleic acid targets in general,[18-21] and broad-spectrum detection of DNA and RNA damage.[2,21] For the design of such a probe, the recognition capabilities of DNA through hybridization reactions are well-established, but adequate reporters

*A version of this chapter has been submitted to Analytica Chimica Acta (January 2013)

are needed to generate a physically measurable signal from the hybridization event. This is normally accomplished by labeling the same DNA probe with a fluorophore-quencher pair so that the Förster resonance energy transfer (FRET) can take place. Despite the wide applications and the exquisite sensitivity and selectivity of MBs, they have some readily-apparent limitations,[22-27] such as the synthetic and purification difficulties, and limitations associated with site-specific labeling of each terminus of the hairpin,[22,23,25,27] incomplete attachment of the quencher,[3,7] and the ability to probe only undamaged DNA.[2,21] For this last limitation, the MB signal is inversely proportional to the damage, or negative detection, lowering the sensitivity and selectivity of the assay.

The main focus of this work is to design an inexpensive probe for the positive detection of DNA damage, in which the produced signal is directly proportional to the amount of DNA damage. We have previously reported two methods for the positive detection of DNA damage. The first is by using a 2-aminopurine (2AP) hairpin probe as discussed in Chapter 4. This probe offers high sensitivity and selectivity for the detection of DNA damage, as well as overcoming most of the MB probe's limitations. However, these are expensive probes, especially with an increasing number of 2AP bases incorporated in the probe to increase sensitivity. A hypochromism probe (Chapter 5) was also designed. The hypochromic effect arises from the formation of the double-stranded hybrid of the undamaged target and hairpin. With accumulated UV exposure, the target-hairpin hybrid concentration decreases and the absorbance increases. This probe (Chapter 5) is more selective and is more than ten times cheaper than MBs, but is less sensitive. The goal of this chapter is to design a more sensitive, selective and cheaper probe for the positive detection of DNA damage.

Terbium(III) (Tb^{3+}) is a trivalent lanthanide cation that possesses low intrinsic luminescence in aqueous solutions owing to its low absorption cross-section and non-radiative deactivation through the O-H vibrations of the coordinated water molecules.[28-35] In the presence of an appropriate ligand, Tb^{3+} ion chelates with the ligand. Upon excitation of the ligand with light, it undergos intersystem crossing from the ligand's excited singlet state to an excited triplet state. Following this

crossing, radiationless energy transfer occurs from the excited triplet state of the ligand to the lanthanide ion. This results in population of the lanthanide ion excited state. This process leads to longer emission lifetimes with significant luminescence enhancement, due to the involvement of the long-lived triplet state.[28-35] This property, which allows for efficient intra-molecular energy transfer from ligand to central atom, along with the fact that there is an insignificant degree of radiationless deactivation in the chelated ion,[36] has made Tb^{3+} ions extremely valuable as fluorescent probes for detecting DNA[37-40] as well as detecting alkaline metal binding sites in proteins,[41-42] tRNA,[43] and rRNA.[44,45] Similarly, lanthanides, especially Tb^{3+}, have been employed to study the structure of tRNA,[43,46] rRNA[44] and DNA.[47-49] In addition, the enhancement of Tb^{3+} emission in the presence of single-stranded oligonucleotides has been utilized in the detection of distorted DNA regions,[50] single base mismatches in DNA duplexes[51] and DNA- and RNA-drug interactions.[52,53]

In this chapter, we explore the enhanced emission of Tb^{3+} as a potential tool to probe UV-induced DNA damage. This is accomplished by the use of a DNA hairpin probe complementary to the DNA target of interest. The Tb^{3+}/hairpin probe detects UV-induced DNA damage through the hybridization of the hairpin probe to the undamaged target DNA. The damaged DNA-hairpin hybrid is destabilized, and the probe preferentially acquires the hairpin structure while the damaged target remains single-stranded. The Tb^{3+} then directly coordinates to the unpaired nucleobases of the single-stranded damaged DNA and the loop of the hairpin probe. This enhances the intrinsic luminescence of Tb^{3+}, producing a detectable signal proportional to the amount of DNA damage. Thus, the recognition of DNA damage is accomplished by the hairpin probes through hybridization reactions and the Tb^{3+} is the reporter that generates a physically measurable signal reflecting the amount of damage. The Tb^{3+}/hairpin probe has superior selectivity and sensitivity for DNA damage compared to conventional DNA MBs, and is almost an order of magnitude less expensive.

6.2. Experimental

6.2.1. Materials

Single-stranded oligonucleotide targets and hairpin probes (Figure 6.1) were obtained from Integrated DNA Technologies Inc. (Coralville, Iowa). The oligonucleotide samples were purified by standard desalting. The terbium (III) chloride ($TbCl_3$) was obtained from Sigma-Aldrich Canada Ltd. (Oakville, Ontario), magnesium chloride ($MgCl_2$) and sodium chloride (NaCl) were obtained from EMD Chemicals Inc. (Gibbstown, New Jersey), and Tris was obtained from ICN Biomedicals, (Aurora, Ohio). All chemicals were used as received. Nanopure water from a Barnsted Nanopure (Boston, Massachusetts) system was used for all solutions. The oligonucleotide samples were each dissolved in nanopure water and kept frozen at –20 °C until needed.

6.1.1. UV Irradiation

Nitrogen-purged aqueous solutions of 10 μM oligonucleotide targets were irradiated in sealed, UV-transparent 1 cm path length cuvettes. The cuvettes were placed in a water bath in a UV-transparent water dish to keep the temperature, which was monitored by means of a Cole-Parmer DiGi-SENSE thermocouple (Niles, Illinois), constant throughout the irradiation. Oligonucleotide samples were irradiated in a Luzchem (Ottawa, Ontario) DEV photoreactor chamber with UVC light from lamps emitting principally at 254 nm with an irradiation dose of 75 W m^{-2}. The samples were constantly stirred during irradiation, and the photoreactor was purged with nitrogen throughout the irradiation to flush out oxygen and any ozone subsequently generated from the UVC lamps. Control samples were handled identically, but were not exposed to UV radiation. The UVC lamps were turned on ~20 min before the start of irradiation to stabilize the lamp output.

6.1.2. Absorption and fluorescence measurements

Absorption spectra were recorded at intervals throughout the irradiation period on a Hewlett-Packard (Sunnyvale, California) 8452A diode array spectrophotometer by placing the irradiated cuvettes containing the target oligonucleotide solutions directly into the spectrophotometer. For the fluorescence measurements, a 10 μL aliquot of each irradiated solution was taken at various time intervals and was later mixed with appropriate amounts of the hairpin probes and 2 mM Tris buffer

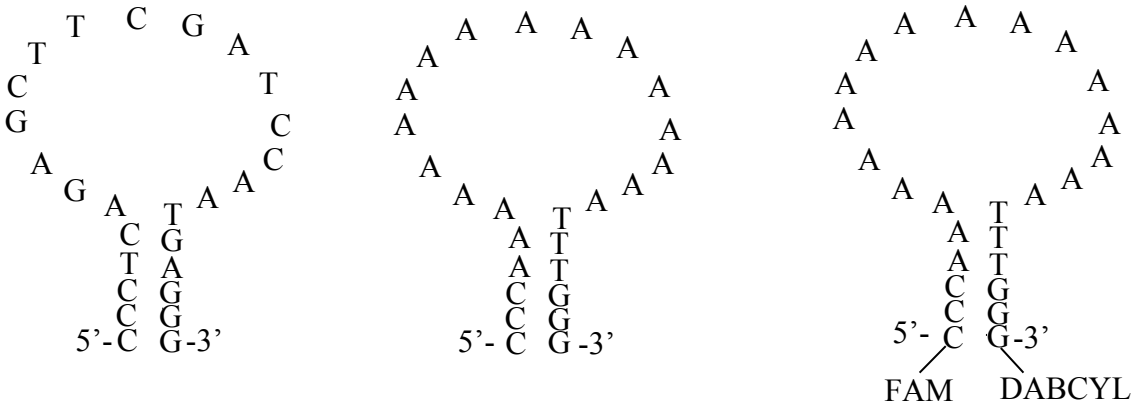

(A) (B) (C)

$T_{dT_{17}}$: 3'-TTT TTT TTT TTT TTT TT-5'

T_{random}: 3'-CTC GAA GCT AGG TTA CT-5'

Figure 6.1. Sequences of the probes used in this work. The Tb^{3+}/hairpin probes are complementary to T_{random} (A) and to $T_{dT_{17}}$ (B). The MB probe is complementary to $T_{dT_{17}}$ (C). "FAM" denotes the 6-carboxyfluorescein fluorophore and "DABCYL" denotes the dabcyl quencher. T_{random} and $T_{dT_{17}}$ are the oligonucleotide targets used in this study.

solution (pH 7.5) to give final concentrations of 1 μM oligonucleotide targets and 1 μM hairpin probes. These solutions were then incubated in the dark at room temperature for about 24 h. A 40 μM $TbCl_3$ solution was added to the hybridized solutions prior to the fluorescence measurements. For the MB fluorescence measurements, a 10 μL aliquot of each irradiated solution was taken at various time intervals and was later mixed with an appropriate amount of the MB probe and 10 mM Tris buffer solution (3 mM $MgCl_2$, 1 mM EDTA, pH 7.5) to give final concentrations of 1 μM oligonucleotide target and 200 nM MB probe. These solutions were then incubated in the dark at room temperature for about 24 h.

Fluorescence spectra of 100 μL aliquots of the incubated hybridization mixtures were measured using a Photon Technologies International (Birmingham, New Jersey) fluorescence spectrophotometer. The spectra were recorded between 450 and 600 nm with excitation at 290 nm for the Tb^{3+} fluorescence measurements, and between 500 and 700 nm with excitation at 490 nm for the MB fluorescence measurements. A 1 cm path length Suprasil quartz fluorescence cuvette was used for these measurements.

The Tb^{3+}/hairpin probe was characterized by a thermal denaturation profile experiment, in which temperature-dependent luminescence measurements were carried out on a buffered 1 μM solution of the hairpin probe incubated in the absence or presence of either the target oligonucleotide sequence or the UV-damaged target sequence at 1 μM concentration. The temperature was varied from 20 to 60 °C in 4 °C increments at a heating rate of 1 °C min^{-1} and 5 min settling time for each step of the heating cycle.

6.3. Results and Discussion

The hairpin probes used in this study are carefully designed to maximize their performance as a specific probe for UV-induced nucleic acid damage. This design ensures that the probes can selectively discriminate single damage sites in oligonucleotides. Figure 6.1 shows the structure of the hairpin probes used in this study. Each probe is composed of a loop and a stem region composed of six base pairs. The design of the hairpin maximizes discrimination of damaged ***versus***

undamaged targets, due to the melting temperatures (T_m's) of the stem and hybrid; designing the hairpin to have a T_m for the stem 5 – 10 °C higher than the T_m of the hybrid ensures maximum selectivity.

The luminescence at 545 nm of Tb^{3+} alone, in the presence of single-stranded DNA (ssDNA) and in the presence of double-stranded DNA (dsDNA) is shown in Figure 6.2. The intrinsic luminescence of Tb^{3+} is enhanced by ~15 times in the presence of ssDNA, while almost complete luminescence quenching occurs in the presence of dsDNA (Figure 6.2). After UV damage, the hairpin probe will hybridize only with the undamaged DNA, while the damaged DNA remains single-stranded and the probe in the hairpin structure, binding Tb^{3+} and enhancing its luminescence. In this way, the Tb^{3+} produces a detectable signal proportional to the amount of DNA damage. In order to optimize Tb^{3+}/hairpin detection of DNA damage to obtain the maximum discrimination between damaged and undamaged oligonucleotides, we studied the effect of ionic strength, oligonucleotide concentrations, and Tb^{3+} concentration on the luminescence of Tb^{3+}.

6.3.1. Optimizing DNA damage detection

The analysis of DNA damage is commonly carried out in the presence of high ionic strength buffers with metal ions such as magnesium and sodium ions present. Such ions are essential for stabilizing the hairpin structure of the probe and the hybrid between the probe and undamaged target.[2,21] We studied the effect of magnesium and sodium ions on the enhancement of Tb^{3+} luminescence in the presence of ssDNA. Figure 6.3A shows the luminescence of the Tb^{3+}-ssDNA complex at 545 nm as a function of different concentrations of magnesium and sodium ions that have been previously used in buffers for the detection of DNA damage.[2,21] The results show that the highest luminescence is from solutions of buffers having no Mg^{2+} and Na^{+}. The Tb^{3+} luminescence decreased with increasing sodium concentrations, with increasing magnesium concentration, and with increasing concentration of both (Figure 6.3A). These results can be attributed to blocking of Tb^{3+} binding sites on the negatively charged phosphate

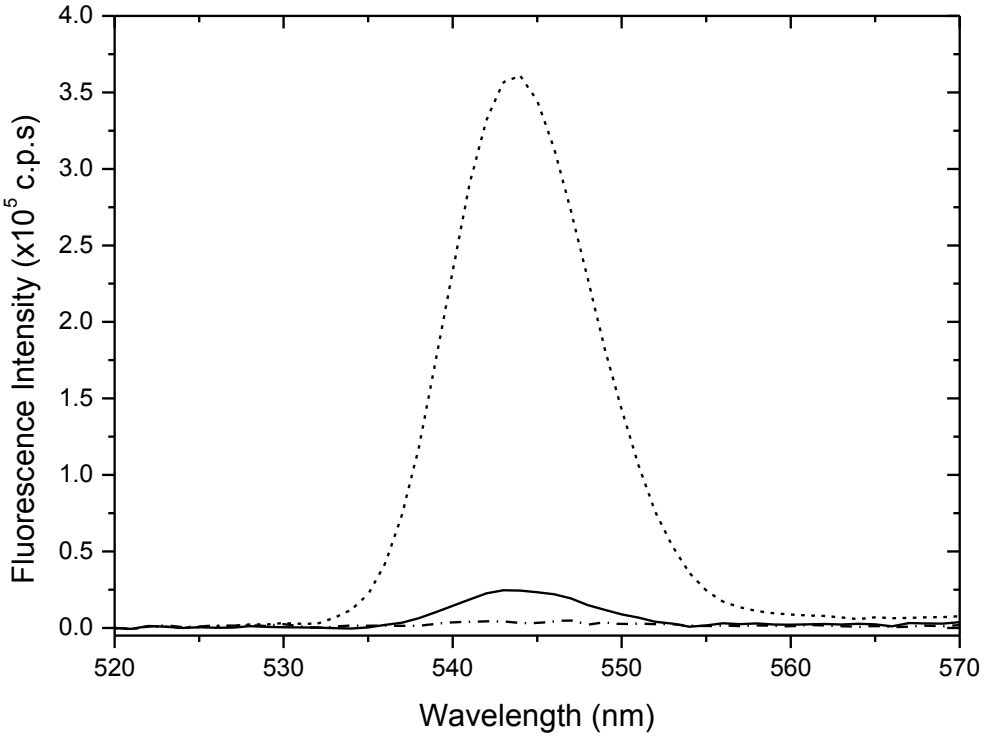

Figure 6.2. The luminescence spectra of Tb^{3+} alone (—), in the presence of single-stranded DNA (------) and in the presence of double-stranded DNA (•-•-•-). The luminescence excitation wavelength was 290 nm and the spectra were recorded at room temperature. "c.p.s." denotes counts per second.

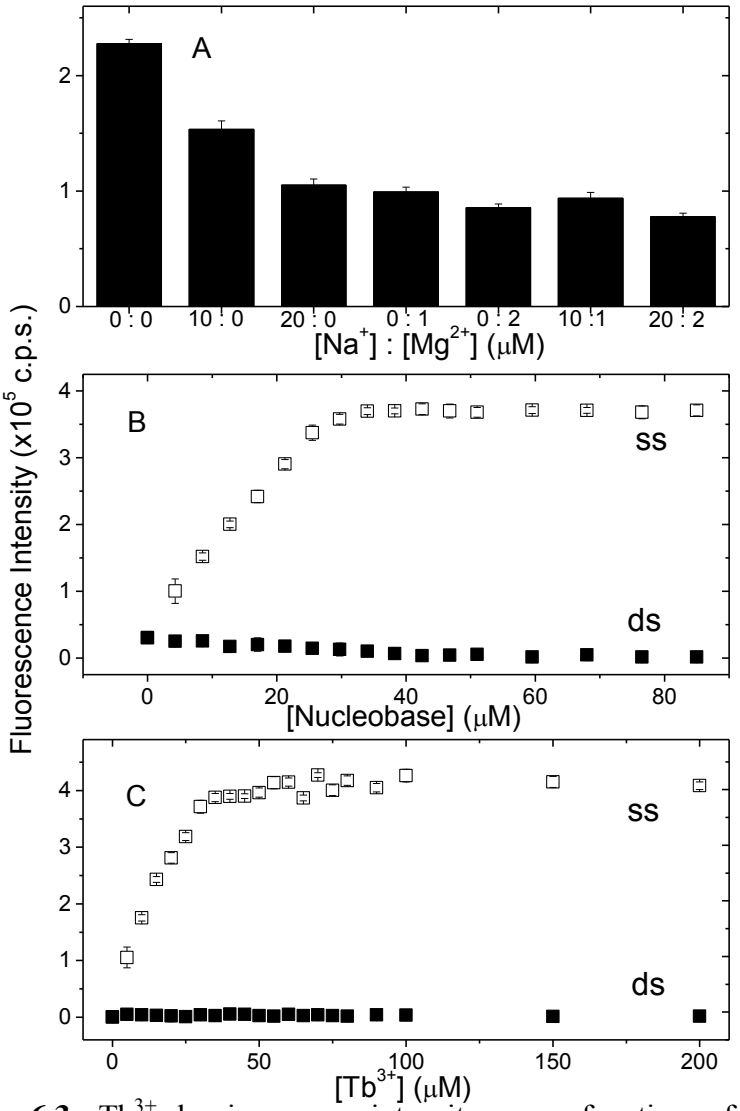

Figure 6.3. Tb^{3+} luminescence intensity as a function of (A) sodium and magnesium ion concentrations in 2 mM Tris (pH 7.5) buffer and 25 μM Tb^{3+}, (B) nucleobase concentration of single-stranded DNA (open squares) and double-stranded DNA (filled squares) in 2 mM Tris buffer (pH 7.5) and 25 μM Tb^{3+}, and (C) Tb^{3+} concentration of single-stranded DNA (open squares) and double-stranded DNA (filled squares) in 2 mM Tris buffer (pH 7.5) and 34 μM nucleobases. Luminescence excitation and emission wavelengths were 290 and 454 nm, respectively. Each data point is an average of three replicate measurements and the error bars correspond to the standard deviation of each measurement. "c.p.s." denotes counts per second.

backbone by the Na^+ and Mg^{2+} ions, lowering the Tb^{3+} luminescence. Figure 6.3A also shows that the presence of Mg^{2+} in the buffer has a more drastic effect on the enhancement of Tb^{3+} luminescence than Na^+, indicating that the higher valance ions lower the enhancement of the Tb^{3+} luminescence more. To maximize the luminescence enhancement of Tb^{3+}, 2 mM Tris buffer with no Na^+ and Mg^{2+} ions added was used for all subsequent measurements.

Figure 6.3B shows a plot of the luminescence of 25 μM Tb^{3+} as a function of the nucleobase concentration of the single-stranded and double-stranded DNA. In the absence of DNA, Tb^{3+} luminescence is very low (Figure 6.3B). Upon addition of the ssDNA, the Tb^{3+} emission increases linearly with increasing ssDNA nucleobase concentration. After the addition of ~29 μM ssDNA bases, the luminescence enhancement starts to gradually level. This result is expected, as the Tb^{3+} concentration is 25 μM, and indicates that one Tb^{3+} binds, on average, to one base. The annealed duplex solutions did not enhance the Tb^{3+} luminescence (Figure 6.3B), as expected, because all the electron donating groups of the nucleoside bases are base-paired and are not free to coordinate to Tb^{3+}. This result confirms that binding to the phosphate backbone, without direct coordination to the base, does not result in efficient energy transfer.[54,55] It is worth mentioning that the luminescence of solutions of both Tb^{3+}- ssDNA and Tb^{3+}-dsDNA complexes did not change over 6 h. This result indicates that the presence of Tb^{3+} with dsDNA does not force the equilibrium to shift to the ssDNA formation over the 6 h period of time and acts only as a multivalent cation stabilizing the hybrid secondary structure.

The luminescence spectra and intensities of Tb^{3+}-ssDNA complexes strongly depend on the amount of complexed Tb^{3+} (Figure 6.3C). In the absence of Tb^{3+}, the solution is non-fluorescent as expected. When Tb^{3+} is added to the annealed duplex solutions, no luminescence enhancement is observed and the luminescence is constant at the background level. After the addition of Tb^{3+} to the ssDNA solutions, the emission of Tb^{3+} is greatly enhanced, and the luminescence intensity increases linearly with increasing Tb^{3+} concentration. As shown in

Figure 6.3C, when the Tb^{3+}:nucleobase ratio reaches 1:1, the luminescence intensity saturates.

6.3.2. Selectivity of Tb^{3+}/hairpin detection of DNA damage

To examine the selectivity of this method for the detection of UV-induced DNA damage, we measured the luminescence at 545 nm of 40 μM Tb^{3+} in the presence of the hairpin probe alone, the annealed duplexes of the hairpin probe with the undamaged target, and with the 3 minute- and 60 minute-UV damaged ssDNA targets for 3 and 60 min as a function of temperature. Figure 6.4 shows their thermal denaturation profiles. At low temperatures, the luminescence of Tb^{3+} in the presence of the hairpin probe remains constant at a slightly enhanced luminescence signal level due to the interaction of Tb^{3+} with the nucleobases in the single-stranded loop of the hairpin probe. At temperatures close to the melting temperature of the stem of hairpin probe (~42 $^{\circ}$C), the Tb^{3+} luminescence gradually increases with temperature, because the proportion of single-stranded DNA increases as the stem melts. For the hybrid between the probe and undamaged target, there is no luminescence enhancement at low temperatures, because the undamaged target is completely hybridized with the probe and all the nucleobases are involved in hydrogen bonding. At temperatures close to the hybrid melting temperature (~39 $^{\circ}$C), the luminescence intensity gradually increases due to the interaction of Tb^{3+} with the unpaired nucleobases of the undamaged target.

It is clear that the thermal denaturation profile of the undamaged target-hairpin probe hybrid in the presence of Tb^{3+} shows an opposite trend to that of the MB probe[2,21] and this is what causes the Tb^{3+} luminescence signal to increase with increasing damage to the target. This result is demonstrated in Figure 6.4, where the hybrid between the hairpin probe and the oligonucleotide target subjected to UVC light for 3 min in the presence of Tb^{3+} shows higher luminescence intensity than that of the hairpin-undamaged target hybrid and is essentially flat with increasing temperature. The slight decrease in luminescence with increasing

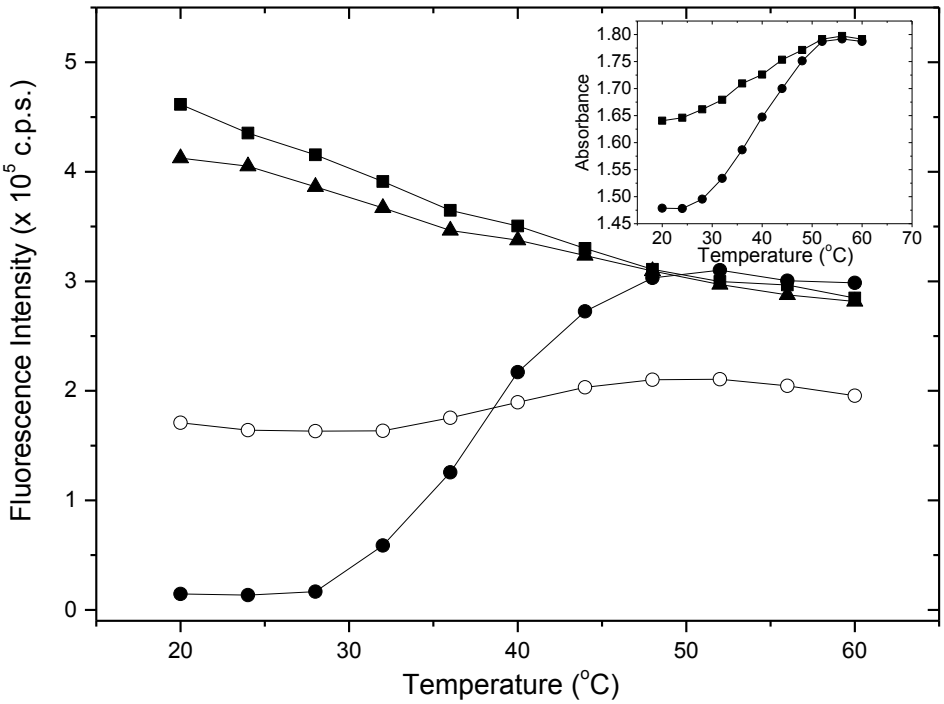

Figure 6.4. Luminescence thermal denaturation profiles for 40 μM Tb^{3+}/hairpin probe alone (open circles), 40 μM Tb^{3+}/hairpin probe in the presence of an equimolar amount of the complementary oligonucleotide target sequence (filled circles), and 40 μM Tb^{3+}/hairpin probe in the presence of an equimolar amount of the UV-irradiated oligonucleotide target sequence for 3 min (filled squares) and 60 min (filled triangles). The inset shows the absorption thermal denaturation curves for the same solutions of 40 μM Tb^{3+}/hairpin probe in the presence the complementary oligonucleotide target (filled circles), and the 3 min UV-irradiated oligonucleotide target (filled squares) in 1 cm cuvettes. The lines are guides for the eye.

temperature has been observed before in Chapters 2 and 4 and is attributed to a higher rate of non-radiative relaxation in the fluorophore at higher temperature. The thermal denaturation profile of the hybrid between the hairpin probe and the oligonucleotide target subjected to UVC light for 60 min in the presence of Tb^{3+} shows a very similar trend to that of the 3 min-irradiated target-hairpin hybrid. This result indicates that most of the oligonucleotide targets are damaged within 3 minutes of UVC irradiation and are in the single-stranded structure with the probe in the hairpin structure causing maximum enhancement of the Tb^{3+} luminescence. As shown in Figure 6.4, there is good discrimination in the luminescence between the undamaged and damaged targets hybridized with the hairpin probe in the presence of Tb^{3+} at 20 $^{\circ}$C. Therefore, we have chosen this hybridization temperature for detecting the formation of the UV-induced photoproducts.

In order to confirm that these are the secondary structures of the probe-target hybrids for the undamaged and 5 minute UV-damaged targets, we also measured the 260 nm absorbance of these solutions as a function of temperature (Figure 6.4 inset). As shown in the inset, the hybrid between the hairpin probe and the UV-damaged target shows a higher absorbance than that of the hybrid between the hairpin and the undamaged target at low temperatures. The increase in absorbance of the damaged solution is due to less hypochromism from the single-stranded damaged target. This confirms that the UV-damaged target-probe hybrid after 5 min is unstable due to damage and the probe preferentially acquires the hairpin structure with the damaged target in the single-stranded form.

To confirm the selectivity of Tb^{3+} to detect single-stranded DNA in the presence of complementary duplexes, we measured the luminescence intensity as a function of the dsDNA:ssDNA concentration ratio at a total nucleobases concentration equal to the Tb^{3+} concentration. Figure 6.5 shows the resulting calibration curve obtained. At zero ssDNA concentration, i.e. only dsDNA is present in the mixture, Tb^{3+} shows no luminescence. Upon increasing ssDNA concentration, the Tb^{3+} luminescence increases linearly. The sensitivity, calculated as the slope of the calibration curve, is 8.21×10^{11} cps M^{-1} and the limit

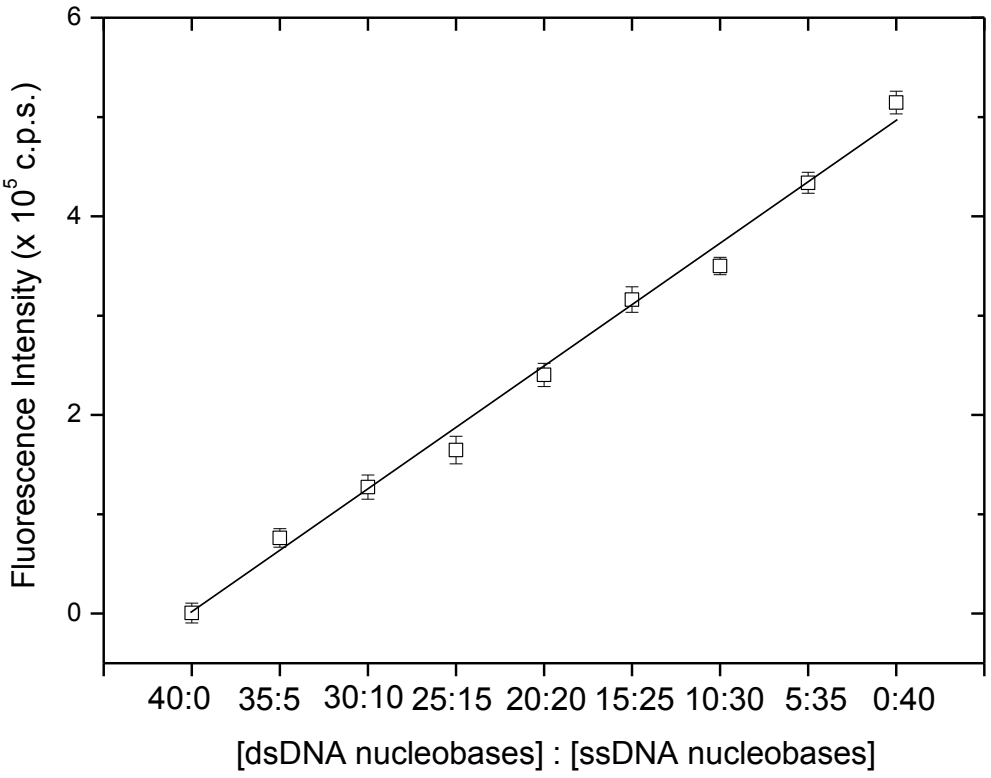

Figure 6.5. Calibration curve of the detection of ssDNA in a mixture of single-stranded and double-stranded DNA with 40 μM Tb^{3+}. [dsDNA nucleobases] and [ssDNA nucleobases] are in μM. Each data point is an average of three replicate measurements and the error bars correspond to the standard deviation of the measurements. The linear regression coefficient squared, R^2, calculated from the calibration curve is 0.993, the sensitivity, calculated as the slope of the calibration curve, is 8.21 x 10^{11} cps M^{-1}, the limit of detection (LOD), calculated as 3 times the standard deviation of the blank divided by the sensitivity, is found to be 28.5 nM, and the limit of quantification (LOQ), calculated as 3.3 times the LOD, is equal to 95.1 nM. For the determination of the blank standard deviation, 20 solutions of 40 μM Tb^{3+} were measured and the standard deviations of these measurements were 0.7×10^4 c.p.s.

of detection (LOD), calculated as 3 times the standard deviation of the blank divided by the sensitivity, is found to be 28.5 nM. By dividing the concentration of the ssDNA bases by the LOD, we are able to calculate that Tb^{3+} can detect one unpaired nucleobase in the presence of ~1060.0 paired ones in double-stranded form.

6.3.3. Detection of UV-induced photoproducts

In order to investigate the selectivity of the Tb^{3+}/hairpin probe to detect nucleic acid damage, T_{random} and $T_{dT_{17}}$ oligonucleotide targets were irradiated separately at constant temperature. The Tb^{3+} luminescence was measured (Figure 6.6) after aliquots of both the irradiated and unirradiated samples of these solutions were incubated with the complementary hairpin probes and Tb^{3+}. It should be noted that the hairpin probes were not irradiated, they were only incubated with aliquots of either the irradiated oligonucleotides or unirradiated controls. As shown in Figure 6.6A and 6.6B, the Tb^{3+} luminescence increases with target UV irradiation dose and continues to increase with increasing dose until it reaches a plateau. This plateau is reached within the first 3 min of target irradiation under the conditions used here. No luminescence is observed from the unirradiated controls. This result indicates that after 3 min irradiation, the entire probe is in the hairpin form and Tb^{3+} exhibits its maximum luminescence enhancement.

The luminescence signal as a function of irradiation time for the T_{random} and $T_{dT_{17}}$ oligonucleotide targets (Figure 6.6A, 6.6B) were fit to a single exponential growth function. This increase in the luminescence intensity represents the decreased stability of the damaged target-hairpin hybrid. Therefore, the faster the increase in the luminescence intensity, the faster the rate of UV-induced damage in the oligonucleotide targets. The damage constants obtained by fitting these luminescence damage curves are shown in Table 6.1 for both the T_{random} and $T_{dT_{17}}$ oligonucleotide targets. It is clear from Table 6.1 that the damage constant of the $T_{dT_{17}}$ target is ~2.8 times faster than that of the T_{random} target. This indicates that

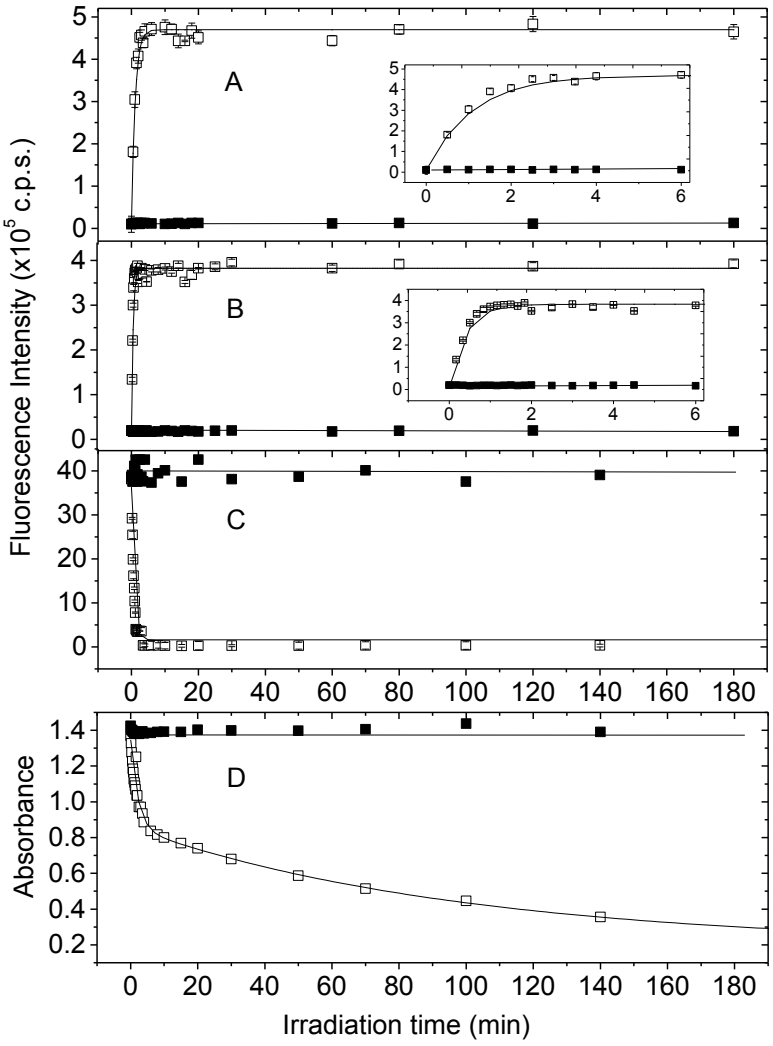

Figure 6.6. UV damage plots of Tb^{3+}/hairpin probe luminescence intensity (λ_{ex} = 290 nm, λ_{em} = 545 nm) as a function of target irradiation time for T_{random} (A) and $T_{dT_{17}}$ (B). (C) MB hairpin probe fluorescence (λ_{ex} = 490 nm, λ_{em} = 520 nm) as a function of target irradiation time for $T_{dT_{17}}$. (D) 260 nm absorbance as a function of target irradiation time for $T_{dT_{17}}$. For all experiments, the 1 μM irradiated oligonucleotide targets (open squares) and the 1 μM unirradiated control (filled squares) were hybridized with the probe at 20 °C. The solid line through the irradiated sample fluorescence points in (A) and (B) is a single exponential growth fit to $I_F = I_{F,0} + a(1 - e^{-t/\tau})$, where (A) $I_{F,0} = (0.10 \pm 0.01) \cdot 10^5$ cps, a = 4.6 ± 0.01, and τ = 1.1 ± 0.02 min, and (B) $I_{F,0} = (0.17 \pm 0.01) \cdot 10^5$ cps, a = 3.7 ± 0.01,

and τ = 0.40 ± 0.01 min. The MB damage curve in (C) is a single exponential decay fit to $I_F = I_{F,0} + a\, e^{-t/\tau}$ where $I_{F,0} = (1.2 \pm 0.04) \cdot 10^5$ cps, a = 2.5 ±0.10, and τ = 2.36 ± 0.10 min. The solid line through the absorbance points (open squares) is the least-squares fit to an offset, double exponential function, $A = A_0 + A_1 e^{t/\tau 1} + A_2 e^{t/\tau 2}$, where the absorbance damage constants are 5.9 ± 0.05 min (τ_1) and 84.3 ± 3.0 min (τ_2), and the amplitudes are A_1 = 0.54 ± 0.01 and A_2 = 0.72 ± 0.02. The offset (A_o) is 0.21 ± 0.02. The control points (filled squares) are fit to a straight line with zero slope by eye.

Table 6.1. Damage constants of the different DNA damage assay methods.

Method	Damage constant (min)[a]
Tb^{3+}/hairpin probe luminescence	$\tau_{dT_{17}} = 0.40 \pm 0.01$
	$\tau_{random} = 1.10 \pm 0.02$
DNA MB fluorescence	$\tau_{dT_{17}} = 2.36 \pm 0.20$
Absorbance	$\tau_1 = 5.9 \pm 0.05$
	$\tau_2 = 84 \pm 3.00$

[a]The damage constants (τ) were obtained from the exponential fits in Figure 6.6.

the $T_{dT_{17}}$ target is more damaged under UV irradiation than the T_{random} target. Comparing the number of photoreactive damage sites in each target reveals that the $T_{dT_{17}}$ target has 8 TT sites that are most prone to UV damage. However, the T_{random} target has only one TT site, one TC site, three CT sites, one AA site and two AT sites. CPDs are produced preferentially at TT and TC sites, whereas CC and CT dipyrimidine sites are poorly photoreactive,[13] and dipurine sites are photostable compared to dipyrimidine sites.[1] So the T_{random} target contains a total of five dipyrimidine sites, in which four of them are less photoreactive than the TT site. Thus, it should exhibit slower photodamage kinetics, consistent with Figure 6.6. This result confirms that we can get information on the amount of UV damage accumulated in different targets by comparing the damage constant values obtained by the same probe.

The selectivity of the Tb^{3+}/hairpin probe was compared to the MB for detecting nucleic acid damage. The MB probe (Figure 6.1) used in this study was designed to have the same sequence as the hairpin probe, i.e. complementary to the $T_{dT_{17}}$ target. In this target, the 260 nm absorption band bleaches with increasing irradiation time, quantifying photoproduct formation via the loss of the C_5=C_6 and yielding an independent spectroscopic marker for DNA damage.

As explained above, the MB fluorescence is quenched in the hairpin position when the FAM fluorophore and DABCYL quencher are in close proximity, and the fluorescence intensity is high in the presence of complementary target when the MB forms a hybrid with the target. As damage accumulates on the target strand, the MB-target hybrid becomes less stable, effectively decreasing the fluorescence intensity until the closed, hairpin form is the more stable form of the MB. This trend is shown in Figure 6.6C, in which the MB fluorescence intensity decreases with longer target irradiation time until reaching a constant minimum corresponding to the quenched fluorescence of the MB in the hairpin structure. The damage curve for MB-detected UV damage was fit to a single exponential decay function. The damage constant obtained is shown in Table 6.1. The

selectivity of the probe is directly related to the damage constant; the faster the fluorescence intensity increases in case of Tb^{3+}/hairpin probe (Figure 6.6B) or decreases in case of the MB probe (Figure 6.6B), the more selective the probe is at detecting UV-induced DNA damage under identical irradiation conditions for the same target. Table 6.1 shows that the damage constant of the Tb^{3+}/hairpin probe is 6 times faster than that of the DNA MB. This proves that the Tb^{3+}/hairpin probe has superior selectivity for detection of UV damage in nucleic acids compared to the DNA MB method.

UV absorbance measurements as a function of $T_{dT_{17}}$ target irradiation time (Figure 6.6D) were used to quantify the amount of UV damage and to develop calibration curves for the Tb^{3+}/hairpin probe. This curve was fit to a double-exponential function and the damage constants are listed in Table 6.1. The results show that the damage constant of the Tb^{3+}/hairpin probe is 15 times faster than the fastest absorption damage constant. The faster the change in the signal with damage, the more selective the probe is to UV-induced damage. This confirms that the fluorescent Tb^{3+}/hairpin probe has superior selectivity for detection of UV damage in nucleic acids over the absorption method.[2,21]

6.3.4. Sensitivity of the Tb^{3+}/hairpin probe

In order to check the sensitivity of the Tb^{3+}/hairpin probe for damage detection, we used the UV absorbance measurements as a function of target irradiation time to quantify the amount of UV damage and to develop calibration curves of the UV-induced photoproducts detected by the Tb^{3+}/hairpin probe. The procedure and calculation of the photoproducts concentration from the absorbance measurements of the irradiated solutions have been explained previously in Chapter 4. Figure 6.7 shows the calibration curve obtained upon plotting the Tb^{3+} luminescence intensity as a function of the concentration of the photoproducts calculated for both the Tb^{3+}/hairpin probe (Figure 6.7A) and the fluorescence signal for the MB probes (Figure 6.7B). In Figure 6.7A, the luminescence at zero concentration of the photoproducts represents the background level corresponding to the quenched

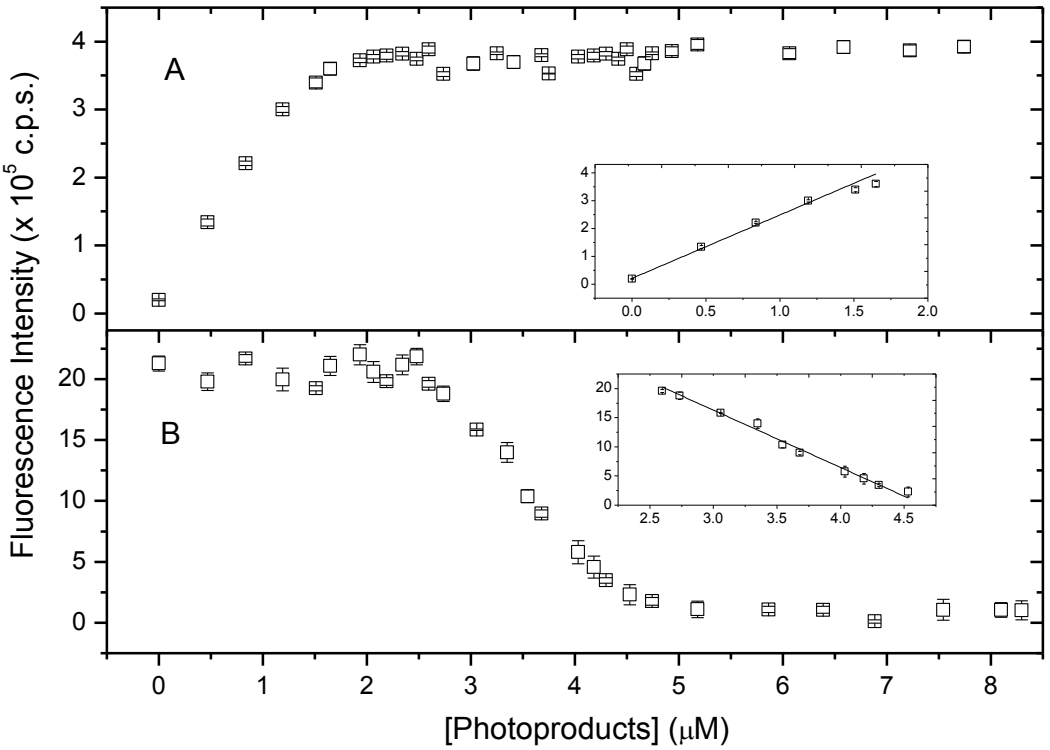

Figure 6.7. Calibration curve of DNA photodamage formed upon UV irradiation of the $T_{dT_{17}}$ target for the (A) Tb^{3+}/hairpin probe and (B) DNA MB. The inset shows the fit to the linear portions of the calibration curves. Each data point is an average of three replicate measurements and the error bars correspond to the standard deviation of the measurements.

Tb^{3+} luminescence as the hairpin probe is completely hybridized with the undamaged target. The Tb^{3+} luminescence increases linearly with increasing damage. At high damage concentrations, the hybrids formed between the hairpin probe and the damaged strands are completely unstable, and the probe acquires the hairpin structure with the damaged target in the single-stranded form leading to maximum enhancement of Tb^{3+} luminescence. Additional formation of photoproducts cannot lead to any more dehybridization, so the luminescence signal shows saturation-like behaviour.

For the DNA MB (Figure 6.7B), any decrease in fluorescence signal requires a minimum 2.59 μM concentration of the photoproducts. The constant fluorescence signal of the DNA MB over the range of 0 – 2.59 μM of the photoproducts concentration can be attributed to the lower selectivity of the DNA MB to UV-induced DNA damage as discussed above. At high photoproduct concentrations, the hybrid formed between the DNA MB and the damaged strand is completely unstable, and the DNA MB preferentially acquires the hairpin structure where the fluorophore and the quencher are in close proximity and the fluorescence is the lowest. Further damage does not lead to any additional decrease in fluorescence and the signal remains constant, showing a saturation-like behaviour.

Although the MB probe used in this study was designed to have the same sequence as the hairpin probe (Figure 6.1), the Tb^{3+}/hairpin probe proved to be more selective and sensitive to UV-induced DNA damage than the MB probe. This can be attributed to the difference in the reporting mechanism between the two probes. In the MB probe, the reporting mechanism is through FRET between a fluorophore-quencher pair on the hairpin probe, while in the Tb^{3+}/hairpin probe, it is through direct emission from the coordinated Tb^{3+} via energy transfer from the unpaired nucleobases. This is reflected in Figure 6.7A where the low luminescence background allowed the Tb^{3+} to show an immediate luminescence increase upon photoproduct formation, leading to better sensitivity. Also, it has been previously shown that single mismatches in the sequence of a duplex DNA lead to selective Tb^{3+} luminescence enhancement.[51] Our result showing that Tb^{3+} is sensitive to very low photoproduct concentrations is consistent with this past

Table 6.2. Analytical parameters for the quantification of UV-induced DNA damage with Tb^{3+}/hairpin probe and DNA MB

Parameter[a]	Detection of UV-damaged DNA	
	Tb^{3+}/hairpin probe	**DNA MB**
Linear Dynamic Range (μM)	0.00 – 1.72	2.59 – 4.53
R^2	0.975	0.995
Sensitivity (cps M^{-1})	2.38×10^{12}	9.84×10^{11}
LOD (nM)	4.36	41.4
LOQ (nM)	14.5	138

For the determination of the blank standard deviation, 20 solutions of 40 μM Tb^{3+} and 200 nM DNA MB were used, respectively. The standard deviations of these measurements were 0.7×10^4 and 1.3×10^4 c.p.s., respectively. [a]In this table, linear dynamic range is the concentration range corresponding to the linear region in the calibration curve, R^2 is the linear regression coefficient squared, sensitivity is the slope of the calibration curve, LOD is the limit of detection and is 3 times the standard deviation of the blank divided by the sensitivity, and LOQ is the limit of quantification and is 3.3 times the LOD.

work. For the MB probe (Figure 6.7B), the high fluorescence background of the quenched fluorophore decreases the sensitivity of this probe.

Table 6.2 shows the parameters for the quantification of UV-induced DNA damage from Figure 6.7. The calibration curve for the Tb^{3+}/hairpin probe shows a similar linear dynamic range to the MB probe (Table 6.2), taking into account the MB threshold response of 2.59 μM photoproduct. The sensitivity of detection is larger by a factor of ~2.5 for the Tb^{3+}/hairpin probe, leading to a lower limit of detection (LOD) and limit of quantification (LOQ) by approximately an order of magnitude. It is worth mentioning that the values recorded in Table 6.2 for the LOD and LOQ for the MB method for the detection of DNA damage is obtained by using the standard deviation of the blank measurements and the sensitivity of the method, while the LOD and LOQ will be practically limited to the threshold 2.59 μM (Figure 6.7B) photoproduct concentration. From this data, we calculate that the Tb^{3+}/hairpin probe can detect one damage site in the presence of ~8000 undamaged sites, compared to one damage site in the presence of ~820 undamaged sites with the MB probe. This again confirms the superior sensitivity of the Tb^{3+}/hairpin probe over the MB probe.

6.4.Conclusions

These results conclusively show that the Tb^{3+}/hairpin probe is a sensitive tool for detecting UVC-induced oligonucleotide damage. Changing the fluorescence reporting mechanism of the probe from a fluorophore-quencher pair attached to the hairpin probe to Tb^{3+} coordinated to ssDNA allows positive detection of DNA damage with a luminescence signal that increases with increasing damage. The Tb^{3+}/hairpin probe proves to have superior selectivity and sensitivity to DNA damage than the MB probe, while also being much cheaper and easier to synthesize. The Tb^{3+}/hairpin probe represents a promising tool in the design of biosensors for the *in vivo* detection of nucleic acid damage.

6.5.References

1) B.P. Ruzsicska, D.G.E. Lemaire, In DNA Photochemistry, CRC Handbook of Organic Photochemistry and Photobiology, P.-S. Horspool, W.M. Song, Eds., CRC Press, New York (1995) pp 1289.
2) S. Yarasi, C. McConachie, G.R. Loppnow, Photochem. Photobiol. 81 (2005) 467-473.
3) B. Ames, L. Gold, W. Willett, Proc. Natl. Acad. Sci. U.S.A. 92 (1995) 5258-5265.
4) T. Lindahl, Nature 362 (1993) 709-715.
5) L. Marnett, P. Burcham, Chem. Res. Toxicol. 6 (1993) 771-785.
6) L. Marrot, J. Meunier, J. Am. Acad. Dermatol. 58 (2008) S139-S148.
7) M. Weinfeld, K. Soderlind, Biochemistry 30 (1991) 1091-1097.
8) X. Le, J. Xing, J. Lee, S. Leadon, M. Weinfeld, Science 280 (1998) 1066-1069.
9) B. Haab, R. Mathies, Anal.Chem. 67 (1995) 3253-3260.
10) J. Wang, G. Rivas, M. Ozsos, D. Grant, X. Cai, C. Parrado, Anal.Chem. 69 (1997) 1457-1460.
11) H. Kaur, B. Halliwell, Biochem. J. 318 (1996) 21-23.
12) T. Douki, M. Court, S. Sauvaigo, F. Odin, J. Cadet, J. Biol. Chem. 275 (2000) 11678-11685.
13) T. Douki, J. Cadet, Biochemistry 40 (2001) 2495-2501.
14) J. Ravanat, T. Douki, J. Cadet, Photochem. Photobiol. B: Biol. 63 (2001) 88-102.
15) A. Kumar, M. Tyagi, P. Jha, Biochem. Biophys. Res. Commun. 318 (2004) 1025-1030.
16) C.C. Trevithick-Sutton, L. Mikelsons, V. Filippenko, J.C. Scaiano, Photochem. Photobiol. 83 (2007) 556-562.
17) J. Xing, J. Lee, S. Leadon, M. Weinfeld, X. Le, Methods 22 (2000) 157-163.
18) S. Tyagi, D. Bratu, F. Kramer, Nat. Biotechnol. 16 (1998) 49-53.
19) S. Tyagi, F. Kramer, Nat. Biotechnol. 14 (1996) 303-308.

20) K. Wang, Z. Tang, C.J. Yang, Y. Kim, X. Fang, W. Li, Y. Wu, C.D. Medley, Z. Cao, J. Li, P. Colon, H. Lin, W. Tan, Angew. Chem. Int. Ed. Engl. 48 (2009) 856-870.
21) S.A. Oladepo, G.R. Loppnow, Anal. Bioanal. Chem. 397 (2010) 2949-2957.
22) K. Stohr, B. Hafner, O. Nolte, J. Wolfrum, M. Sauer, D. Herten, Anal. Chem. 77 (2005) 7195-7203.
23) J. Knemeyer, N. Marme, M. Sauer, Anal. Chem. 72 (2000) 3717-3724.
24) A. Misra, P. Kumar, K.C. Gupta, Anal. Biochem. 364 (2007) 86-88.
25) T. Heinlein, J. Knemeyer, O. Piestert, M. Sauer, J. Phys. Chem. B. 107 (2003) 7957-7964.
26) Y. Kim, C.J. Yang, W. Tan, Nucl. Acids Res. 35 (2007) 7279-7287.
27) A. Misra, M. Shahid, Bioorg. Med. Chem. 17 (2009) 5826-5833.
28) N. Sabbatini, M. Guardigli, J. Lehn, Coord. Chem. Rev. 123 (1993) 201-228.
29) S. Rigault, C. Piguet, G. Bernardinelli, G. Hopfgartner, Angew. Chem. Int. Ed. 37 (1998) 169-172.
30) N. Martin, J. Bunzli, V. McKee, C. Piguet, G. Hopfgartner, Inorg. Chem. 37 (1998) 577-589.
31) C. Piguet, J. Bunzli, G. Bernardinelli, G. Hopfgartner, S. Petoud, O. Schaad, J. Am. Chem. Soc. 118 (1996) 6681-6697.
32) V. Alexander, Chem. Rev. 95 (1995) 273-342.
33) G. Choppin, Z. Wang, Inorg. Chem. 36 (1997) 249-252.
34) P. Valente, S. Lincoln, K. Wainwright, Inorg. Chem. 37 (1998) 2846-2847.
35) M. Wolbers, F. van Veggel, B. SnellinkRuel, J. Hofstraat, F. Geurts, D. Reinhoudt, J. Am. Chem. Soc. 119 (1997) 138-144.
36) R.C. Leif, L.M. Vallarino, M.C. Becker, S. Yang, Cytometry A. 69A (2006) 767-778.
37) M. Li, P.R. Selvin, Bioconjug. Chem. 8 (1997) 127-132.
38) A. Saha, K. Kross, E. Kloszewski, D. Upson, J. Toner, R. Snow, C. Black, V. Desai, J. Am. Chem. Soc. 115 (1993) 11032-11033.
39) P. Ioannou, T. Christopoulos, Anal. Chem. 70 (1998) 698-702.

40) P. Hurskainen, P. Dahlen, J. Ylikoski, M. Kwiatkowski, H. Siitari, T. Lovgren, Nucl. Acids Res. 19 (1991) 1057-1061.

41) S. Ghosh, A. Misra, A. Ozarowski, A. Maki, J. Phys. Chem. B. 107 (2003) 11520-11526.

42) A. Leonov, B. Voigt, F. Rodriguez-Castaneda, P. Sakhaii, C. Griesinger, Chem.-A Europ. J. 11 (2005) 3342-3348.

43) M.J. Belousoff, P. Ung, C.M. Forsyth, Y. Tor, L. Spiccia, B. Graham, J. Am. Chem. Soc. 131 (2009) 1106-1114.

44) M. Lambert, J. Hoerter, M. Pereira, N. Walter, RNA 11 (2005) 1688-1700.

45) A. Trentani, P. Testillano, M. Risueno, M. Biggiogera, Eur. J. Histochem. 47 (2003) 195-200.

46) M. Roy, L. Wittenhagen, S. Kelley, RNA 11 (2005) 254-260.

47) B. Jolles, A. Laigle, J. Liquier, L. Chinsky, Biophys. Chem. 46 (1993) 179-185.

48) S. Klakamp, W. Horrocks, J. Inorg. Biochem. 46 (1992) 175-192.

49) D. Gersanovski, P. Colson, C. Houssier, E. Fredericq, Biochim. Biophys. Acta 824 (1985) 313-323.

50) Z. Balcarova, V. Brabec, Biophys. Chem. 33 (1989) 55-61.

51) P. Fu, C. Turro, J. Am. Chem. Soc. 121 (1999) 1-7.

52) L. Pearlman, H. Simpkins, Biochem. Biophys. Res. Commun. 131 (1985) 1033-1040.

53) Y. Ci, Y. Li, X. Liu, Anal. Chem. 67 (1995) 1785-1788.

54) A. Canfi, M. Bailey, B. Rocks, Analyst 114 (1989) 1405-1406.

55) A. Abusaleh, C. Meares, Photochem. Photobiol. 39 (1984) 763-769.

Chapter 7

General Conclusions and Future work

7.1. Conclusion

The research described in this thesis involves the development of various DNA and RNA hybridization probes with different reporter groups for the detection and quantification of UV-induced damage in single-stranded oligonucleotides. The importance of these studies, which is apparent throughout the thesis, is due to the fact that nucleic acids are the fundamental essence of life, as they carry the genetic potential of all organisms.

The goal of this thesis is to design new sensitive and selective hairpin probes (Figure 7.1) for the quantification of UV-induced DNA damage in order to overcome the limitations of conventional DNA MBs mentioned in Chapter 1. In Chapter 2, we used Locked Nucleic Acid MBs (LNA MBs) which contains different numbers of LNAs (Figure 7.1). We studied the factors affecting the selectivity of LNA MBs to detect UV-induced nucleic acid damage. Results show that high ionic strength and low target concentration improves the performance of these MBs in detecting UV-induced DNA damage, as demonstrated by the shorter damage constants. Increasing the LNA ratio in the MB design leads to longer damage constants, reflecting a decrease in the selectivity of these MBs to detect damage. Such results show that, although LNA MBs have greater selectivity to single base-pair mismatches than conventional MBs, they have lower specificity for detecting UV-induced nucleic acid damage.

In Chapter 3, we used another type of backbone modification in which RNA bases replaced DNA bases of the conventional MBs in regions complementary to the oligonucleotide target, the chimeric RNA-DNA MBs (chMBs). Results show that the RNA bases incorporated in the MB loop increased the stability of the hybrids formed between the chMB and the oligonucleotide targets compared to that of the conventional DNA MB, allowing the chMB to have superior sensitivity and selectivity compared to the DNA MB. However, the chMB (Figure 7.1) still

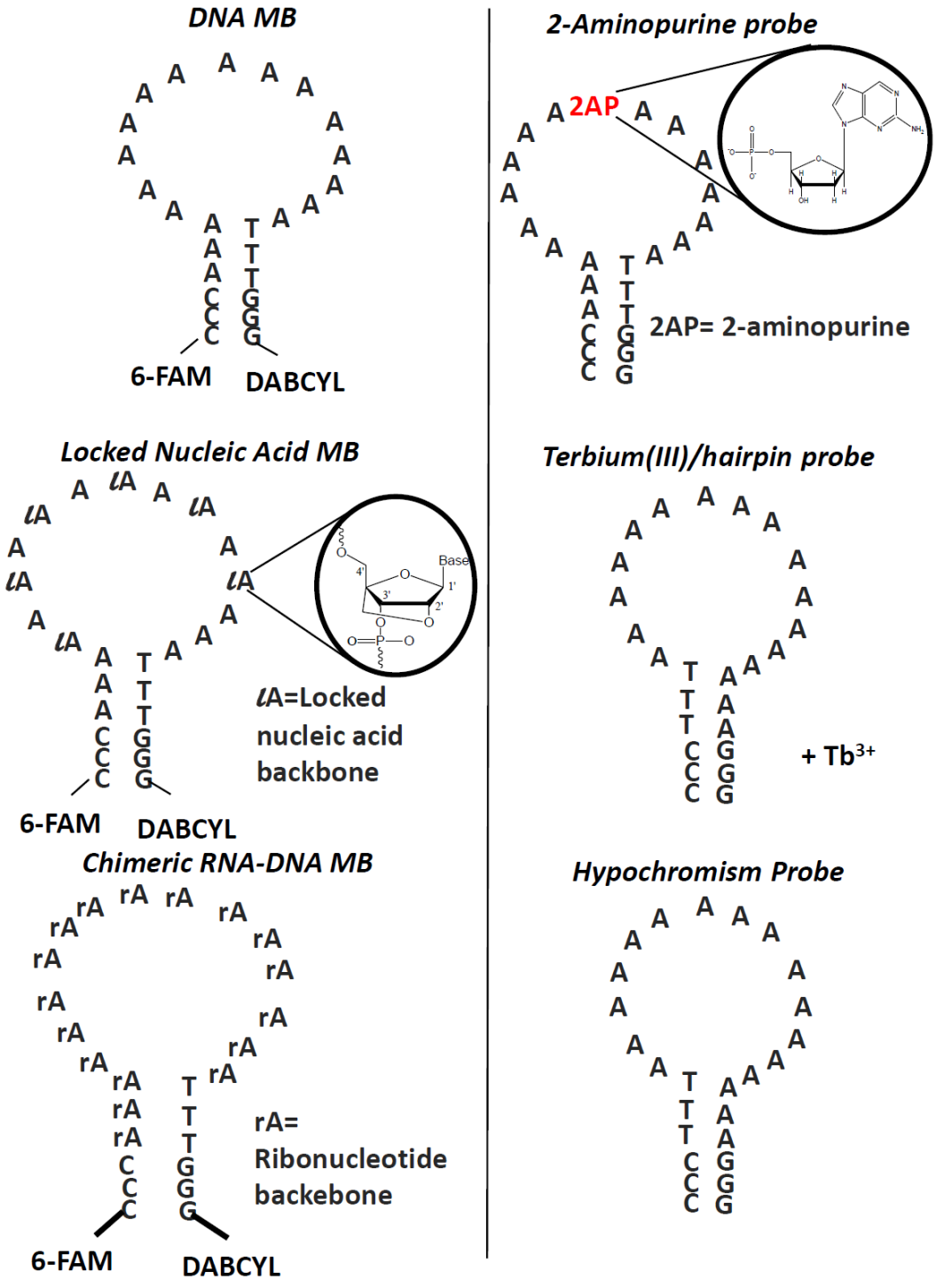

Figure 7.1. Schematic diagram of all the probes discussed in this thesis

suffer from some important limitations of the MBs, such as, the need of site-specific labeling of both termini of the hairpin and the negative detection of DNA damage (Figure 7.2). For this reason, probes that do not require terminal labeling and can positively detect DNA damage have been developed and discussed in Chapters 4 - 6 to address these specific limitations.

2-Aminopurine (2AP) hairpin probes (Figure 7.1) are discussed in Chapter 4. The 2AP hairpin probe is designed so that 2APs are incorporated in the loop of the hairpin probe with the two hairpin termini free. The probe forms a hybrid with the undamaged target and the fluorescence is significantly quenched. While the hybrid with the damaged targets is unstable, the 2AP hairpins will preferentially acquire the hairpin structure, emitting maximum fluorescence. Thus, the more damaged DNA targets there are in solution, the more 2AP probes will be in the hairpin structure and the higher the fluorescence intensity will be. The results show that the 2AP hairpin probe is a sensitive tool to detect UV-induced oligonucleotide damage. The more 2AP nucleotides incorporated in the probe, the more the sensitivity and selectivity of the 2AP probes appears to be enhanced, allowing these probes to have superior selectivity compared to conventional MBs. In contrast to MBs, the use of 2AP probes has overcome most of the MB limitations, mainly the feasibility of further modification at any of the two termini of the hairpin and positive detection (Figure 7.2) of DNA damage (i.e. fluorescence intensity increases with the increase of damage). However, the cost is still an issue, as the more 2APs added to the hairpin, the more expensive is the synthesis of this probe. Thus, the need for an inexpensive probe was the motivation to design the hypochromism probe.

In Chapter 5, the design of the hypochromism probe (Figure 7.1) is discussed. The hypochromic effect,[2,3] which is the decrease in UV absorbance of DNA associated with the better stacking of purine and pyrimidine residues in double-stranded oligonucleotides compared to single-stranded ones, is the characteristic of DNA that allows the positive detection of DNA damage. As a result, the absorbance signal significantly increases with increasing DNA damage due to more ssDNA as damage accumulates. The results show that the hypochromism

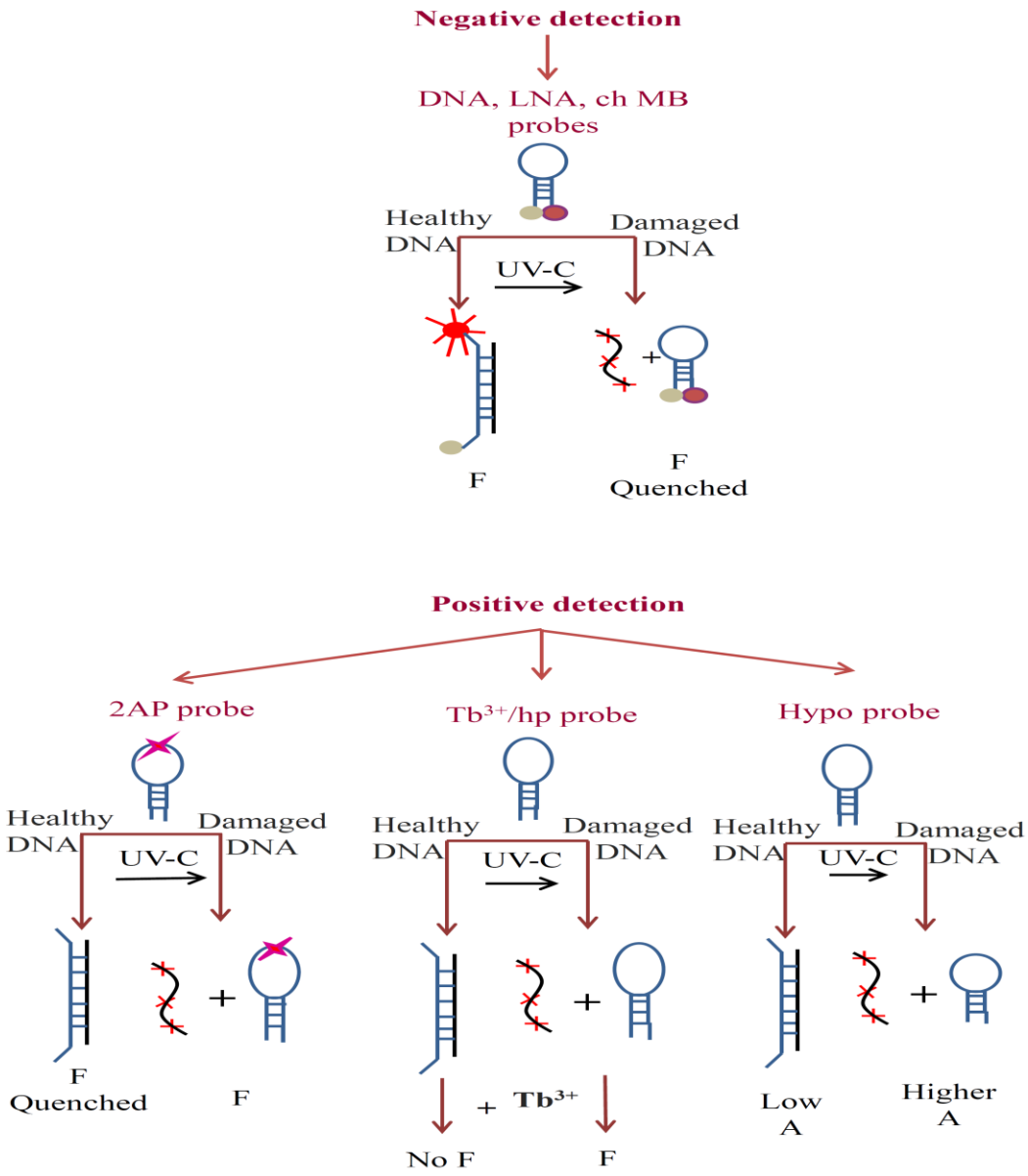

Figure 7.2. Schematic diagram of the positive and negative detection of UV-induced DNA damage. "F" and "A" denote fluorescence and absorbance, respectively.

probe has superior selectivity to detect UV-induced oligonucleotide damage over conventional MBs. Although its sensitivity is not as good as DNA MB probes, it is 10 times cheaper than the DNA MBs, making it an attractive tool for high-throughput qualitative analysis for UV-induced DNA damage.

The need for a sensitive and inexpensive probe for high-throughput quantitative analysis for UV-induced DNA damage was the main motivation for designing the terbium (III)/hairpin probes (Figure 7.1) discussed in Chapter 6. With the aid of a DNA hairpin probe complementary to the oligonucleotide of interest, the Tb^{3+}/hairpin probe is applied to detect UV-induced DNA damage. The hairpin probe hybridizes only with undamaged DNA, while the damaged DNA remains single-stranded. The ssDNA can bind and enhance the intrinsic fluorescence of Tb^{3+}, producing a detectable signal directly proportional to the amount of DNA damage (Figure 7.2). The results show that the Tb^{3+}/hairpin probe has superior selectivity and sensitivity to DNA damage than conventional MBs. In addition, the Tb^{3+}/hairpin probe is almost one order of magnitude less expensive than MBs, it allows the positive detection of UV-induced DNA damage and the possibility of further modifying the hairpin. These advantages allow the Tb^{3+}/hairpin probe to overcome the main limitations of MBs and introduce this probe for the detection and quantification of various DNA damage forms in multiplexing assays.

7.2. Future Work

The different probes presented in the preceding chapters of this thesis involve the detection of UV-induced damage in single-stranded DNA (ssDNA). Therefore to expand the benefit of these probes, the following future experiments should be directed to the detection of UV-induced damage in double-stranded DNA (dsDNA). This approach could ultimately lead us to successful intracellular analysis of UV-induced DNA damage.

7.2.1. Detection of UV-induced damage in double-stranded oligonucleotides

The use of peptide nucleic acid[4] (PNA) openers is a recently developed approach that allows probe hybridization to dsDNA. This approach allows the detection of

short DNA sequences within genomic DNA without the need for DNA denaturation[4] which may introduce additional damage to DNA. PNAs are oligonucleotide analogues in which the sugar-phosphate-backbone has been replaced by a pseudopeptide skeleton (Figure 7.3) through synthetic amide linkages.[5] The PNA structure represents a radical departure from the standard oligonucleotide chemistry, providing PNA molecules with exceptional chemical, physical and biological properties.[5] As compared to ordinary oligonucleotides and their analogue, the pseudopeptide backbone gives PNAs excellent chemical and biological stability,[5,6] superior specificity and affinity of binding to ssDNA or RNA, [7,8] and a unique ability to invade dsDNA.[9-13] In the repertoire of various PNAs capable of strand invasion,[9-13] PNA openers[4,14-15] (Figure 7.4) are composed of two homopyrimidine PNA oligomers connected by a flexible linker (bis-PNAs). A pair of PNA openers initiates the local opening of dsDNA yielding an extended strand-displacement complex. This structure is able to accommodate different hybridization probes by formation of PD-loop complexes.[4,14-15] As a result, affinity capture[16] and topological labeling[17] of dsDNA and highly selective detection of specific sequences[4,14] and mismatches[15] within dsDNA have become possible. Our goal for future work is to extend the use of PNA openers with the aid of the hybridization probes described in this thesis for the detection of UV-induced damage in dsDNA.

Figure 7.5 shows a schematic diagram of the proposed approach for the detection of UV-induced damage in dsDNA. It consists of two main steps. The first step involves the local opening of a known DNA target sequence by a pair of strand-invading PNA openers, thus, exposing one DNA strand within the double-helix.

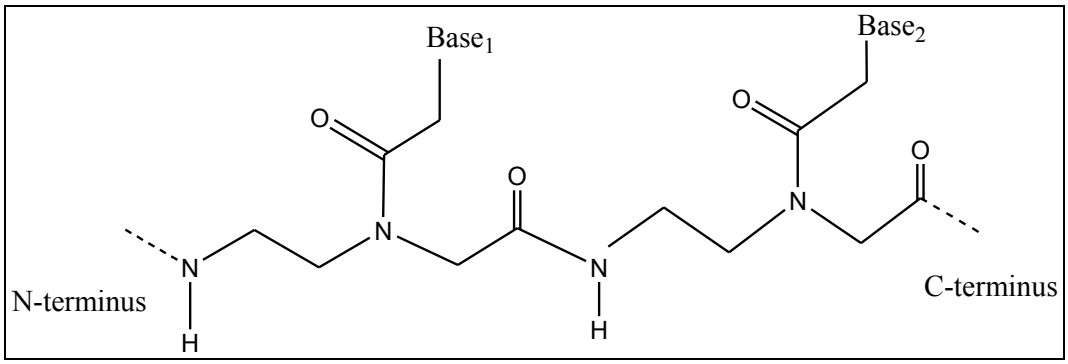

Figure 7.3. Pseudopeptide skeleton of the peptide nucleic acid (PNA).

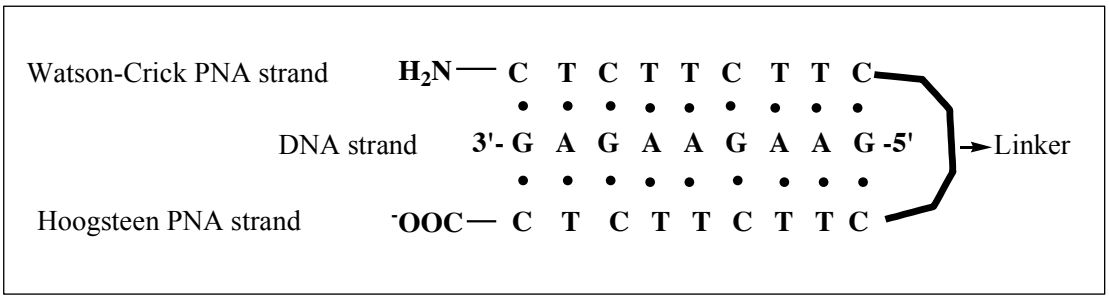

Figure 7.4. PNA opener with two homopyrimidine PNA oligomers connected by a flexible linker and hybridizing to a DNA strand

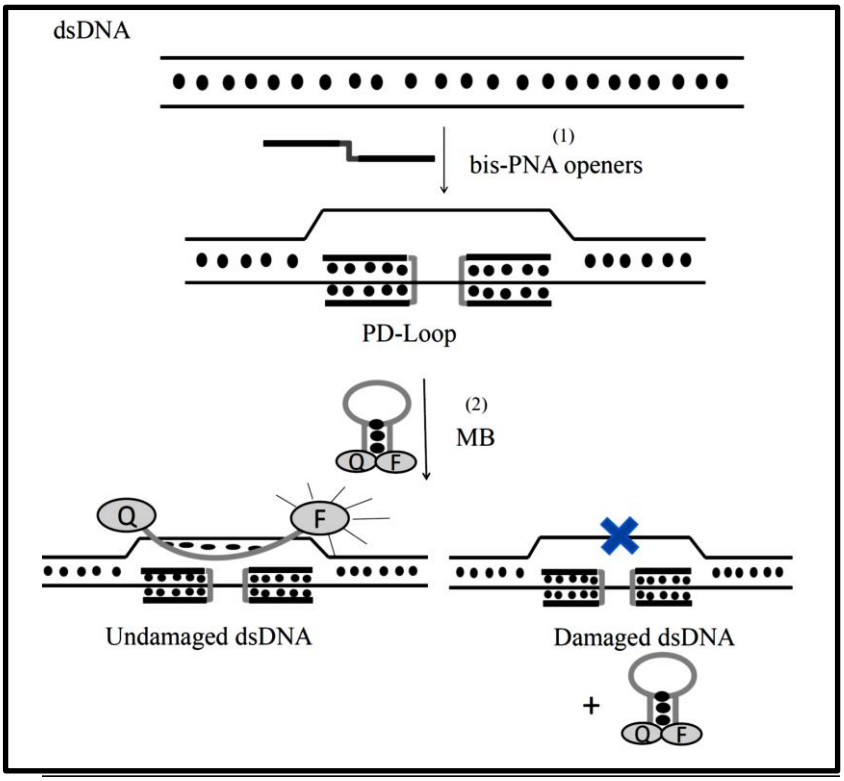

Figure 7.5. Schematic diagram for the use of PNA openers with MB probes for the detection of UV-induced damage in dsDNA (See text for details).

The second step involves the detection of the exposed ssDNA with one of the hybridization probes described in this thesis. In Figure 7.4, a MB probe was chosen as a representative example for the detection of damage in dsDNA. For all MB probes, including the chMB and LNA MBs, the increase in damage upon exposure to UV light would be reflected as a decrease in the fluorescence signal. While for the 2AP probe and the Tb^{3+}/hairpin probe, the fluorescence signal will increase with the increase of damage as explained before, and for the hypochromism probe, an increase in absorbance will be accompanied with the increase in damage.

The choice of the hybridization probe will depend on the intended application. For example, for the *in vitro* detection of UV-induced damage in dsDNA, the chMB or the Tb^{3+}/hairpin probe would be the probe of choice out of all those discussed in this thesis because of their high selectivity and sensitivity for UV-induced DNA damage. With Tb^{3+}/hairpin probe being much cheaper than MBs then it would be the first choice for a sensitive and inexpensive the *in vitro* analysis of UV-induced DNA damage.

7.2.2. *In vivo* detection of UV-induced damage in intracellular double-stranded DNA

For the intracellular detection of DNA damage, we have to consider several other factors that would limit the use of some of the discussed hybridization probes. For example, the degradation of RNA/DNA probes with intracellular enzymes such as RNA and DNA nucleases, the non-specific binding of the RNA/DNA probe to RNA and DNA binding proteins or disruption of the probe stem or change in the secondary structure due to changes in pH. In addition, the ubiquitous endogenous fluorescent components in the cellular matrix, such as flavins, nicotinamide adenine dinucleotides, and porphyrins,[18-20] may affect the assay's background fluorescence level. All these factors would affect the accuracy of the assay. This explains why intracellular DNA isolation is a prerequisite step in most of the various methods developed for the detection of intracellular DNA damage. However, the isolation step is the step where most of the experimental artifacts

are introduced. This is because that step includes the use of harsh chemicals, such as sodium hydroxide and sodium dodecyl sulfate for cell lysis, followed by the chromatographic separation. Thus, the intracellular DNA is subjected to several steps prior to damage detection. This may introduce additional damage to the DNA affecting the sensitivity of the developed assay and increasing the complexity of the assay to be more elaborate and time consuming. Therefore a future experiment is to develop probes for the detection of DNA damage that resist degradation and non-specific binding to cellular components, and which can produce a signal that is selectively detected in the presence of the endogenous fluorescent background.

7.2.2.1. Probes not affected by cellular components

LNA MBs[21] are well-known for their resistance to nuclease activity and non-specific binding to RNA and DNA binding proteins. This makes their use, with the aid of PNA openers, beneficial for the *in vivo* detection of intracellular dsDNA. However, their low selectivity to UV-induced DNA damage, discussed previously in Chapter 2, restricts their potential use.

PNA MBs[14,15] have the same characteristics of LNA MBs regarding nuclease resistance and resistance to non-specific protein binding. In addition, because of their neutral pseudopeptide backbone, they are not affected by changes in pH and thus are more stable than LNA and DNA MBs. PNA MBs have been previously used for the detection of specific sequences of dsDNA[14] and mismatches in dsDNA[15] with the aid of PNA openers. Therefore, the use of a PNA MBs and a pair of PNA openers would allow the intracellular detection of UV-induced damage in dsDNA and avoid false results due to nuclease degradation, non-specific protein binding and MB stem disruption.

7.2.2.2. Probes not affected by the background fluorescence interference

Most endogenous components emit fluorescence from the ultraviolet range to the visible range. To reduce background fluorescence, several near-infrared organic dyes,[22,23] fluorescent proteins,[24,25] and inorganic nanomaterials[26-28] were used. However, the detrimental photophysical properties of these fluorescent molecules,

such as photobleaching and blinking, and the significant toxicity of the nanomaterials inevitably restrict their *in vivo* applications.

A more efficient approach for elimination of background fluorescence in complex environments is time-resolved fluorescence or room-temperature phosphorescence (RTP) measurement. RTP has gained significance as a very useful mode for optical sensing applications as it offers many advantages over steady-state fluorescence.[29] In particular, the longer emission lifetime of the triplet excited state of phosphorescence allows an appropriate delay time so that any fluorescent emission and scattering light can be easily avoided.[30] However, few attempts so far have been made to design a RTP-based MB. In comparison to common organic fluorophores, lanthanide ion complexes have the advantage of a long luminescence lifetime, large Stokes shift, and relatively high quantum yield as discussed in Chapter 6. The long-lived luminescence of the lanthanides allows background-free measurement using the RTP technique. For these reasons, sensitization of lanthanide luminescence has been exploited for a number of useful signalling systems in the fields of medicine, biotechnology, and biological science.[31-36] For application of lanthanide ions in nucleic acid probes, significant efforts have been directed toward FRET study in the dye-DNA conjugates.[37-39]

Recently a new RTP-based MB[40] for detection of ssDNA in cell samples has been developed. The MB contains a europium(III) (Eu^{3+}) complex of chlorosulfonylated tetradentate β-diketone as a luminescent signalling reporter and black hole quencher 2 (BHQ-2) as a luminescent t quencher.[40] In the MB, the luminescence of the Eu^{3+} complex was quenched by BHQ-2 due to the MB's stem-closed conformation. In the presence of a complementary target, the MB hybridizes with the target and the luminescent complex is separated from BHQ-2 obtaining a Eu^{3+} emission signal proportional to the target concentration. Using RTP assays enabled direct and sensitive detection of ssDNA in cell media without any need of a sample clean-up process.[40]

In conclusion, a potential probe, suitable for the *in vivo* detection of UV-induced damage in dsDNA, would be a MB with a PNA backbone and phosphorescent signalling reporter and quencher with the aid of PNA openers.

The PNA openers will allow the local opening of dsDNA at specific sequences under non-denaturing conditions. The PNA MB would avoid nuclease degradation, non-specific protein binding, and MB's stem disruption. While the luminescent signalling reporter with RTP detection would avoid interferences from the endogenously fluorescent background and obtain a luminescent signal proportional to the complementary undamaged DNA. Therefore, this design would allow the efficient, simple, mix-and-read detection of specific DNA sequences within genomic DNA in complex biological environments.

7.3. References:

1) S. Nakano, T. Kanzaki, N. Sugimoto, J. Am. Chem. Soc. 126 (2004) 1088-1095.
2) A. Rich, I. Tinoco, J. Am. Chem. Soc. 82 (1960) 6409-6411.
3) I. Tinoco, J. Am. Chem. Soc. 82 (1960) 4785-4790.
4) I.V. Smolina, H. Kuhn, C. Lee, M.D. Frank-Kamenetskii, Bioorg. Med. Chem. 16 (2008) 84-93.
5) E. Uhlmann, A. Peyman, G. Breipohl, D.W. Will, Angew. Chem. Int. Ed. 37 (1998) 2796–2823.
6) V.V. Demidov, V.N. Potaman, M.D. Frank-Kamenetskii, M. Egholm, O. Buchardt, S.H. Sonnichsen, P.E. Nielsen, Biochem. Pharmacol. 48 (1994) 1310–1313.
7) H. Perry-O'Keefe, X.-W. Yao, J.M. Coull, M. Fuchs, M. Egholm, Proc. Natl. Acad. Sci. U.S.A. 93 (1996) 14670–14675.
8) M. Egholm, O. Buchardt, L. Christensen, C. Behrens, S.M. Freier, D.A. Driver, R.H. Berg, S.K. Kim, B. Norden, P.E. Nielsen, Nature 365 (1993) 556–568.
9) L.C. Boffa, E.M. Carpaneto, V.G. Allfrey, Proc. Natl. Acad. Sci. U.S.A. 92 (1995) 1901–1905.
10) S.V. Smulevitch, C.G. Simmons, J.C. Norton, T.W. Wise, D.R. Corey, Nat. Biotechnol. 14 (1996) 1700–1704.
11) P. Wittung, P.E. Nielsen, B. Nordin, Biochemistry 36 (1997) 7973–7979.

12) J. Lohse, O. Dahl, P.E. Nielsen, Proc. Natl. Acad. Sci. U.S.A. 96 (1999) 11804–11808.
13) V.V. Demidov, M.D. Frank-Kamenetskii, Methods 23 (2001) 108–122.
14) H. Kuhn, V.V. Demidov, B.D. Gildea, M.J. Fiandaca, J.C. Coull, M.D. Frank-Kamenetskii, Anti. Nucl. Acid Drug Dev. 11 (2001) 265-270.
15) H. Kuhn, V.V. Demidov, J.M. Coull, M.J. Fiandaca, B.D. Gildea, M.D. Frank-Kamenetskii, J. Am. Chem. Soc. 124 (2002) 1097-1099.
16) N.O. Bukanov, V.V. Demidov, P.E. Nielsen, M.D. Frank-Kamenetskii, Proc. Natl. Acad. Sci. U.S.A. 95 (1998) 5516
17) H. Kuhn, V.V. Demidov, M.D. Frank-Kamenetskii, Angew. Chem. Int. Ed. Engl. 38 (1999) 1446.
18) N. Billinton, A.W. Knight, Anal. Biochem. 291 (2001) 175–197.
19) J.R. Mansfield, K.W. Gossage, C.C. Hoyt, R.M. Levenson, J. Biomed. Opt. 10 (2005) 41207.
20) T. Troy, D. Jekic-McMullen, L. Sambucetti, B. Rice, Mol. Imaging 3 (2004) 9–23.
21) C.J. Yang, L. Wang, Y. Wu, Y. Kim, C.D. Medley, H. Lin, W.H. Tan, Nucl. Acids Res. 35 (2007) 4030-4041.
22) N.W.S. Kim, M. O'Connell, J.A. Wisdom, H. Dai, Proc. Natl. Acad. Sci. U.S.A. 102 (2005) 11600–11605.
23) S. Zhang, V. Metelev, D. Tabatadze, P.C. Zamecnik, A.J. Bogdanov, Proc. Natl. Acad. Sci. U.S.A. 105 (2008) 4156–4161.
24) J. Lippincott-Schwartz, G.H. Patterson, Science 300 (2003) 87–91.
25) J. Yu, J. Xiao, X.J. Ren, K.Q. Lao, X.S. Xie, Science 311 (2006) 1600–1603.
26) E.S. Jeng, A.E. Moll, A.C. Roy, J.B. Gastala, M.S. Strano, Nano Lett. 6 (2006) 371–375.
27) P.W. Barone, S. Bik, D.A. Heller, M.S. Strano, Nat. Mater. 4 (2005) 86–92.
28) S.J. Yu, M.W. Kang, H.C. Chang, K.M. Chen, Y.C. Yu, J. Am. Chem. Soc. 127 (2005) 17604–17605.

29) A.M. Powe, S. Das, M. Lowry, B. El-Zahab, S.O. Fakayode, M.L. Geng, G.A. Baker, L. Wang, M.E. McCarroll, G. Patonay, M. Li, M. Aljarrah, S. Neal, I. Warner, Anal. Chem. 82 (2010) 4865–4894.
30) J. Kuijt, F. Ariese, U.A.T. Brinkman, C. Gooijer, Anal. Chim. Acta 488 (2003) 135–171.
31) J.L. Yuan, L. Matsumoto, Anal. Chem. 70 (1998) 596–601.
32) A. Beeby, S.W. Botchway, I.M. Clarkson, S. Faulkner, A.W. Parker, D. Parker, J.A.G. Williams, J. Photochem. Photobiol. B 57 (2000) 83–89.
33) J. Karvinen, P. Hurskainen, S. Gopalakrishnan, D. Burns, U. Warrior, I. Hemmila, J. Biomol. Screening 7 (2002) 223–231.
34) K. Matsumoto, T. Nojima, H. Sano, K. Majima, Macromol. Symp. 186 (2002) 117–121.
35) J.C. Frias, G. Bobba, M.J. Cann, C.J. Hutchison, D. Parker, Org. Biomol. Chem. 1 (2003) 905–907.
36) N. Weibel, L.J. Charbonniere, M. Guardigli, A. Roda, R. Ziessel, J. Am. Chem. Soc. 126 (2004) 4888–4896.
37) A. Tsourkas, M.A. Behlke, Y.Q. Xu, G. Bao, Anal. Chem. 75 (2003) 3697–3703.
38) U. Karhunen, L. Jaakkola, Q. Wang, U. Lamminmaki, T. Soukka, Anal. Chem. 82 (2010) 751–754.
39) L.N. Krasnoperov, S.A.E Marras, M. Kozlov, L. Wipsza, A. Mustaev, Bioconjugate Chem. 21 (2010) 319–327.
40) J. Li, W. Zhou, X. Ouyang, H. Yu, R. Yang, W.H. Tan, J. Yuan, Anal. Chem. 83 (2011) 1356–1362.